Republic of Iraq
Ministry of Higher Education
and Scientific Research
University of Kerbala
College of Engineering
Civil Engineering Department

Shear Behavior of Hybrid Deep Beams with Reactive Powder and Normal Strength Concrete

A Thesis

Submitted to the Department of Civil Engineering, University of Kerbala in Partial Fulfillment of the Requirements for the Degree of Master of Science in Civil Engineering (Infrastructure Engineering)

By
Ali Younis Saad Al-Asady
(B.Sc. in Civil Engineering 1994)

Supervised by
Asst.Prof. Laith Shakir Rasheed

August 2018 A.D
Jumada I 1439

بسم الله الرحمن الرحيم

وَمَا تَوْفِيقِي إِلَّا بِاللَّهِ ۚ

عَلَيْهِ تَوَكَّلْتُ وَإِلَيْهِ أُنِيبُ

صدق الله العلي العظيم

[هود من الآية:88]

Abstract

The main aim of the present research was to study the usefulness of the use of hybridization technique in the deep beam by investigation the shear behavior of reinforced concrete deep beams with hybrid cross-section containing two different types of concrete, reactive powder concrete (RPC) and normal strength concrete (NSC) experimentally and numerically.

The experimental program included testing of eight simply supported reinforced concrete deep beams under the effect of symmetrical concentrated two-point load. The dimensions of all beams are (150 × 300 × 800) mm. The specimens were divided into four groups: group (A) normal beam, group (B) hybrid beam with RPC (75 mm in tension region), group (C) hybrid beam with RPC (75 mm in compression region), and group (D) hybrid beam with RPC (125mm in tension region), to study the effect of: Shear span / total depth (a / h= 2/3 and 1.25/3), the thickness of the RPC layer (75 and 125) mm, and the location of the RPC layer (tension or compression region) on the first cracking load and ultimate load, load-vertical midspan deflection, and type of failure. The experimental results showed that the use of hybridization technique improved the behavior of the deep beams and increase in the first crack and ultimate loads, the largest increase in first crack and ultimate loads about (17.8 and 54) %, respectively when RPC (125 mm) in tension region with compared with the normal strength concrete deep beam. The ultimate load of the hybrid deep beam with RPC layer in tension region is greater than the hybrid deep beam with RPC in the compression region about (6.7 and 28.7) % when (a/h= 2/3 and 1.25/3) respectively. Also, the first crack and ultimate loads increased with increasing the thickness of RPC layer about (2.4 and 8.6) %, respectively at (a/h=1.25/3). The load-midspan deflection behavior in deep beams was more ductility with increased (a/h), the load-vertical

midspan deflection in hybrid deep beams is stiffer than the normal deep beams, the load-vertical midspan deflection in hybrid deep beams was stiffer with increased thickness of RPC layer. The best behavior of the load-vertical midspan deflection curve was in the hybrid deep beam with RPC (125 mm in tension region) and (a / h=1.25/3). The ultimate loads increased with decreasing (a/h) about (21.5, 27.4, 5.6, and 22.6) % in groups (A, B, C, and D) respectively, but the negligible effect of the a/h on first cracking load.

The numerical part included the use of the Finite Element Method (FEM) to simulate the specimen's behavior and improving the search by adding more variables. Analysis conducted with (ANSYS-2016- R 17.2) showed an acceptable agreement between the experimental and the numerical results. The experimental ultimate loads to the numerical ultimate loads were between (0.19 – 6.67) %.

SUPERVISOR CERTIFICATE

I certify that the preparation of this thesis titled ***"Shear Behavior of Hybrid Deep Beams with Reactive Powder and Normal Strength Concrete"***, is prepared by ***"Ali Younis Saad Al-Asady"***, under my supervision at the Department of Civil Engineering in the University of Kerbala in partial fulfillment of the requirements for the degree of Master of Science in Civil Engineering (Infrastructure).

Signature: L. Sh. Rash

Name: ***Asst. Prof. Laith Shakir Rasheed***

Date: 25/ 4/ 2018

Examination Committee Certification

We certify, as an examining committee, that we have read the thesis entitled "SHEAR BEHAVIOUR OF HYBRID DEEP BEAMS WITH REACTIVE POWDER AND NORMAL STRENGTH CONCRETE", *and examined the student* "**Ali Younis Saad**", *in its contents and in our opinion, it meets the standards of the thesis for the degree of Master of Science in Civil Engineering (INFRASTRUCTURE)*.

L. Sh. Rasheed

Dr. Laith Sh. Rasheed
Asst. Professor
(Member and Supervisor)
Date 26 / 4 / 2018

Dr. Sadjad Amir Hemzah
Asst. Professor
(Member)
Date 26 / 4 / 2018

Sarmad shafeeq

Dr. Sarmad Shafeeq Abdul-qader
Asst. Professor
(Member)
Date 26 / 4 / 2018

Hayder Talib

Dr. Hayder Talib Nimnim
Asst. Professor
(Chairman)
Date 26 / 4 / 2018

Approved by Civil Engineering department:

Waqed. H. H

Dr. Waqed H. Hassan Al-Muhammed
Asst. Professor
(Head of civil engineering department)
Date 6 / 5 / 2018

Approved by College of Engineering- University of Kerbala:

Dr. Basim Khlail Nile
Asst. Professor
(Dean of College of Engineering)
Date 6 / 5 / 2018

University Of Kerbala
Dean Office
College Of Engineering

To the people of Iraq

Ali Younis Saad

2018

ACKNOWLEDGEMENT

In the name of Allah, the most compassionate the most merciful.

All thanks and praise be to **God** our Lord who helped me and enabled me to achieve this work. I would like to express my sincere thanks to my supervisor; Asst. Prof. **Laith Sh. Rasheed** for his constructive suggestions, fruitful guidance and continuous encouragement to me throughout the research period. Special thanks to **my family** for helping and encouraging me throughout the research period. I also extend my thanks and gratitude to my friends who helped me and encouraged me throughout the research period, especially **Dr. Wajdi Shuber**, **Dr. Ali Hadi**, **Dr. Bahaa Hussain, Abaader Majid** and **Mustafa Amoury**. Thanks to all **staff** of Civil Engineering Department/College of Engineering of Kerbala University for their facilities and assistance throughout this study.

Ali Y. S. Al-Asady

2018

List of Contents

Notation

Symbol	Description
A_v	Area of web reinforcement perpendicular to flexural tension reinforcement within a distance s, (mm^2).
A_{vh}	Area of web reinforcement parallels to flexural tension reinforcement within a distance s_2, (mm^2).
a	Shear span (mm).
b_w	Web width (mm).
E_c	Concrete modulus of elasticity (MPa).
E_s	Steel modulus of elasticity (MPa).
f	Stress at any strain (ε) (MPa).
f'_c	Cylinder compressive strength of concrete (MPa).
f_{sp}	Splitting tensile strength of concrete (MPa).
f_{cu}	Cube compressive strength of concrete (MPa).
f_u	Ultimate tensile strength of steel (MPa).
f_y	Yield stress of steel (MPa).
h	Total depth of deep beams(mm).
L	Total length (mm).
ln	Clear span (mm).

P_{cr}	Cracking load (kN).
$P_{cr(EXP.)}$	Cracking load obtained from experimental tests (kN).
$P_{cr(FEM)}$	Cracking load obtained from finite element analysis (kN).
P_u	Ultimate load (kN).
$(P_u)_{EXP.}$	Ultimate load obtained from experimental tests (kN).
$(P_u)_{FEM}$	Ultimate load obtained from finite element analysis (kN).
V	Shear force (kN).
V_c	Shear resistance of concrete (kN).
V_s	Shear strength of web reinforcement (kN).
Vu	Factored shear force (kN).
Mu	Factored moment at the critical section, kN.m.
u, v, w	Displacement components in (X, Y, and Z) directions, respectively.
X, Y, Z	Global coordinate system (denoting Cartesian coordinate).
$(\Delta s)_{EXP.}$	Experimental mid-span deflection of beam models at service load(mm).
$(\Delta s)_{FEM}$	Numerical mid-span deflection of beam models at service load(mm).
ρ	Ratio of longitudinal tensile reinforcement $({}^{A_s}/_{bd})$.
ε	Strain at any stress f_c.
$\varepsilon_\circ$	Strain at the maximum compressive strength f'_c .
ε_u	Ultimate strain of concrete.
σ	Stress at any strain ε(MPa).
υ c	Poisson's ratio of concrete.
υ_s	Poisson's ratio of steel.
β_c , β_o	Shear transfer coefficient for closed and opened crack.
σ_1 σ_2 σ_3	Principal stresses.
[B]	Strain-nodal displacement relation matrix.

[D]	Constitutive matrix.
$[k^e]$	Element stiffness matrix.
[K]	Overall structural stiffness matrix.
[N]	Shape function.
[T]	Transformation matrix.

Abbreviations

Abbreviation	*Description*
ACI	**A**merican **C**oncrete **I**nstitute
ASCE	**A**merican **S**ociety of **C**ivil **E**ngineers
ASTM	**A**merican **S**ociety for **T**esting and **M**aterial
BS	**B**ritish **S**tandards
IQS	**I**ra**q**i **S**pecifications
ANSYS	**An**alysis **Sys**tem program
EXP.	**Exp**erimental
FEM	**F**inite **E**lement **M**ethod
RPC	**R**eactive **P**owder **C**oncrete
HSC	**H**igh **S**trength **C**oncrete
NSC	**N**ormal **S**trength **C**oncrete
No.	**N**umber (issue)
et al	And others
Ref.	**Ref**erence
MPa	**M**ega **Pa**scal (N/mm^2)
pp.	From **p**age to **p**age
Vol.	**Vol**ume

List of Figures

List of Plates

List of Tables

Chapter One

1

INTRODUCTION

CHAPTER ONE

INTRODUCTION

1. 1 General

Reinforced concrete deep beams are structural members that carry heavy loads over short spans such as transfer girder in bridges and tall buildings. They are widely used in infrastructure, bridges and buildings, such as wall footings, foundation pile caps, floor diaphragms, bunkers, tanks etc. **(Attarde and Barbal, 2015),** as in shown plate (1-1).

The term deep beam is applied to any beam with a depth-to-span ratio that is sufficiently large to cause nonlinearity in the elastic flexural stresses over the beam depth as well as to make the distribution of shear stress non-parabolic (**Kang-Hai, 1995).**

According to American Concrete Institute **(ACI-318, 2014)**, deep beams have the following properties:

a) For the distributed load case, the clear span to total depth ratio (ln /h) is not more than 4.

b) For the point load case, the shear span to the effective depth ratio (a/d) is not more than 2.

At deep beam, a large amount of applied load transmitted to the support point by a compression force that combines the load and the reactions. This leads to the distribution of the strain being non-linear, as well as the shear disfigurements are more obvious than the flexural disfigurements.

Plate (1-1) Some applications of deep beams (from Google Website)

1.2 Types of Failure Patterns of Deep Beams

Two main patterns of failure that deep beams suffer from which are shear and flexural failures. The shear failure is divided into three patterns **(Salamy et al, 2004)** and **(Subedi and Kubota, 1986)** as follows:

1. Shear tension failure, this type of failure is due to the effect of the flexural load, which causes the tensile crack expansion in the compressive zone. The beam fails by flexural failure in the compressive zone, as shown in Figure (1-1 a). 1
2. Shear compression failure, this type of failure is the result of a decrease in the compressive zone due to the presence of diagonal cracks and their expansion in the compression zone, also, concrete crushing that occurs because of compressive stresses are exceeding, as shown in Figure (1.1 b).
3. Struts compressive or shear proper failure, this type of failure often occurs in deep beams that have a low of (a/h), in which arc formation is evident. The deep beams fail by compressive crush in direction of strut axis or by sudden tensile crack parallel to the strut axis, as shown in Figure (1.1 c).

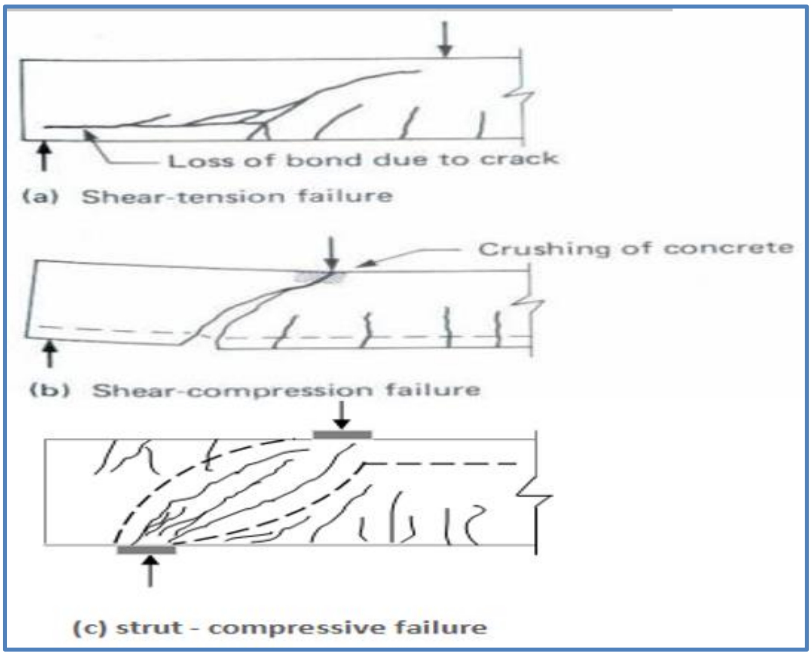

Figure (1.1) Patterns failure of deep beams (Subedi and Kubota,1986)

1.3 Deep and Simple Beams: A comparison

According to design proposition, the differences between simple and deep beams are as follows:

1- Two-Dimensional Action, the simple beams have a one-dimensional action, while deep beams have a two-dimensional action due to their dimensions.

2- Plane section is not a remaining plane in the deep beam design.

3- The shear deformations are neglected in simple beams, but they cannot be neglected at deep beams. The distribution of stresses is nonlinear even in the elastic stage as well as the distribution of shear stresses at ultimate limit state is not of parabolic shape.

1.4 Reactive Powder Concrete

Reactive powder concrete (RPC) is a distinct type of concrete with superior mechanical properties and excellent durability. It was first developed in the 1990s by the Bouygues' Laboratory in France for the purpose of obtaining superior properties such as high strength and durability **(Yao, and Zhou, 2005)**. Defects such as small micro-cracks and interior voids should be minimized. RPC can be developed through the technique of enhancing microstructural of the cementitious materials. Both Cheyrezy and Richard referred to a set of key principles for developing RPC **(Richard, and Cheyrezy, 1995):**

1- Exclude coarse aggregates to enhance the homogeny.

2- Utilize silica fume as it possesses the pozzolanic characteristics.

3 - Increase the density by improving the granular mix.

4- Utilize superplasticizer to reduce the water-cement ratio to obtain the required workability.

5- Apply pressure during casting.

6- Employ fibers to improve ductility.

7- Post-set heat-treatment to improve the microstructure.

RPC has unique features that make it an interesting subject for researchers. The Sherbrooke pedestrian/bikeway bridge which was created in Canada in July 1997, was the first practical application of RPC technology **(Blais, and Counture, 1999),** as shown plate (2.1).

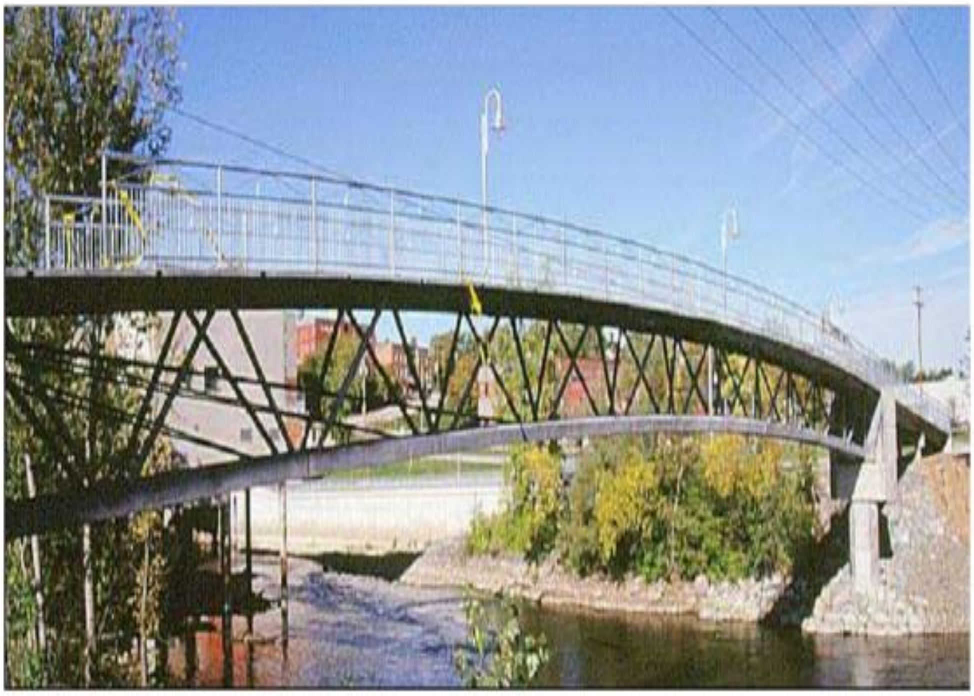

Plate (1.2) Sherbrooke bridge, Quebec, Canada

The outstanding mechanical properties of RPC such as high strength, excellent durability, superior resistance to abrasion and corrosion, and limited shrinkage make it beneficial as following **(O'Neiland Dowd, 1995):**

1- Enable creating concrete members with smaller cross-sections, resulting in a reduction in the dead loads and increase in the internal area.
2- RPC provides improved seismic performance due to lightweight of RPC members
3- RPC can be used in panels and structures exposed to explosions because of its high capacity to absorb energy.
4- It is also used in places where the gases and fluids cannot be transported and penetrated due to the non-interconnection and extremely low porosity.
5- It provides longer life for factory floors and bridge decks due to the high resistance to abrasion.
6- RPC structures require low maintenance in their service life.
7- It is used in pre-stressed members because RPC has very low shrinkage and creep.
8- RPC has high shear strength, eliminating the need for complementary shearing and other auxiliary reinforcing bars as compared to normal concrete.
9- RPC is easy to use in very thin precast structures, concrete members that have a large amount of reinforcement, complex members, and various structural sections that is because RPC possesses casting ease and good liquidity.
10- Economic benefits of reducing the cost of labor and reduce the supplementary reinforcing steel and ease the formation of various cross-sections of the members **(Dauriac, 1997).**

11- Provides self-healing under cracking conditions due to high cement content in RPC as it provides a large amount of unhydrated cement **(U.S. Department of Transportation, 2005).**

1.5 Ingredients of RPC

1- Cement:

The content of cement used in the RPC mixture has a significant role in its performance due to the high content of cement (from 900 to 1000 kg / m^3).

2- Fine Sand:

Fine Sand, whose granules are less than 600 micrometers, is used in RPC mixes instead of coarse aggregates in order to obtain more homogenous materials, as well as to increase the density of the RPC paste, which increases RPC strength and improves the durability.

3- Silica Fume:

Silica fume is an ultrafine powder of a pozzolanic nature collected as a by-product of the production of silicon and ferrosilicon alloys. The size of particles of silica fume is smaller than the size of cement particles by hundreds of times. Thus, silica fume fills in the cement paste matrix resulting in a lower content of voids, which makes RPC denser, as shown in Figure 1.2 **(Burke, 2008).**

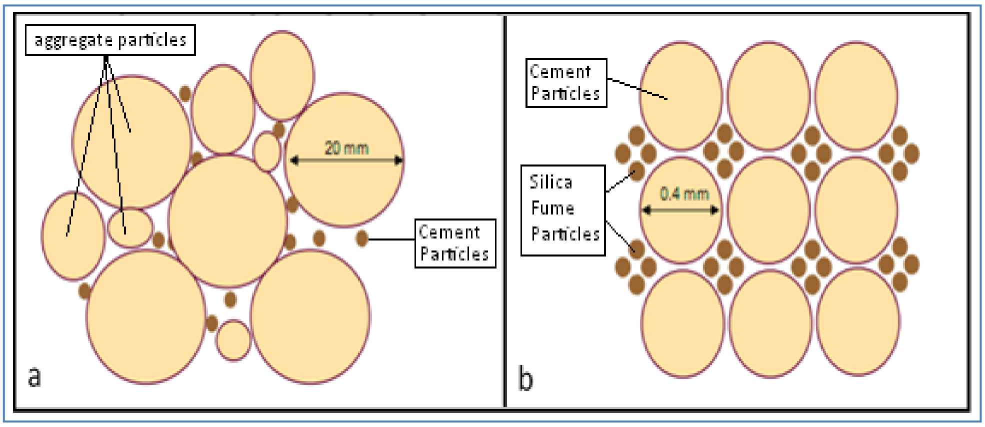

Figure (1.2) Particle of material in (a) normal strength concrete and (b) UHPC **(Burke, 2008).**

4- Fibers:

The addition of fibers to RPC can improve the tensile cracking resistance, ductility, and energy absorption capacity, post-cracking strength **(Wille et. al, 2011).** There are many types of fibers that can be used in RPC such as steel, carbon, polypropylene and other types of fibers.

5- Superplasticizer:

Superplasticizers are chemical materials used as admixtures to reduce the water to cement ratio to keep an acceptable workability **(Ramachandran, 1995).** There are many types of superplasticizers that are used in RPC such as GLENIUM® 51, GLENIUM54, Structuro335, Structuro480, Sika Visco Crete PC-20, Sikament®-163N ،PC200, and other materials.

1.6 Concept of Hybrid Concrete Members

Bernard et. al, (1998), explained that structural elements, which consist of the addition of a new concrete layer to an old concrete layer, is a structural member of a hybrid and is often designed to strengthen or repair structural elements.

In Hybrid layered systems, if the cross section consists of more than one layer of different material, the section element is defined as a hybrid.

Strength, workability, durability, cost and availability of important structural material advantages, it is difficult to find a structural material that has all these advantages to the required level. For the best performance of the structural member, more than one structural material is used in the same structural member taking into account the full utilization of the characteristics of the materials involved in its construction. This type is hybrid structural member **(Yam, 1981).** However, with the development of construction engineering technology, the structural member can be a hybrid by using two or more different layers of concrete in the same cross-section of the structural member so that each layer is used to obtain its better advantage. In this study, the deep beam is defined as a hybrid deep beam by containing two different layers, the first one is normal concrete and the other layer is RPC.

1.7 Objective of the Present Work

The objectives of the current study can be divided into the following:

1- Experimental investigation of hybrid deep beams behavior with RPC and normal strength concrete, in terms of the variables of; a/h, thickness and the location of the RPC layer in the compression zone or tension zone. Then, compare it with the normal deep beam.

2- Use the finite element method (ANSYS (version 17.2)) to simulate hybrid deep beams and study many parametric studies which effect on the behavior of hybrid deep beams.

1.8 Layout of Thesis

The current thesis includes six chapters. **Chapter one** provides a general information about deep beams and their differences from simple beams, with an overview of the (RPC), with a clarification of the concept of hybrid concrete elements, and presents the main objectives of the current study. **Chapter two** reviews most of the previous studies conducted in relation to this study in addition to a summary of the conclusions of these studies. **Chapter three** presents the practical program, details of the samples, characteristics of the materials and testing procedures. **Chapter four** presents and discusses the results obtained from the examination of the test samples. **Chapter five** deals with the finite element program (ANSYS) and the new cases that have been added to the program. **Chapter six** indicates a synopsis of conclusions of the current work and recommendations for the future works.

Chapter Two

2

LITERATURE REVIEW

CHAPTER TWO

LITERATURE REVIEW

2.1 Introduction

The technique of reinforced concrete (RC) members made of more than one type of concrete has good economic and environmental benefits. The published research on the behavior of concrete deep beams made of a homogeneous section (one type of concrete such as normal concrete, reactive powder concrete (RPC), etc.) or hybrid section (consisting of more than one class of different concrete properties) with a summary of these studies are presented through this chapter.

2.2 Behavior of RC Deep Beams

Many experimental studies had been conducted on the behavior of concrete deep beams according to the characteristics of the member (one type of concrete for all parts of the member or more). Some that related to the current study were as follow:

2.2.1 Homogeneous Section of RC Deep Beams

2.2.1.1 Normal Concrete Deep Beams

In (1965) De Paiva and Siess tested nineteen simply supported deep beams under the effect of two-point loads. All beams had a constant length of 24in, and cross-section dimensions were (9×3) in or (7×4) in. To study the effect of the longitudinal reinforcing steel ratio, the web reinforcement ratio, the concrete strength, the length-depth ratios, and the web reinforcement mode (vertical or inclined stirrups) on the behavior of the deep beams. The experimental results showed that ultimate load of the beam was increased and the mode of failure changed from flexural to shear by increasing the percentage of the longitudinal reinforcing steel. The increase in the concrete strength had no significant effect on the ultimate strength of beams failing in flexure. As well as, the formation of inclined cracks was not affected by the web reinforcement, and the web reinforcement had a weak effect on the ultimate strength of the beams.

Ramakrishnan and Ananthanarayana (1968), studied the effect of diagonal cracks on the ultimate shear loading of deep beams according to span to depth ratio of (0.94-2.1). The loading type used was uniformly distributed, two points concentrated loading and centrally concentrated loading. These beams were divided into the 3 groups according to the shape of the failure, first group failed in shear, the second group in flexure-shear while the third in flexure. The sudden fracture of the deep beam along the line connecting the loading point and the support was a shear failure, which was described as the failure of the diagonal tensile; in uniformly load the failure line was connecting between the support and the point that located under the uniform load near the one-third of the span. The failure resulting from the crushing of the concrete confined between the two parallel inclined cracks connecting the loading point and support was the diagonal compression failure. The splitting of the compression zone was the third type of failure that occurred by a vertical fracture in the compression zone. The sudden formation of the diagonal tension cracks, that causing the fall of the deep beam was the flexural shear mode. Thus, the mode of failure for these beams was a shear failure due to diagonal tension

(Manuel et al. 1971) investigated the effect of both the shear span to depth ratio (a/h) and the span to depth ratio on the behavior of concrete deep beams. The ultimate shear and mode of failure were more affected by (a/h), while it was insignificant by the span to depth ratio.

In (1982) fifty-two simply supported deep beams under the effect of two-point loads were tested by **Smith and Vantsiotis**. All beams had constant cross-section dimensions of (102×356) mm, the ratio of longitudinal reinforcing steel to tensile 1.94% and to compression 0.1%. The objective was to study the influence of horizontal web reinforcement amounts (0.23 – 0.91) %, amounts of vertical web reinforcement (0.18 – 1.25) %, and shear span / effective depth ratio (0.77, 1.01, 1.34, and 2.01) on the behavior of deep beams. The experimental results showed that the web reinforcement moderately affected the ultimate load of the deep beams but it did not affect the formation of cracking. The contribution of the stirrup (web reinforcement) of the ultimate shear strength did not exceed the calculated value of the equation $1/3\sqrt{f'_c}$ bd. The horizontal web reinforcement had insignificant effect on the ultimate shear strength, while its effect was clearer for the (a/h) less than one. The ultimate load capacity increased with increasing concrete compressive strength but decreased with an increase in shear span to effective depth ratio.

In (2001) Jung-Keun Oh and Sung-Woo Shin studied fifty-three simply supported deep beams under the effect of the concentrated two-point load, as shown in Figure (2.1). Different variables were covered, compressive strength of concrete (f'_c) (23 to 74) MPa, quantity of vertical web reinforcement (0 – 0.34) %, quantity of horizontal web reinforcement (0 – 0.94) %, effective span to depth ratio (3 – 5), and (a/h) (0.5 – 2). The tests indicated that the (a/h) controlled the ultimate shear failure mode with regardless of the (f'_c). For a low (a/h), the failure models produced from concrete with high compressive strength or normal compressive strength are abruptly and without warning. At low (a/h) and high (f'_c), the horizontal web reinforcement has a little effect to the ultimate load.

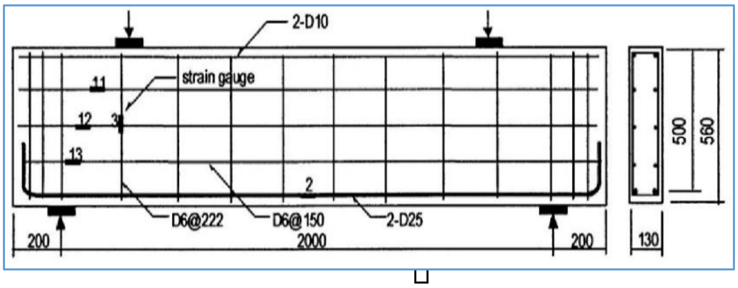

Figure (2.1) Details of deep beams adopted by Oh and Shin

(Salamy et. al, 2005) tested nineteen simply supported deep beams under the effect of the concentrated two-point load. The objective of this study to simulation abilities using the finite elements through the analytical results to estimate the behavior of deep beams for each of the load failure, pattern failure, and the spread of cracking, as well as to make a comparison with experimental results. Considered variables were:

1 - Ratio of shear span to effective depth (0.5, 1, and 1.5)

2 - The effective depth of the deep beam (400, 600, 800,1000, 1200, and 1400) mm

3 - Lateral reinforcement ratio varies by 0.0%, 0.4% and 0.8% in shear span.

The results showed a reliability of the analytical results compared to the results obtained from the experiments. The simulation ability can be used with the finite elements to estimate the behavior of the deep beams in order to reduce the time taken in the experimental work and reduce the cost.

The general behavior of tested beams investigated by **(Abolfazl et. al, 2011).** Observations made on mid-span and loading point deflections, cracks form, failure modes, and shear strengths. Based on test results, the shear capacity of beams its more affected by vertical and horizontal web reinforcement, as well as, the orthogonal shear reinforcement when placed perpendicular to the diagonal crack axis it is more active. The ultimate shear strength of deep beam improved by concentrated the shear reinforcement in the middle of shear span. The ultimate strengths predicted by ACI code were unsafe or scattered when compared with experimental results. The performed investigations deduced that ACI code provisions need to be revised.

(Londhe, 2011) tested twenty-seven simply supported deep beams under the effect of the concentrated two-point load. The experimental results indicated that the load transfer capacity of transfer (deep) beam increased significantly with distributed longitudinal reinforcement. The vertical shear reinforcement changed the failure from brittle mode to ductile mode. The vertical shear reinforcement more effect than horizontal reinforcement on the shear capacity. The shear capacity and failure pattern of the transfer beam were more affected by orthogonal web reinforcement.

In (2012) Nabeel studied the behavior of RC deep beams with Porcelanite lightweight aggregate. The studied parameters were the (a/h), (f'_c), and vertical and horizontal web reinforcement. All specimens had simply supported under the effect of the concentrated load at two-points and its dimensions were (150 × 400 × 1400) mm. The experimental results indicated that the ultimate load increased but the vertical midspan deflection decreased with increasing of the compressive strength of concrete. Also the vertical midspan deflection decreased but the ultimate load increased with decreasing of the (a/h), the ultimate load of specimens affected by the horizontal web reinforcement less than the vertical web reinforcement. The good correlation between the experimental results and the nonlinear finite element analysis results by using the ANSYS 14 program was found. In addition, the maximum shear capacity calculated by the STM (Strut-Tie Model) based on ACI 318M-11 code was less than the experimental strength for the Porcelanite RC deep beams.

Under the central point load, five simply supported deep beams were investigated by **(Pandurang and Girish, 2012).** A comparison between the analytical and experimental shear capacities of beams was carried out. It was concluded from that; a load of failure increased when the shear span to depth ratio was reduced, the shape of failure was shear where the shear span to depth ratio was less than or equal to two while others failed in flexure. The experimental results showed higher values than the analytical one for all failure loads.

In (2014) Jasim Al-Khafaji et. al, investigated eight simply supported self-compacting concrete deep beams under the effect of two-point concentrated load. Dimensions of this specimens were (100×330×1050) mm. The goal of the research was to study the shear behavior for such type of beams. The parameters considered were the (f′c), (a/d), and steel fiber volumetric ratio. Experimental results indicated that the cracking strengths and ultimate shear strengths increased about (28.6 and 23.3) %, respectively, with decreased (a/h), the cracking strengths and ultimate shear strengths increased about (11.7 and 38.8) %, respectively, with increased (f′c), the ultimate shear strengths increased about (10.1) % with increased the steel fiber ratio.

(Amornpinnyo & Teerawong, 2014) investigated the effect of horizontal to vertical reinforcements ratio, and (a/h) on the shear behavior of the RC deep beams. The test variables including the (a/h) ratios were between 1.5 to 2, and horizontal to vertical reinforcements ratio (1, 3.11, and 0.32). The conclusions were as follows:

1-Horizontal to vertical reinforcements ratio did not affect the ultimate load capacity of deep beams that had the same (a/h).

2- Horizontal to vertical reinforcement changing from less to more in deep beams with a/d ratio of 1.5 effects the failure modes from shear compression failure to diagonal compression failure.

Also, the ultimate load capacity calculated by used the ACI 318-11 was less than experimental results.

(Suresh, and Kulkarni, 2016), investigate eighteen RC deep beams of dimensions (150 × 350 × 700) mm were tested under effect of the concentrated two-point loads. The aim of this study was to study the behavior of reinforcement concrete deep beams when changing a percentage of tension reinforcement and (f′c) experimentally and compare them with the numerical results used in the ANSYS- 14.5 programs, which is one of the finite element programs. The experimental and numerical results showed that the first cracking and ultimate loads increased with the increase of the (f′c) and the tension reinforcement. The (f′c) increased the shear strength and moment capacity of the deep beams. The analytical results hold good with the experimental results, as well as the crack patterns were similar between FEA and experimental result.

(Ismail, 2016) tested twenty-four simply supported concrete deep beams under effect of the two-point concentrated load. All samples were divided into two groups. All samples of the first group have the same dimensions (100 × 400 × 1800) mm and the same percentage of longitudinal reinforcement as shown in figure (2.2). For the second group, all samples have the shear span to depth ratio 1.67 and the percentage of longitudinal reinforcement 1.4%, while geometric samples were different as shown in figure (2.3). The aim of this group was to study the influence of size without web reinforcement. The objective of this study was to know the effect of the shear span to depth ratio (0.91, 1.29, and 1.67), concrete strength, horizontal shear reinforcement (0 - 0.215) %, stirrups (0 - 1.26) %, and member depth, on the behavior and shear strength of the RC deep beams. The conclusions of the work were: The arch action which was the mechanism of shear transfer in the RC deep beams was affected by the change of the (a/h), thus, this ratio controlled the shear capacity and the behavior of RC deep beams. In RC deep beams the load was transferred to the support by arch action and for this reason, the strength of the compression of the concrete effected the ultimate shear capacity and the general behavior of the reinforcement concrete deep beams. The analysis showed that the shear strength of the RC deep beams increased approximately 20% when using the minimum amount of shear reinforcement but the capacity of deep beams did not improv with more increase of the shear reinforcement.

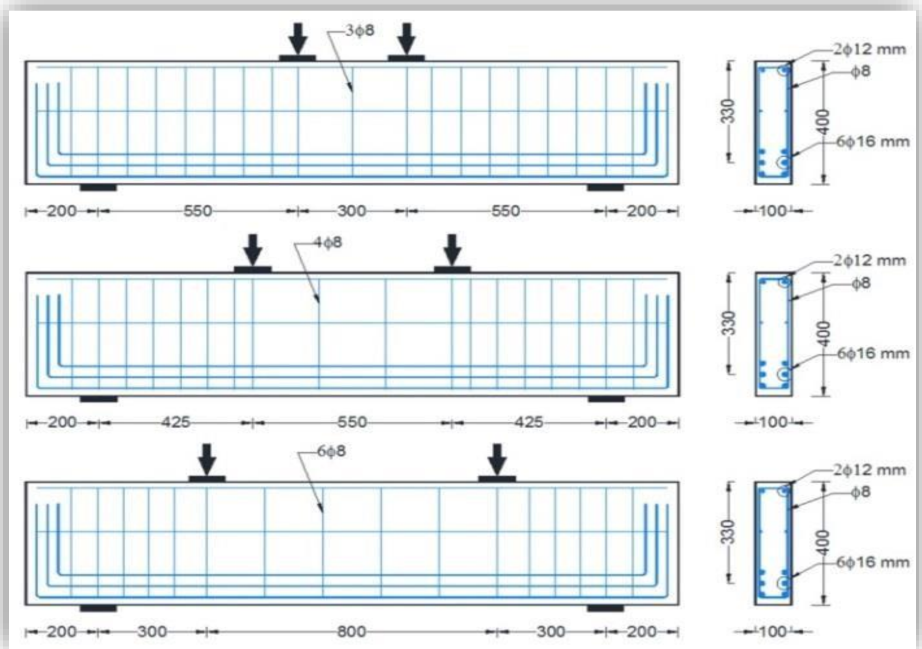

Figure (2.2) Details of the deep beams in the first group (Ismail, 2016)

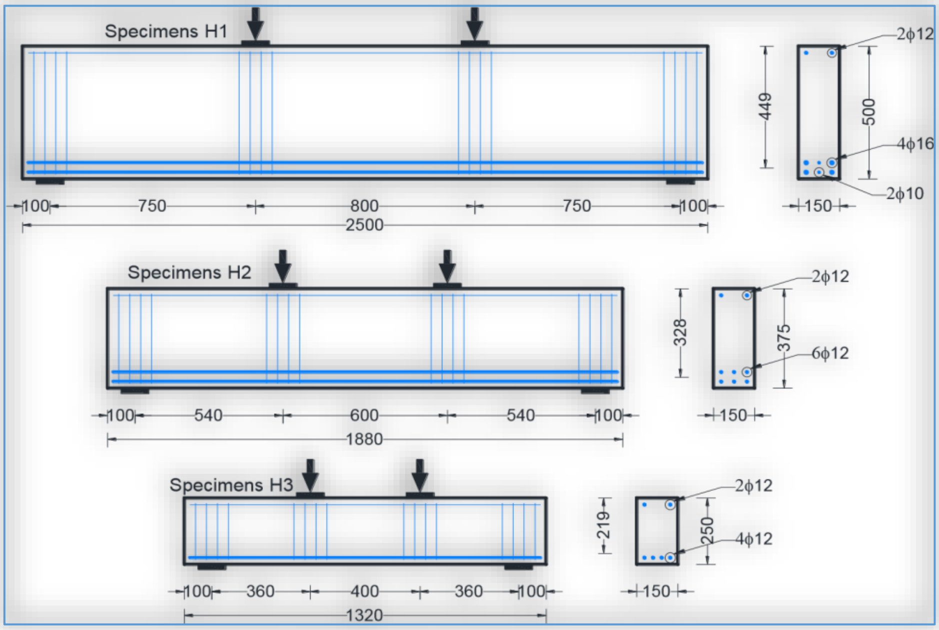

Figure (2.3) Details of the deep beams in the second group (Ismail, 2016)

2.2.1.2 High Strength Concrete Deep Beams

(Shengbing & Lihua, 2012) examined eighteen simply supported hybrid fiber reinforced high-performance concrete deep beams under two-point concentrated load, with the same dimensions (150×500×1040) mm, percentage longitudinal reinforcement (1.356 %), (a/h=1), and span to depth ratio (1.6). The aim of the research was to investigate the shear strength and diagonal cracking strength of hybrid fiber reinforced high-performance concrete deep beams. The research aimed to study the effect of the volume fraction of steel fiber and polypropylene fiber, the shape and aspect ratio of the steel fiber, the addition of the effect of the vertical and horizontal web reinforcement on the diagonal cracking strength and the shear strength of the hybrid fiber reinforced high-performance concrete deep beams. The experimental results showed that the hybrid fiber improved the shear strength and the diagonal cracking strength of the hybrid fiber deep beams. The diagonal cracking strength increased about 83.3% when using together (0.165 and 1) % of polypropylene fiber and steel fiber, respectively. The diagonal cracking strength more influenced by increasing the volume fraction of polypropylene fiber. However, the effect of the polypropylene fiber on the shear strength was less, also the increase in shear strength was 35.2% when using 1.0% of the steel fiber and 0.165% of the propylene fiber with web reinforcement.

(Omar & Msheer, 2013) tested fifteen simply supported deep beams without stirrups under two-points loading. The research aimed to investigate the shear strength and behavior of Ultra-high-performance fiber reinforced concrete deep beams without stirrup. Considered variables were; the compressive strength of concrete, the shear span to depth ratio (a/d) and overall depth of the beam (h=180, 240 and 300 mm), while the width of all beams was (120 mm). The experimental results showed, by increasing the compressive strength of concrete from 42 to 63.75 then to 134.5, the diagonal cracking load increased by 31% and 150% respectively and increased the failure load by about 44% and 150% respectively. (a/d) has high significant effect on failure load, it can be seen that by increasing (a/d) ratio from 1 to

1.5 then to 2, lead to decreasing the failure load by 30% and 150% respectively.

(Hani, et al, 2013), tested seven simply supported reactive powder concrete deep beams under two-points concentrated loading. All test samples have the same amount of longitudinal reinforcement (2.44) % and dimensions of (110×300×1400) mm. From the experimental results in this investigation on the behavior of reactive powder concrete deep beams, the (a/h) greatly influenced the behavior of the reactive powder concrete deep beam and determined the mode of the failure. The shear strength and cracking load increased with the decreasing of the (a/d). The deflection decreased and thus the model was stiffer with the decreasing of the (a/d). As the silica fume increases, the cracking load and shear strength increases and model was stiffer.

(Bashandy et. al, 2014) studied the effect of cement content on the behavior of load deflection of the beams produced from the reactive powder concrete, using two types of reinforcement and steel fiber. The experimental conclusion indicated that the ultimate load and the cracking load were significantly affected by the cement content and the steel fiber content of these types of beams. The shear reinforcement had a greater impact on the behavior of these beams in case steel fiber was not used. The use of a non-linear finite element computer program was also found to be effective for these types of beams.

Sixteen simply supported concrete deep beams where tested by **(Sinan, 2016)** without web reinforcement. The shear strength and behavior of these beams under two-point loading were investigated. The variables considered were the compressive strength of concrete (f′c) (40–120 MPa), shear span-to-depth ratio (1, 1.5, 2, 2.5, and 3), and the flexural steel bar ratio (1.35%, 2.40%, 3.76%, and 6.108%). Experimental results showed that increasing of concrete compressive strength and flexural steel bar ratio increased the ultimate shear capacity. By contrast, increasing (a/h) and (span/depth) reduced ultimate shear capacity.

2.2.2 Hybrid Reinforced Concrete Deep Beams

(Hassan, 2015) investigated twelve simply supported deep beams under the effect of two-point concentrated loads, all deep beams having dimensions of (100×330×1050) mm. Three of these deep beams were made of normal concrete (CC), three with ultra-high-performance concrete (UHPC) and six as hybrid deep beams. Ultra-high-performance concrete was used in the top layer and normal concrete in the bottom layer of hybrid deep beams. The deep beams tested variables included the thickness of the ultra-high performance concrete layer and steel fibers volumetric ratio from 0% to 1%. Experimental results generally showed that stiffer load-deflection behavior was obtained with the increase of ultra-high performance concrete layer thickness and steel fibers volumetric ratio for hybrid beams with ultra-high-performance concrete in compression. The presence of 0.5 % of steel fibers increases the ultimate load by a range of 6.75 % to 44.23 % (the average of increase is 25.49 %). While using of 1 % of steel fibers increases the ultimate load with a range of 25.67% to 62.98 % (the average of increase is 44.33 %). The enhancement is larger in UHPC beams when compared with CC beams. The predicted hybrid deep beam strength using the ACI strut and tie model are underestimated with comparison in the experimental values by up to about 28%.

(Ammar & Maha, 2015), tested nine simply supported deep beams under the effect of the concentrated two-point loads experimentally. All the deep beams had dimensions (100×400×1400) mm. Details of both the hybrid section and the loading are shown in Figure (2.4). The aim of the research was to investigate the overall shear behavior of hybrid RC deep beams made from two different types of concrete strength, normal strength concrete (NSC) and high strength concrete (HSC). The test variables included the thickness of the high strength concrete layer, the method of casting concrete layers (at the same time or at different times), and the effect of the presence of web reinforcement. The experimental test results obtained from the adopted hybridization technique of (HSC) and (NSC) have shown that for beams made from (HSC) (about 45MPa) with a layer in compression zone of thickness (25 - 50) % of total beam depth, the ultimate shear strength was increased about (11.2 - 19.5) % for beams without web reinforcement and (16.75 - 22.25) % for beams with minimum web reinforcement. It has also shown that, the first cracking load was increased about (32.8 - 48) % and (43.4 - 57.9) % for beams without and with web reinforcement, respectively.

The hybrid concrete beams that cast monolithically, have exhibited an increase in ductility about (13.3- 22.6) % and (17.3 - 26.3) % for specimens without and with web reinforcement, respectively.

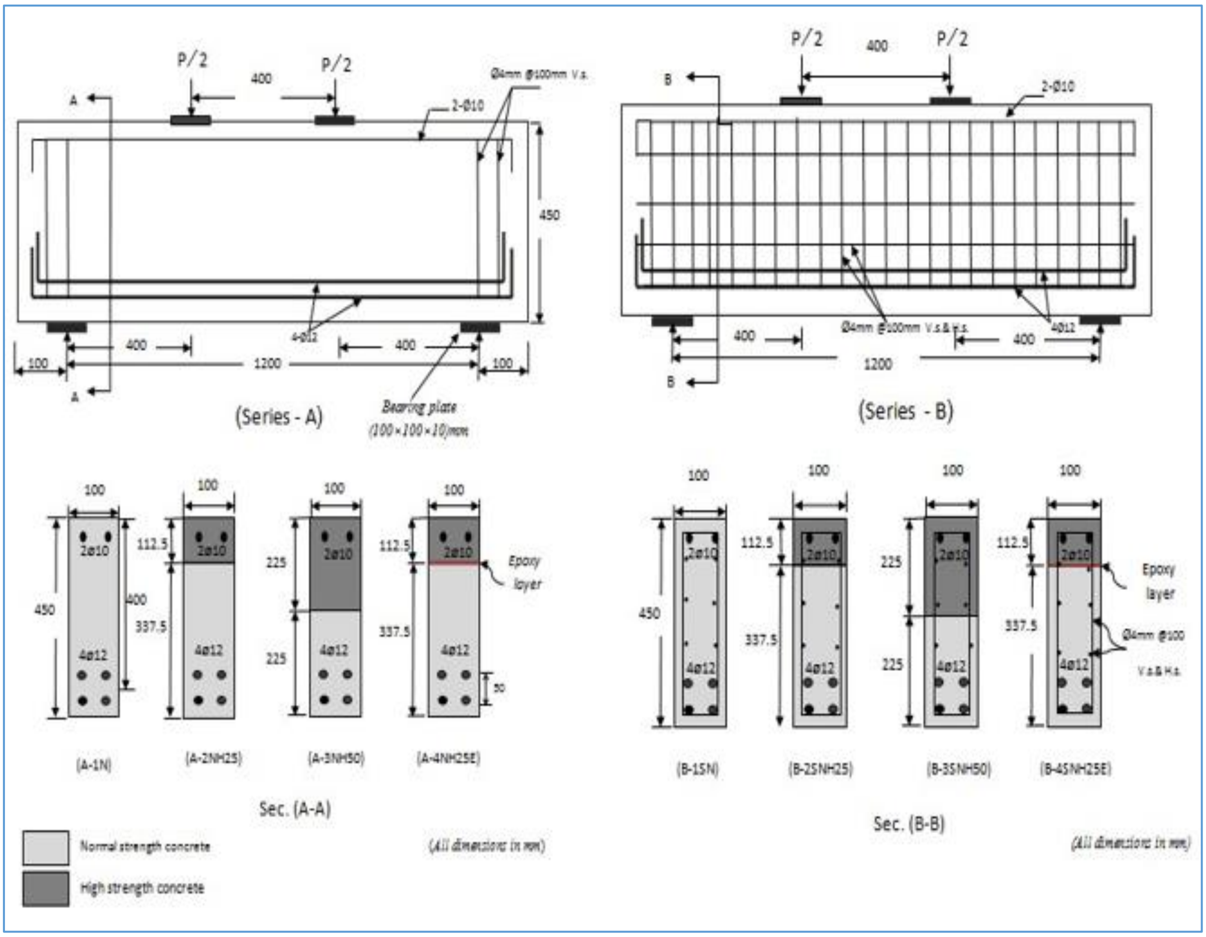

Figure (2.4) Loading and specimen's details (Ammar & Maha).

(Sawsan & Ghsoon, 2016), examined twelve simply supported hybrid deep beams under the effect of concentrated two-point loads. All tested specimens have same dimensions as shown in figure (2.5). Bearing plates were used below the two loading points and above the support to prevent concrete crushing at loading. The aim of the research was to study the behavior of hybrid deep beams (adding steel fiber to the shear spans) experimentally and theoretically according to the following variables, type of loading (monotonic or repeated), type of deep beam (hybrid or non-hybrid), quantity of steel fibers (0, 1, and 2) %, and quantity of web reinforcement (0, 0.003, and 0.004). Refer to the experimentally results concluded that;

1- Under monotonic loading system. the ultimate load increased by 29.73% and 50.81% when the steel fiber content 1% and 2% located at a shear span, respectively compared with a reference beam of no steel fiber.
2- The increase in web reinforcement ratios from 0.0 to 0.003 and 0.004 under monotonic loading system leads to increase in the ultimate load are 34.08% and 42.46%, respectively
3- The experimental results showed that the ultimate load was greater than the expected ultimate load using the ACI 318M-11 Code.
4- Under monotonic loading, the ultimate load of the deep beams containing 1% of steel fiber for all its parts was 5.21% greater than the ultimate load of the hybrid deep beams containing the steel fiber in the shear zone, this increase was not important.
5- The percentages decrease between the hybrid deep beams without web reinforcement when subjected to monotonic and repeated loading is of negligible value (1.96%).

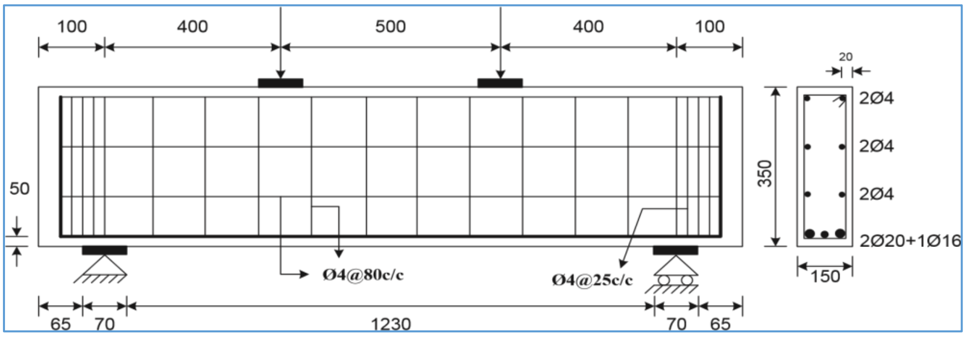

Figure (2.5) Details of Beams (Hassan & Faroun).

2.3 Summary of Literature

The following are the observations drawn from previous studies that dealt with the behavior of RC deep beams with a homogeneous section (containing one type of concrete) and hybrid RC deep beams (hybrid cross-section):

1- The behavior of the RC deep beams is affected by a number of parameters, including, (a/h), (f'c), longitudinal reinforcement ratio, vertical and horizontal shear reinforcement ratios, clear span to depth ratio.

2- The shear span to depth ratio is one of the parameters that had a significant impact on the behavior of concrete deep beams and its effect is greater than the effect of the clear span to depth ratio.

3- The ultimate shear capacity of reinforced concrete deep beams increases with increasing concrete strength when the ratio of shear span to depth is low.

4- The addition of fiber improves the behavior of deep beams, increasing the shearing and diagonal cracking capacity.

5- Web reinforcement reduces the width of the crack but has no effect on the form of cracking. The vertical shear steel affects the shear capacity of the RC deep beam more than the horizontal shear steel.

Through a review of experimental studies and previous theoretical programs concerning the behavior of deep beams, it was found there is an important need to study the behavior of hybrid deep beams, because, it is considered as new a technique that needs to know more about its advantages. In addition, reactive powder concrete material is considered an expensive material and needs special attention during work, casting and curing. Therefore, the current study focused on the behavior of RC hybrid deep beams consisting of two different layers of concrete, one of which was the normal strength concrete and the other layer of reactive powder concrete. This was done in order to find the best ratio of the thickness of the reactive powder concrete layer to the total thickness of the deep beams, and also the best location of the reactive powder concrete layer in the deep beam in the compression zone or the tensile zone. These hybrid concrete deep beams may have good advantages and economic strength.

Chapter Three

3

EXPERIMENTAL PROGRAM

CHAPTER THREE

EXPERIMENTAL PROGRAM

3.1 Introduction

This chapter describes construction materials, properties of materials, details of test samples, testing procedure, tools and equipment used in the work, as well as experimental tests of control specimens.

3.2 Experimental Procedures

3.2.1 Depiction of the Samples

The experimental program includes a testing of all construction materials used in the current work, with casting and testing of control samples (cylinders and concrete cubes) and reference concrete deep beams.

The specifications of (**ACI–318R-14)** were adopted to design the deep beams in this work to ensure that the specimens fail in shear rather than flexure, as shown in Appendix A.

Eight samples in the experimental program were divided into four groups (A, B, C, and D). Group (A) had normal strength concrete (NSC). Group (B) had hybrid deep beam used two different layers (NSC and RPC) whereas the thickness of RPC layer in tension zone (25) % of total depth. Group (C) had hybrid deep beam used two different layers (NSC and RPC) whereas the thickness of RPC layer in compression zone (25) % of total depth. Group (D) had hybrid deep beam used two different layers (NSC and RPC) whereas the thickness of RPC layer in tension zone (41.6) % of total depth, Figure (3.1) shows the details of the concrete layers of the samples.

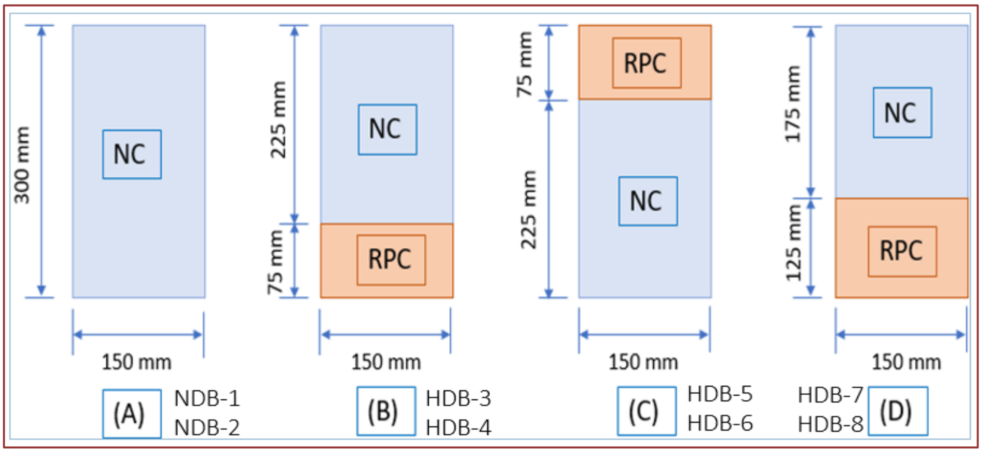

Figure (3.1) Thickness of RPC and NSC layers in all samples

The variables depended in this work included the thickness of RPC layer (25 and 41.7) % from total depth, the location of RPC layer (compression or tension region), and shear span to depth ratio (a/h= 2/3, and 1.25/3). All specimens of deep beams had the same; dimensions, vertical and horizontal shearing reinforcement, and longitudinal tension and compression reinforcement. Appellation and specifics of all tested beams are reported and presented in Table (3.1).

Table (3.1) Appellation and specifics of specimens

Groups	**Beam No.**	**Beam Appellation**	**a / h**	**Location RPC & total depth %**
(A) Normal Deep	A-1	NDB-1	2/3	without
	A-2	NDB-2	1.25/3	without
(B) Hybrid Deep	B-1	HDB-3	2/3	tension (25)
	B-1	HDB-4	2/3	tension (25)
(C) Hybrid Deep	C-1	HDB-5	2/3	compression (25)
	C-2	HDB-6	1.25/3	compression (25)

Table (3.1) Continue

Groups	Beam No.	Beam Appellation	a / h	Location RPC & total depth %
(D) Hybrid Deep	D-1	HDB-7	2/3	tension (41.7)
	D-2	HDB-8	1.25/3	tension (41.7)

3.2.2 Description of the Tested Beams

Eight simply supported RC deep beam models were tested with vertical and horizontal shear reinforcement having a total length (l=800mm), clear span (ln=600mm), cross-section (150×300) mm, with a/h=2/3 and 1.25/3 to ensure that tied-arch action of the deep beam would be developed. **(ACI-Code 318-14).**

All specimens tested under the two-point concentrated loads in the top edge, as detailed in Figure (3-2). Five (ø12mm) diameter of deformed bars were provided as longitudinal tension reinforcement in order to ensure shear failure to occur rather than flexure failure. Reinforcing bars (2ø12mm) were used as compressive bars to hold the stirrups and to prevent abrupt crushing failure of compression zone.

All beams were owned vertical and horizontal shear reinforcement (ø 6mm @50 mm c ⁄c). The concrete cover of 25 mm was from all sides, as shown in figure (3-2), and plate (3.1).

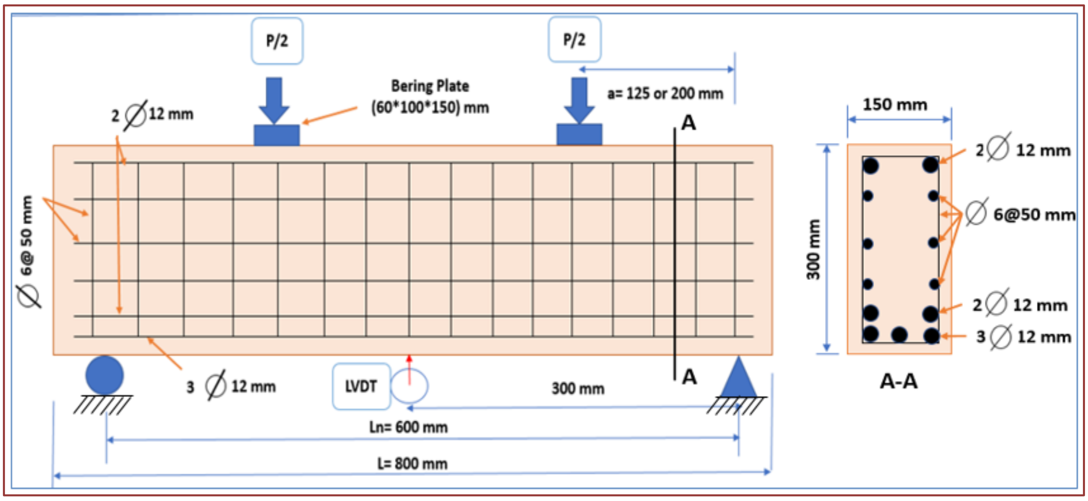

Figure (3.2) Loading and specimen's details

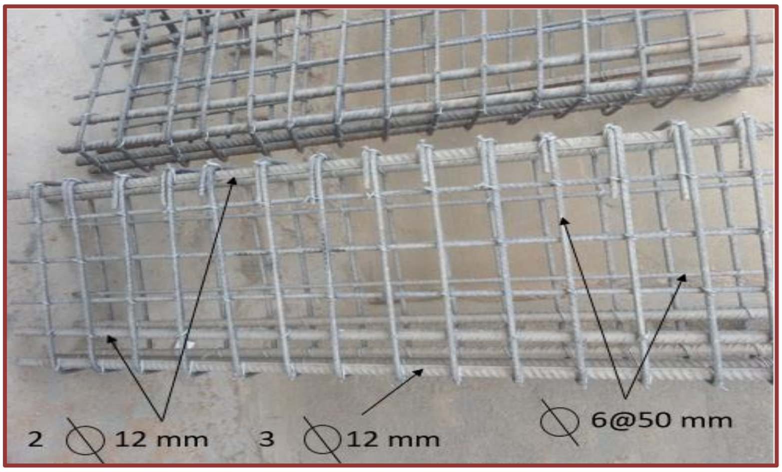

plate (3.1) Distribution of reinforcing steel.

3.3 Properties of Construction Materials

The American Society for Testing (**ASTM**), British Standards Institution (**BS**), and Iraqi Specification (**IQS**) were adopted to evaluate the properties of construction materials used in the current work. All tests of construction materials were made with the help of the concrete laboratory in the College of Engineering / University of Kerbala.

3.3.1 Cement

The resistant Portland cement (type-V), which was manufactured by the well-known industrial LAFARGE Company (LAFARGE - JESSER) in (Karbala / Iraq), was used in current study. The results of the chemical and physical testing of resistant Portland cement (type-V) are shown in Table

(3.2). Test results indicated that the cement specifications used in the current work are conform to the **(Iraqi specifications No.5/1984**)

Table (3.2) Cement test results

Compound (Oxide)	Laboratory results	Iraqi specifications No.5/1984
Silica (SiO_2%)	22.01	-----------
Alumina (Al_2O_3%)	3.41	-----------
Iron oxide (Fe_2O_3%)	4.22	-----------
Magnesia (MgO%)	2.9	≤ 5
Sulfate (SO_3%)	2.1	≤ 2.5 if $C_3A < 5\%$ ≤ 2.8 if $C_3A > 5\%$
Free Lime	1.008	------------
Fe_2O_3/ Al_2O_3	0.74	------------
Loss on ignition (L.O. I) %	2.6	≤ 4
Insoluble residue (I.R) %	0.86	≤ 1.5
Lime saturation factor (L.S.F)	0.85	(1.02) -- (0.66)
Tricalcium Silicate (C_3S%)	38.42	------------
Dicalcium Silicate (C_2S%)	34.11	------------
Tricalcium Aluminate (C_3A%)	1.89	≤ 3.5
Tetracacium aluminoferrite (C_4AF%)	12.84	-----
Physical Test		
Area of Specified surface m^2 /kg	240	Minimum 230
Setting time (min) **initial** **Final**	 98 309	 Minimum 45 Maximum 600
Fineness (Blaine) m^2/kg	368	Minimum 250
Compressive strength (MPa) **3 days** **7 days**	 17.5 28	 Minimum 15 Maximum 23

3.3.2 Fine Aggregate (Sand)

The sand used was washed and provided from the western region of Kerbala governorate (Al-Ekhaider zone). Sieve analysis results and physical properties of sand used in current work are as shown in Table (3.3). Test results are within the limits of the **(IQS. 45/1984)**

Table (3.3) Physical sand specification.

NO.	**Sieve size (mm)**	**Passing %**	
		Fine aggregate%	**Limit of IQS (45/1984), zone 2**
1	10	100	100
2	4.75	100	90-100
3	2.36	76	75-100
4	1.18	63	55-90
5	0.6	39	35-59
6	0.3	13	8-30
7	0.15	4	0-10
Passing 0.075 mm%		0.133	Max. 0.5
Sulfate test			
Sulfate content SO_3%		0.3	Max. 0.5

3.3.3 Very Fine Sand

In reactive powder concrete mixtures (RPC) used fine sand of maximum size not more than (600μm). This fine sand was isolated from the washed sand provided from the western region of Karbala governorate (Al-Ekhaider zone) by sieving, as shown in plate 3-2. Table (3.4) and Table (3.5) show the sieve analysis and the sulfate content for the very fine sand, respectively. The properties of the very fine sand used in the current study conform to the **(IQS. 45/1984).**

Table (3.4) Very fine sand particle size

Size of the Sieve Openings	**Total Passing**	**Limit of IQS (45/1984), zone 4**
10 mm	100 %	≥ 100
4.75 mm	100 %	95 - 100
2.36 mm	100 %	95 - 100
1.18 mm	100 %	95 - 100
0.60 mm	100 %	80 - 100
0.30 mm	47 %	15 - 50
0.15 mm	8 %	≤ 15

Table (3.5) Sulfate content for the very fine sand

Compound	**Laboratory results**	**Limit of IQS (45/1984)**
Sulfate test (SO3) %	0.3	≤ 0.5

Plate (3.2) Separated the washed sand

3.3.4 Coarse Aggregate (Gravel)

The crushed white gravel used was provided from the western region of Karbala governorate (Al-Ekhaider zone). Sieve analysis results and physical properties of the gravel used in current work are as shown in Table (3.6). Test results conform to **(IQS. 45/1984).**

Table (3.6) Properties of gravel.

No.	**Sieve size (mm)**	**Passing %**	
		Coarse aggregate	**IQS (45/1984) Limit of**
1	19	100	95-100
2	14	60	-
3	10	38	30-60
4	5	2	0-10
5	Clay %	1	≤ 2
Sulfate test			
	% of SO3	0.05	≤ 1

3.3.5 Properties of Reinforcing Steel

The original Ukrainian reinforcement bars of 12 mm and 6 mm diameter was used in the current study. Reinforcement bars diameter 12mm were used as the main longitudinal reinforcement in the compression and tensile zones. Reinforcement bars of 6 mm diameter were used as shear reinforcement the vertical and horizontal arm (stirrups).

All reinforcement bars were inspected in the laboratories of the College of Engineering at the University of Karbala, and the results were compiled according to the specifications **(ASTM A615M-05a)** and were identical to the limits of the above specification as shown in the table (3.7). Minimum elongation for small bars (6 mm) is 4.5 % according to **(ASTM A496-02)**.

Table (3.7) Properties of reinforcing steel

Diameter Bar (mm)	Actual Diameter Bar (mm)	Yield strength f_y (N/mm^2)	Tensile strength (N/mm^2)	Elongation %	Limit according ASTM A615M-05a		
					f_y (N/mm^2)	Tensile strength (N/mm^2)	Elongation %
6	5.622	510.4	540.5	7.3	420	620	4.5
12	11.89	14.3	636.2	706.8	420	620	9

3.3.6 Admixtures (Superplasticizer)

A Superplasticizer used throughout this work was "**Glenium 51**" with a nominal dosage of (0.5 to 2.5 liter per 100kg of cement) as recommended by the manufacturer. Glenium 51 conformed to **(ASTM C494, 1986) type A** and manufactured by **BASF FZE** Company in United Arab Emirates. Table (3.8) shows the properties of superplasticizer (**Glenium 51**) supplied by the manufacturer.

Table (3.8) Information of superplasticizer (Glenium 51)

Main action	Concrete Superplasticizer
Composition of a chemical mixture	Sulphonated Melamine and Naphthalene Formaldehyde condensates
Color	Light brown
Shape	Viscous liquid
Relative density @20°C	1.1 g/ml
pH	6.6
Viscosity	128µ 30 cps at 20 C^0
Transport	Not classified as dangerous
Labeling	No hazard label required
Chloride content	None

3.3.7 Water

The clean water supplied by the water circuit was used to mix all concrete mixtures as well as to cure the specimens. For concrete mixing, the water-cement ratios (w/c) for NC, and RPC were (0.42) and (0.25), respectively.

3.3.8 Silica Fume

Silica fume used in the current work was supplied by Sika Company and conformed to the **(ASTM C1240-04).** The size of the silica fume particles is very small and its size is about 1/100 of the cement particles size. Table (3.9) contains the chemical composition of silica fume and the specification of the **(ASTM C1240, 2004).**

Table (3.9) Chemical characteristics the silica fume *

Index Items	Oxide Content	Limits the (ASTM C 1240)
SiO_2(Silicon Dioxide) (%)	94.87	Not less than 85.0
Al_2O_3(Aluminum Oxide) (%)	1.18	-
Fe_2O_3 (Iron Oxide) (%)	0.09	-
CaO (Calcium Oxide) (%)	0.23	-
MgO (Magnesium Oxide) (%)	0.02	-
SO_3(Sulfate) (%)	0.25	-
K_2O (Potassium Oxide) (%)	0.48	-
Loss on Ignition (L.O.I) @ 975℃ (%)	2.88	Not more than 4.0
Moisture Content (H_2O) (%)	0.48	Not more than 3.0

*Supplied by the manufacturer.

3.3.9 Polypropylene Fiber

Polypropylene fibers are thermoplastics that produced from propylene gas. Polypropylene fibers are chemically inactive, alkaline resistant, safe, easy to use, cheap and available. It is added to the concrete to overcome the problem of micro-cracks that occur in the concrete as a result of the curing. Whereas these cracks are which spread rapidly when the load is applied, which causes the low tensile strength of concrete. The benefit of Polypropylene fibers is to control the cracks in cement compounds with increasing tensile strength, toughness, wear resistance, as well as to increase the flexural strength and reduces water permeability. In this study, polypropylene fiber of Sika company product was used. Specification for polypropylene fibers is shown in Table (3.10).

Table (3.10) Information on polypropylene fibers*

Properties	Remark
Melting Point	160^0 C
Absorption Water	Nil
Acid Resistance	High
Tensile Strength	300 – 400 N/mm^2
Fiber Diameter	18 microns – nominal
Specific Surface Area of Fibers	250 m^2 /kg
Alkali Resistance	100%
Fiber length	12 mm
Specific Gravity	0.91 g/cm^3
Modulus of Elasticity	~ 4000 N/mm^2
Volumetric ratio	0.01
Aspect ratio	660

*Supplied by the manufacturer.

3.4 Wood Mold Preparation

The smooth face block was used to make the molds for the deep beams specimens. It was cut and installed to have dimensions from inside of (150×300 × 800) mm, as shown in the plate (3.3).

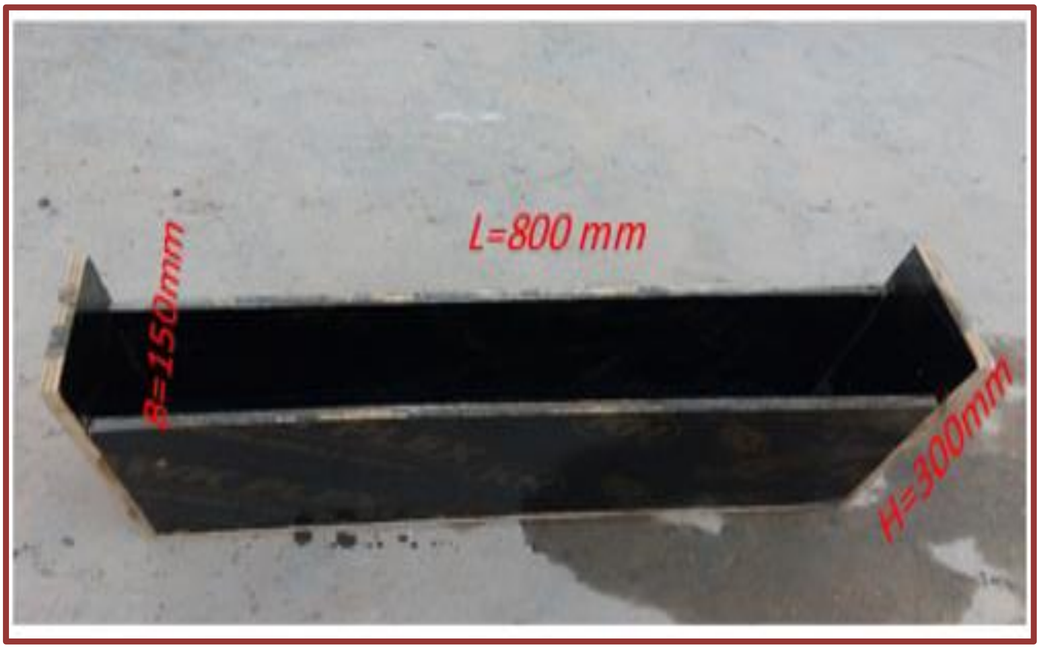

Plate (3.3) Wood mold preparation.

3.5 Properties of Concrete:

3.5.1 Concrete Mix Design:

3.5.1.1 Normal Strength Concrete (NSC)

Three trial concrete mixes were selected through this work with different weights of cement, sand, and gravel. Each was made with concrete cubes with dimensions of (10 x 10 x10) cm, and cylinders of (10 cm diameter, 20 cm height) to examine the compressive strength and the splitting tensile strength, respectively, to determine the weight ratio of the first construction materials adopted in this study. The compressive strength target was (26.4 N/mm^2) at 7 days, for this reason, the weight mixing ratios adopted were 1: 1.20: 1.40 cement, sand, and gravel, respectively, and water/cement is 0.42. Table 3.11 shows the mixing ratios of the trial mixtures.

Table (3.11) Properties of NSC mixes

No.	Water/cement ratio	Mix Design Ratio (By Weight) cement: sand: gravel	Compressive Strength (N/mm^2) 7-day	Tensile Strength (N/mm^2) 7-day
1	0.43	1:1.5:2	26.2	1.83
2	0.42	1:1.2:1.4	26.4	2.08
3	0.42	1:1.25:1.6	25	1.39

3.5.1.2 Reactive Powder Concrete (RPC)

Different trials of experimental mixes were made during the current work, with different ratios of weights for silica fume/cement, and cement content in the mix. Each was made with concrete cubes with dimensions of (5 x 5 x5) cm, and cylinders of (10 cm diameter, 20 cm height) to examine the compressive strength and the splitting tensile strength to determine the ratio of the weight of the materials (silica fume, very fine sand, cement, polypropylene fibers, and superplasticizer) which were for two mixes in this study. The mixing ratios shown in Table (3.12) were sufficient to give adequate operation and strength through the results of experimental mixtures, the mix 2 was selected.

Table (3.12) Properties of RPC Mixes

Parameter	Mix. 1	Mix. 2
Water/ binder (L/ m^3)	300	288
Cement (Kg/m3)	960	960
Very fine sand(kg/ m^3)	1000	1000
Water/ binder (L/ m^3)	300	288
Cement (Kg/m3)	960	960
Very fine sand(kg/ m^3)	1000	1000

Table (3.12) continue

Parameter	Mix. 1	Mix. 2
Water/ binder (L/ m^3)	300	288
Cement (Kg/m3)	960	960
Very fine sand(kg/ m^3)	1000	1000
Water/ binder (L/ m^3)	300	288
Cement (Kg/m3)	960	960
Very fine sand(kg/ m^3)	1000	1000
Silica fume (Kg/m3)	240	192
Superplasticizer (L / m^3)	24*	23.04*
Polypropylene Fiber (kg/ m^3)	9.6	9.6
Compressive Strength (N/mm^2) **7-day**	42.49	43.69
Tensile Strength (N/mm^2) **7-day**	4.67	4.81

* 2 Liter/ 100 kg binder (cement+silica fume)

3.5.2 Concrete Mix Preparation

The hybrid deep beams consist of two different layers of concrete, one of which is normal concrete (NSC) and the other is of reactive powder concrete (RPC). The mix properties for these types are as follows.

3.5.2.1 NSC Mix Preparation

The mixture of normal concrete was mixed by weight 1: 1.2: 1.4, of cement, sand, and gravel, respectively. The percentage of water in this mixture was 0.42 of the weight of the cement. The deep beams (Group A) were completely casted with this mix, as was the casting of the layer composed of normal concrete for hybrid deep beams (Groups B, C, and D).

This mixture was also used for casting the control samples (cylinders and cubes).

3.5.2.2 RPC Mixes Preparation

The reactive powder concrete (consisting of silica fume, cement, very fine sand, polypropylene fiber, Superplasticizer, and water) was used to cast the other layer into the hybrid deep beams (Groups B, C, and D) according to the quantities specified in the Table (3.12). This mixture was also used for casting the control samples (cylinders and cubes).

3.5.3 Mix Procedure

Cubes, cylinders and wooden molds for the deep beams were cleaned and coated with lubricating oil before casting. The first construction materials (cement: sand: gravel) were weighed and placed in special containers. The small rotary mechanical mixer of capacity of 0.1 m3 was used to mix the normal strength concrete to obtain the required homogeneity and workability. At the first, materials were mixed dry for four minutes by mechanical mixers, then, wet by adding water and mixing the mixture for two minutes to record a total mixing time of about six minutes.

All RPC mixes were implemented using the electric mixer. First, the silica fume was mixed with cement for a period of three minutes, to ensure homogeneity of the distribution of silica fume among the cement particles. Then add the very fine sand to the mixture of silica fume and cement and continue mixing for another three minutes to ensure that the sand atoms are distributed homogenously in the mixture. The superplasticizer was dissolved in water and mixed well to obtain a homogeneous mix. 50% of the polypropylene fiber was poured into the mixture (cement, fine sand and silica fume) and 80% of the water with superplasticizer was gradually added. Mixing continued for five minutes. To ensure well mixing for the all components of the mixture especially for the parts that do not reach the blender blades have been stopped mixing and continued by hand. Finally, add the remaining of the water with superplasticizer and the fiber to the mixture and re-mix using the mixer for five minutes to record a total mixing time of about eighteen minutes, as shown in Plate (3.4).

Plate (3.4) Mixing of reactive powder concrete.

3.5.4 Casting Procedure

3.5.4.1 Casting Procedure of Normal Deep Beams

After cleaning the internal surface of the wooden molds with a smooth face and coating it with a thin layer of lubricating oil, the reinforcement bars were placed in its location inside the mold to make a concrete cover of 25 mm around the reinforcement bars. All specimens were filled with the concrete layer of 75mm height. In order to obtain compressed and high-density concrete, an electric vibrator with a steel rod of 25 mm diameter was used to reduce the air voids after casting of each layer for 75 seconds. After completing the casting, the upper face of the deep beam was leveled off and smoothed by using a steel trowel. All control models consisted of three concrete cubes (100 × 100× 100) mm and three cylinders (100 × 200) mm for each casting stage with layers of (50 to 70) mm thickness and a steel rod was used to reduce the air voids after casting of each layer. The final layer was coated with a steel trowel. All samples and control samples were covered with polyethylene sheets to prevent moisture loss for 24 hours after casting, as shown in Plate (3.5).

Plate (3.5) Compact the concrete using an electric vibrator.

3.5.4.2 Casting Procedure of Hybrid Deep Beams

The hybrid deep beams are made from two types of concrete mixes. The NC and RPC layers were cast directly (at the same time) for all hybrid deep beams. After cleaning the internal surface of the wooden molds with a smooth face and coating a thin layer of lubricating oil, the reinforcement bars were placed in the location inside the mold to make a concrete cover of 25 mm around the reinforcement bars. Each type of concrete was cast on two layers, each layer on two stages with 1.5 minutes compaction by an electric vibrator having a metal rod with a diameter of 25 mm to minimize the air voids and to get well-compacted concrete for each stage. Then, the upper face of the lower layer was settled and made rough before placing the other layer, the top face of the upper layer was leveled off and finished with a steel trowel. All control models consisted of three concrete cubes (100 × 100 ×100) mm and three cylinders (100 × 200) mm for NSC, and three cubes (50 ×50 × 50) mm and three cylinders (100 × 200) mm for RPC, for each casting stage with layers of 5 to 7 cm thickness and coated by the steel bar for each layer, the final layer coated by an iron trowel. All samples and control samples were covered with polyethylene sheets to prevent moisture loss for 24 hours after casting.

3.5.5 Curing Procedure

For NSC, after 24 hours of casting, deep beams and control specimens were taken out of the molds and placed in a water tank at room temperature not less than 20 ° C for 28 days. The water of curing was replaced every (3 to 4) day.

For RPC, after 24 hours of casting, hybrid deep beams and control specimens were taken out of the molds and placed in a water tank at a temperature not less than 60 ° C for 3 days. After 72 hours, the temperature of the treated water was reduced gradually to 20 ° C to continue processing for 28 days from the date of casting. The water of curing was replaced every (3 to 4) day, as shown in Plate (3.6).

Plate (3.6) Sample in the water tank.

3.6 Test Procedure

The test included testing control specimens and deep beams with both normal and hybrid.

3.6.1 Testing of Control Specimens

3.6.1.1 Compression Test

The compressive strength of the concrete cubes was tested with a dimension of (100×100×100) mm for the (NSC) and (50×50×50) mm for the (RPC) at age 28 days after casting according to **(BS 1881-116).** The digital test machine ELE with a capacity of 2000 kN was used to load each cube continuously up to failure. The average compressive strength of three cubes was adopted for every mix. Plate (3.7) displays the test machine. Plate (3.8) shows the cubes of the two types of concrete (NSC and RPC) at failure.

Plate (3.7) Compressive testing layout.

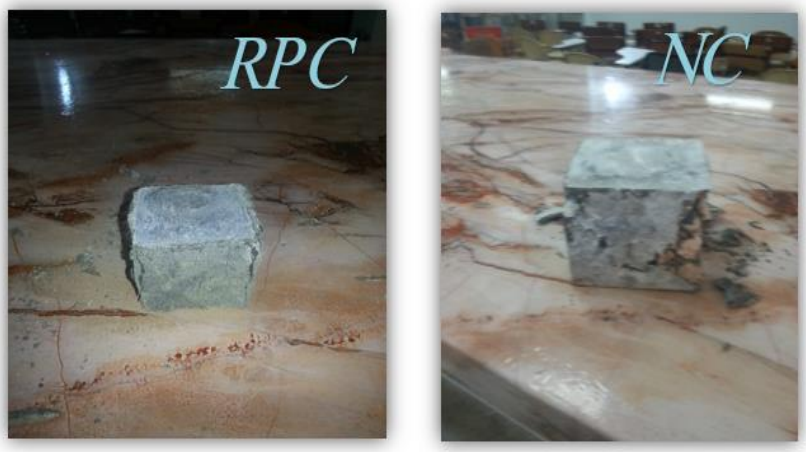

Plate (3.8) NSC and RPC cubic after the test.

3.6.1.2 Splitting Tensile Strength

After completing the curing period for the control specimens (cylinders 100×200 mm), they were taken out from the curing tank and left to dry. The **(ASTM C 496-04)** was adopted to carry out splitting tensile strength tests. The digital test machine ELE with a capacity of 2000 kN was used to load each cylinder continuously up to failure. The average splitting tensile strength of three cylinders was adopted for every mix. Plate (3.9) displays the test machine. Plate (3.10) shows the cylinders of the two types of concrete (NSC and RPC) at failure.

Plate (3.9) Splitting testing layout.

Plate (3.10) NC and RPC cylinder after the test.

3.6.2 Testing of Deep Beams

After the duration of the curing (28 days after casting) the deep beams and control specimens (cubes and cylinders) were extracted from the water basins and left to dry. The deep beams were painted with white water paint to see more clearly the cracks that occur at testing. All the deep beams were tested using the hydraulic machine with capacity (2000 kN) that available in the concrete laboratory in the college of Engineering at Kerbala University, as shown Plates (3.11).

Before starting the test procedures, the efficiency of the fracture machine and the following test tools were verified by testing of backup concrete deep beams:

1- The supports composed of install a steel bar of (25 mm) diameter on a piece of steel I-beam, as shown Plate (3.12a).
2- LVDT was used to measure deflection, as shown Plate (3.12b).
3- Load beam, which is a mass of steel installed on it pieces of steel bars with a diameter (25 mm), was used to transfer loads from the loading machine to the concrete deep beams. The load was concentrated in two points, where the dimensions between them were according to the (a/h), as shown Plate (3.13)
4- The computer was used to display data (load and deflection), as shown Plate (3.14).
5- Steel plate (10 × 60×150) mm was placed below the loading points to prevent the concentration of loads in the narrow areas that cause concrete crushing under load point, as shown Plate (3.15).
6- The compressor in the hydraulic machine and load cell were as shown Plate (3.15).

Each deep beam was placed on simple supports at 100 mm from each end in the machine with a clean span between the two supports of (600 mm). The load was applied in sequent increments of approximately (20 kN) at each loading step. In each increment, the cracks were marked and recorded the load value. When the deep beam reached the failure point, load failure was recorded, then the applied load was removed.

The LVDT was used to measure the vertical deflection in the center of the deep beam. All readings of vertical deflection and weighted load values were recorded automatically by the computer connected to the measuring instruments of the LV DT as well as the load cell.

Plate (3.11) Hydraulic loading machine.

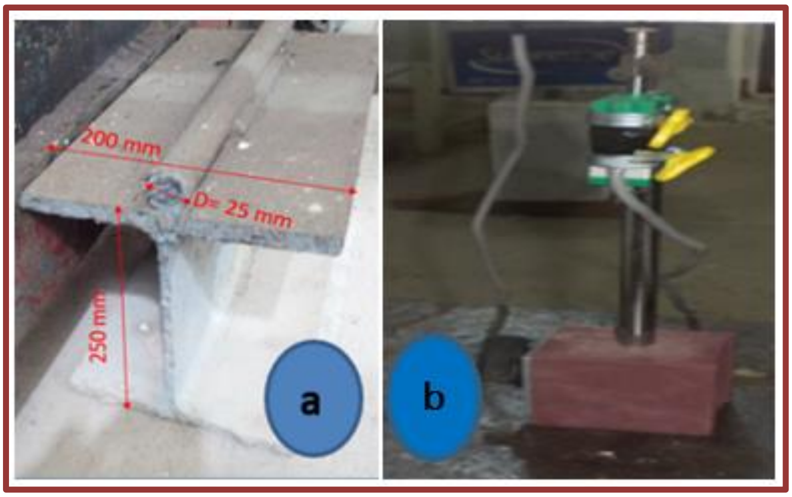

Plate (3.12) Support condition and LVDT

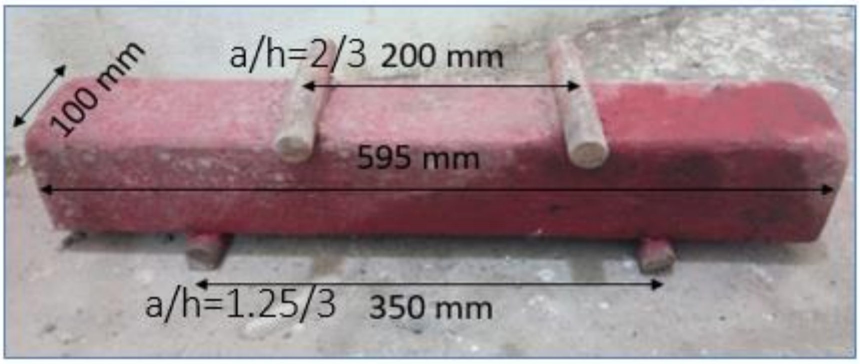

Plate (3.13) Load beam used to distribute load

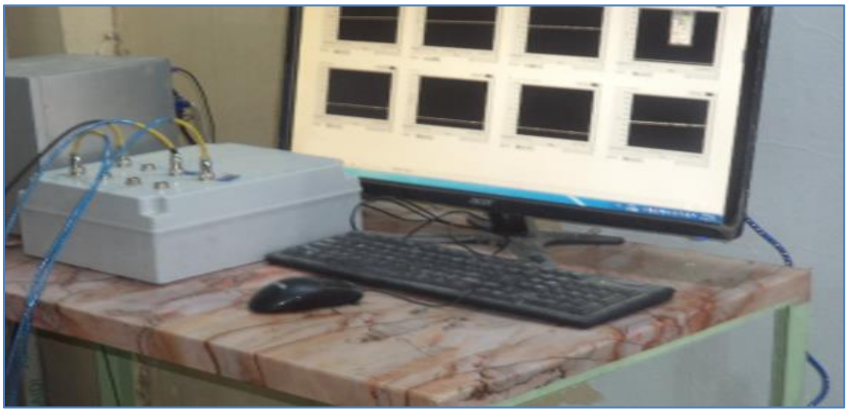

Plate (3.14) Computer used to record the data

Plate (3.15) Deep beam in mechanic test

Chapter Four

4

EXPERIMENTAL RESULTS AND DISCUSSION

CHAPTER FOUR

EXPERIMENTAL RESULTS AND DISCUSSION

4.1 General

The results of the experimental program described in Chapter 3 are presented and discussed in this chapter. The study includes the effect of hybridization technology on the first cracking load, ultimate load, and load-deflection response of reinforced concrete deep beam girders made from two different types of concrete for the same section, one of which was reactive powder concrete (RPC) and the other layer of normal concrete (NSC), cast at the same time (monolithically).

The initial crack load and the load-deflection response were recorded, as well as the ultimate load for each beam specimen tested during the experimental work. The results of the concrete control samples of cubes and cylinders for both types of concrete (RPC and NSC) were included here.

According to **(ACI-318 Code),** the shear failure was adopted on the design of all specimens in this study, because the design and mechanical behavior of deep beams are governed by shear.

4.2 Mechanical Properties of Control Samples

The concrete cubes were tested after completion of curing duration (age 28 days from the cast). The dimensions of tested cubes were (100 × 100 × 100) mm for (NSC) and (50 × 50 × 50) mm for (RPC) for compressive strength, tested according to **(BS1881-116).** The concrete cylinders dimensions were (100 × 200) mm for each type of concrete (RPC and NSC) were used for splitting tensile strength and tested according to **(ASTM-C496, 2004)**. The mechanical properties of control samples (cubes and cylinders) are shown in Table (4.1). Each value represents an average of three samples.

Table (4.1) Results of mechanical properties of controlled concrete samples

Designation Name \ Type of test		Compressive Strength Cubic f_{cu}(N/mm²)	Compressive Strength Cylinder f'_c(N/mm²) *	Tensile Splitting Strength f_{sp} (N/mm²)	Modulus of Elasticity, Ec(N/mm²) **
NDB-1 & NDB-2	NSC	36.813	29.45	3.07	25506
HDB-3 & HDB-4	NSC	40.5	32.4	3.42	26753
	RPC	75.25	60.2	5.33	32659
HDB-5 & HDB-6	NSC	39.813	31.85	3.33	26525
	RPC	75.875	60.7	5.39	32659
HDB-7 & HDB-8	NSC	40.5	32.4	3.42	26753
	RPC	75.25	60.2	5.33	32659

$*f'_c = 0.8 f_{cu}$ **(BS8110-85)** **$Ec_{(NSC)} = 4700\sqrt{f'_c}$ ***(ACI-318M-14),***

$** \ Ec_{(HSC)} = 3320\sqrt{f'_c} + 6900$ ***(ACI 363R-92)***

4.3 General Behavior of Tested Deep Beams

The general behavior included the study of the effect of the thickness of RPC layer (75 mm and 125 mm), the location of (RPC) layer (compression region or tension region), and (a/h= 2/3 and 1.25/3) on the load-deflection response, the first visible cracking load, the ultimate load, the type of failure, and crack pattern of the concrete deep beams.

The Figures from (4.1) to (4.8) illustrate load-vertical deflection curves of tested deep beams. The plates from (4.1) to (4.8) show the failure of pattern and the development of cracking with applying load. Table (4.2) included a review of the experimental results of the deep beams tested (first cracking load, ultimate load, and vertical deflection in mid-span of tested deep beams at the first cracking load and the ultimate load).

Table (4.2) The experimental results of the tested deep beams

Deep beam	Location RPC	Thickness RPC layer (mm)	First Crack Load, Pcr (kN)	First crack deflection, Δcr (mm)	Ultimate Load, Pu (kN)	Ultimate deflection Δu (mm)	$\frac{\Delta u}{\Delta cr}$	Failure mode
NDB-1 a/h=2/3	/	/	180	0.52	435	1.354	2.60	Diagonal compression
NDB-2 a/h=1.25/3	/	/	180	0.36	528.52	1.192	3.31	Diagonal compression
HDB-3 a/h=2/3	Tension	75	205	0.612	588	2.942	4.81	Diagonal compression
HDB-4 a/h=1.25/3	Tension	75	207	0.343	749.23	2.515	7.33	Diagonal compression
HDB-5 a/h=2/3	Compression	75	206	0.543	551	1.544	2.84	Bearing
HDB-6 a/h=1.25/3	Compression	75	210	0.36	582	1.21	3.36	bearing
HDB-7 a/h=2/3	Tension	125	192	0.448	664	2.844	6.35	Diagonal compression
HDB-8 a/h=1.25/3	Tension	125	212	0.248	814	2.262	9.12	Diagonal compression

4.3.1 Pilot Beam

This beam has been tested to verify testing of the system and adequacy of loading plates, supports, and applied loading steel beam (divided the applied load to two points) as well as to ensure that shear failure will occur before flexural failure. The diagonal compression failure occurred finally at load about (580 kN).

4.3.2 Control Deep Beams

Group (A) included NSC deep beams with a homogeneous cross-section (NDB-1) and (NDB-2)

4.3.2.1 Normal Deep Beam NDB-1

This beam was casted from NSC only, and a/h=2/3. The first visible inclined shear cracks appeared at a load of (180 kN) in the shear span region with deflection about (0.52 mm), the ($\frac{Pcr}{Pu}$) of this specimen about (41.4) %. With increasing the load, the shear cracks developed to the direction of the loading points with occurring of more inclined shear cracks in the strut direction and developed until shear failure of concrete. The first flexural crack appeared when loading (240 kN) in the mid-span. The final load caused the failure of beam NDB-1 was (435kN) with final deflection (1.354 mm). Figure (4.1) shows the load-deflection of this specimen. Plate (4.1) shows the formation and spread of cracks at ultimate load as well as the formation of the arch pattern at the final diagonal shear failure.

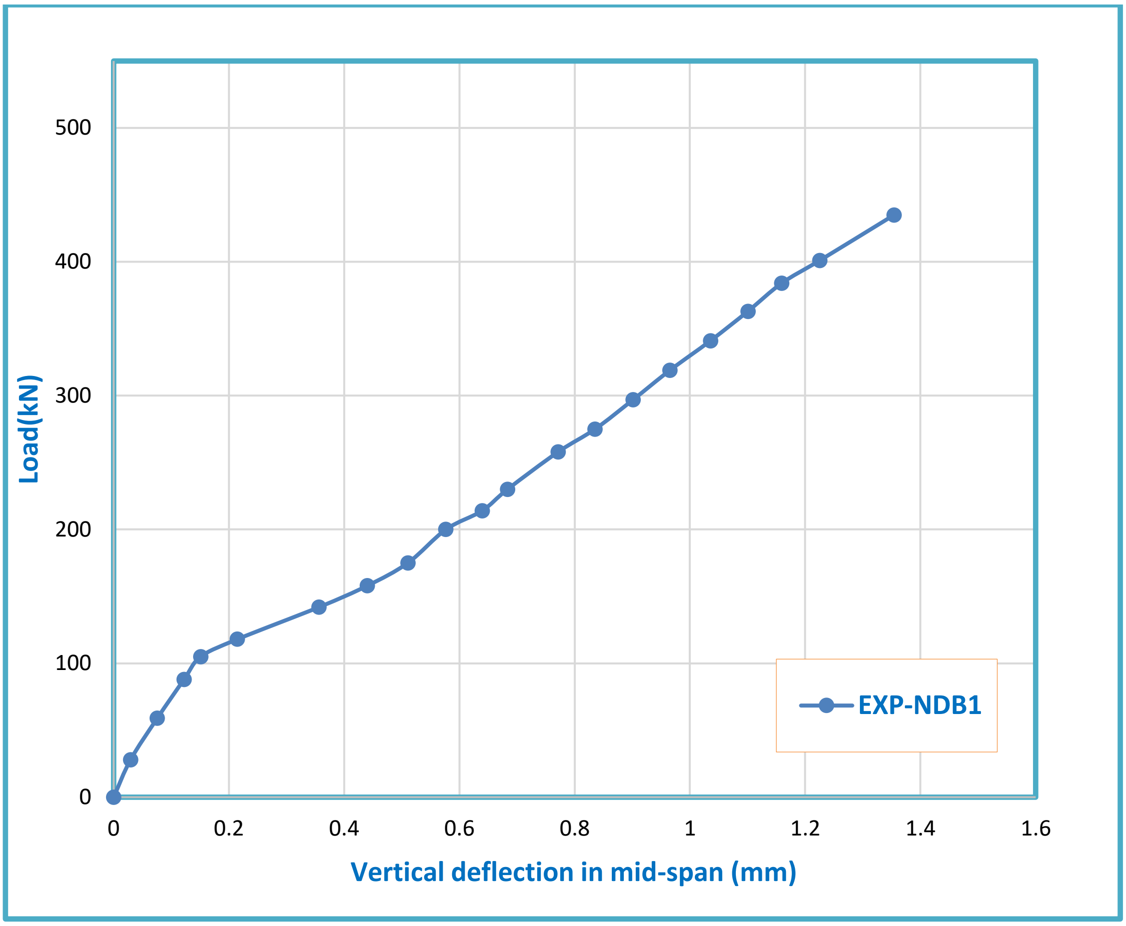

Figure (4.1) Load-vertical deflection of the beam NDB-1 at a/h=2/3

Plate (4.1) Crack pattern of specimen NDB-1 at failure.

4.3.2.2 Normal Deep Beam NDB-2

This specimen was similar to the beam (NDB-1) but the shear span to the total depth ratio was (1.25/3). At applied load of about (180kN), the first visible crack appeared at the support point in the shear span zone, the vertical deflection at first visible crack load was about (0.36 mm), the ($\frac{Pcr}{Pu}$) of this specimen was about (34.1) %, its less than NDB-1, with increasing the applied load; inclined shear cracks were developed towards loading point direction until diagonal crashing concrete failure at ultimate load about (528.52 kN) with final vertical deflection (1.192 mm). At the applied load (240 kN), the first visible flexural crack appeared in the mid-span region. Figure (4.2) shows the load-deflection of this specimen. Plate (4.2) shows the formation and spread of cracks at ultimate load as well as the pattern of final failure.

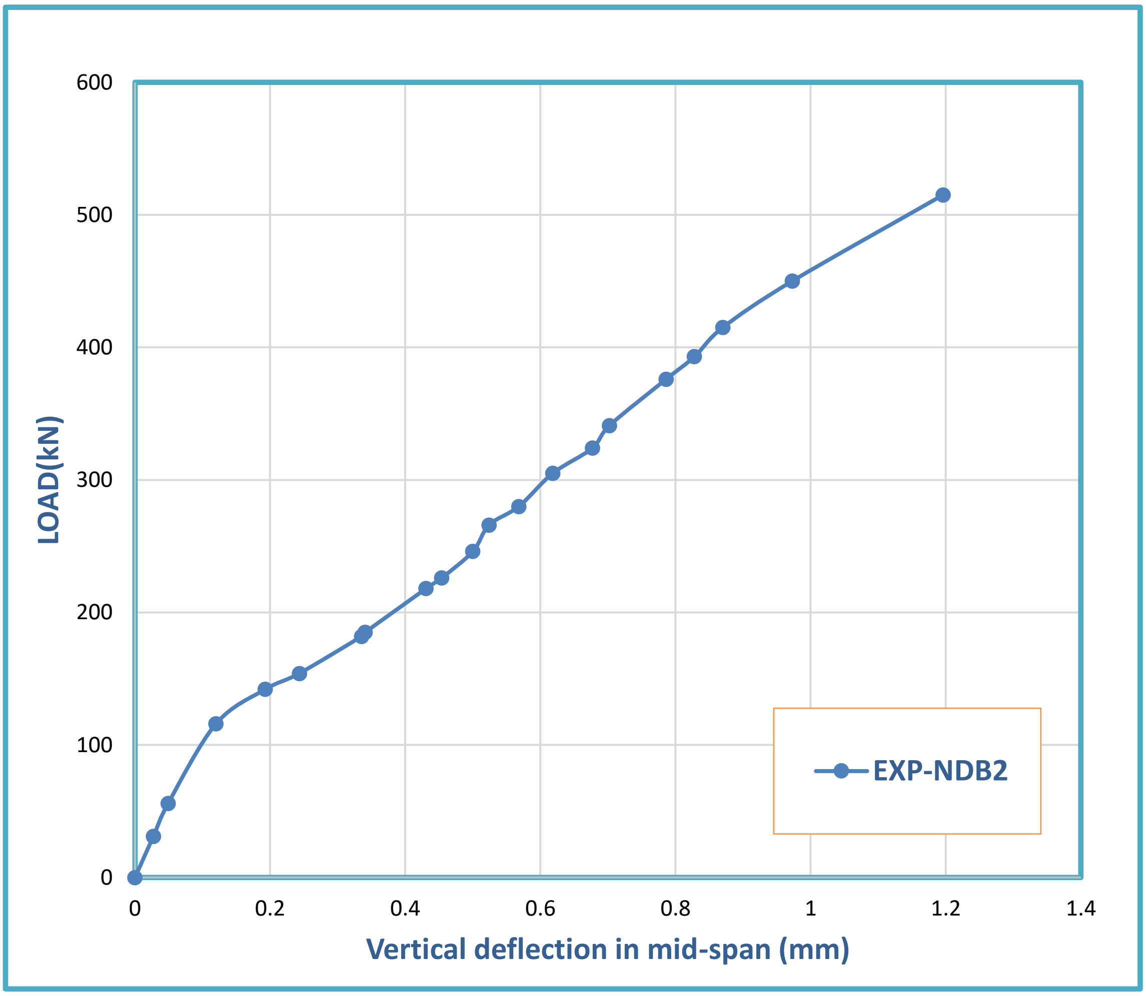

Figure (4.2) Load-vertical deflection of the beam NDB-2

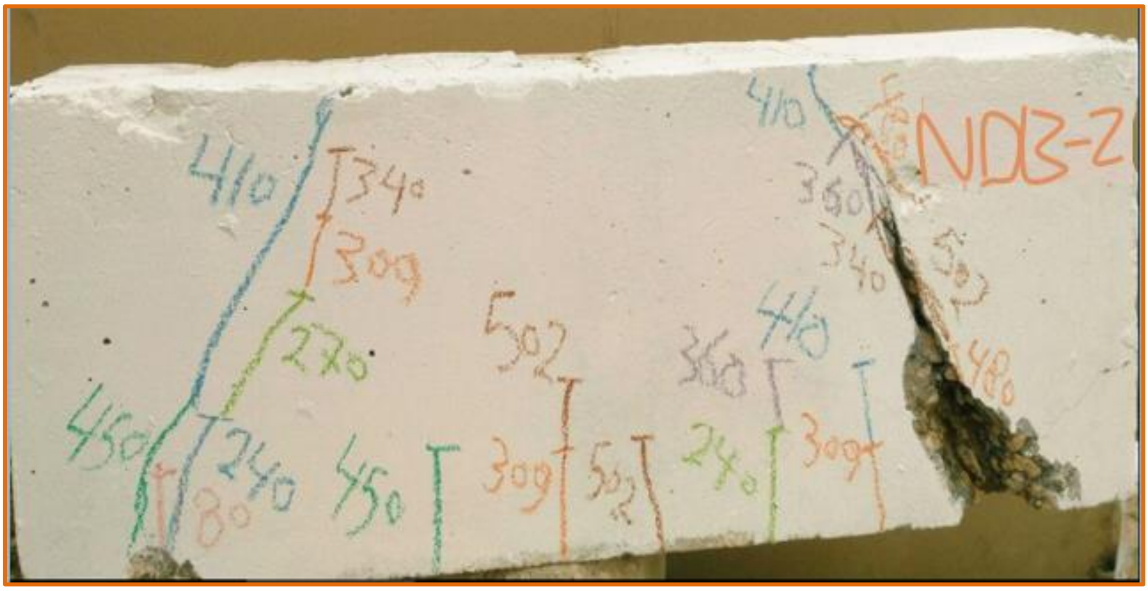

Plate (4.2) Crack pattern of beam NDB-2 at failure.

4.3.3 Hybrid Deep Beams

Those deep beams were including three gropes, group (B) included (HDB-3 and HDB-4), group (C) included (HDB-5 and HDB-6), and group (D) included (HDB-7 and HDB-8). The technique of casting the hybrid deep beams was active to provide bonding between the two concrete layers (RPC and NSC) and did not showing any horizontal cracks of the surface between this concrete layer at all stages of the loading.

4.3.3.1 Hybrid Deep Beam HDB-3

This deep beam was made from two different types of concrete at the same cross-section, RPC (75 mm) in tension zone, and NSC (225 mm) in the compression zone, with a/h=2/3. The first visible cracks formed in shear span at the load about (205 kN), where the vertical deflection in midspan at first cracking load and ultimate load was about (0.612 mm and 2.942 mm), respectively, the ($\frac{\mathbf{Pcr}}{\mathbf{Pu}}$) of this specimen about (34.9) %. With increasing the applied load, the diagonal shear crack was formed and developed to the loading point with the strut direction and diagonal compression failure occurred at ultimate load about (588 kN). At the applied load (255 kN) the first visible flexural crack appeared in the mid-span region, with increasing applied load the flexural cracks developed to the middle depth of specimen and other flexural cracks appeared in the span region between support points, some of which evolved to the middle of the depth of the deep beam. The load-vertical deflection of beam HDB-3 was shown in Figure (4.3). Plate (4.3) shows the formation and spread of cracks at ultimate load as well as the pattern of final failure.

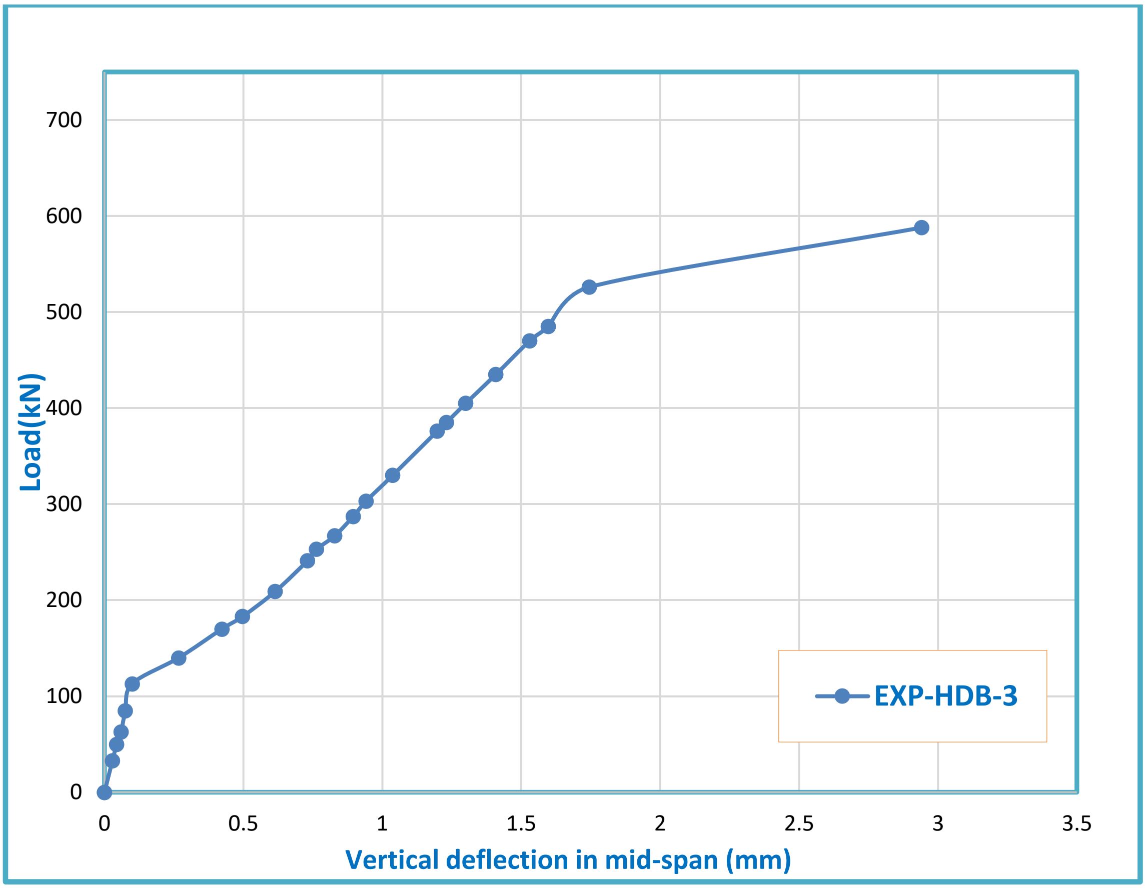

Figure (4.3) Relationship between the vertical mid-span deflection and the applied load for the hybrid deep beam HDB-3 at (a/h=2/3)

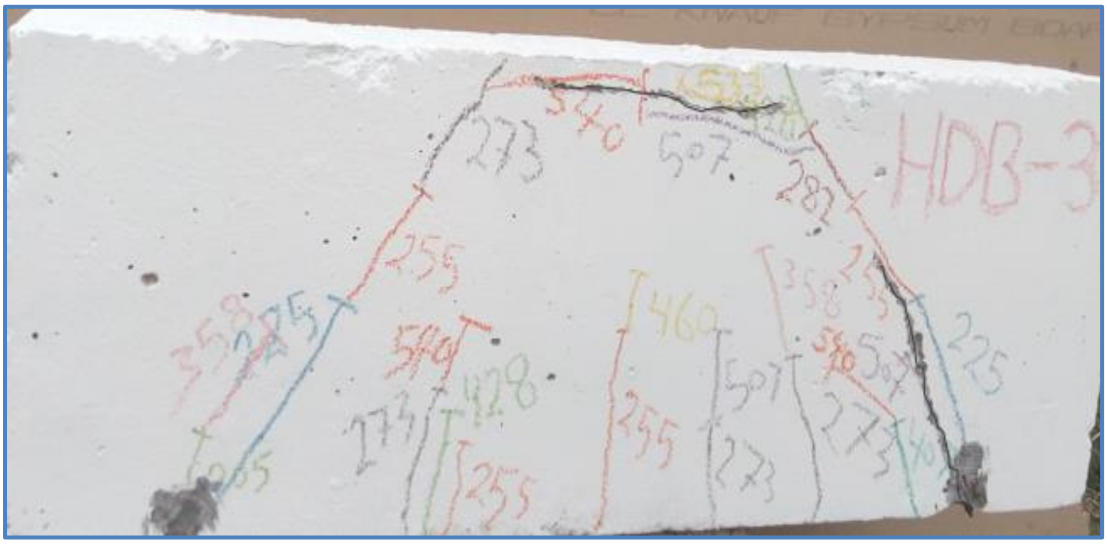

Plate (4.3) Crack pattern of hybrid deep beam HDB-3 at failure

4.3.3.2 Hybrid Deep Beam HDB-4

This specimen is similar to the hybrid deep beam (HDB-3) but a/h=1.25/3. The first visible cracks were the inclined shear cracks in the shear span zone under the applied load about (207 kN), the vertical deflection at the midspan under the first visible crack load of beam HDB-4 was (0.343 mm). the ($\frac{\mathbf{Pcr}}{\mathbf{Pu}}$) of this specimen about (27.6) %, its less than HDB-3. With increased applied load, the first visible cracks developed to the loading point and other shear cracks appeared in the strut region until the diagonal shear failure occurred at the final load of (749.23 kN). The vertical deflection at the midspan under the effect of the ultimate load was (2.515 mm). The first visible flexural cracks appeared in the mid-span region at the load about (207 kN), with increased applied load the first visible flexural cracks developed to the middle depth of the specimen and other flexural cracks appeared in the region between support points. The load-deflection of beam HDB-4 is shown in Figure (4.4). Plate (4.4) shows the formation and spread of cracks at ultimate load as well as the pattern of final failure.

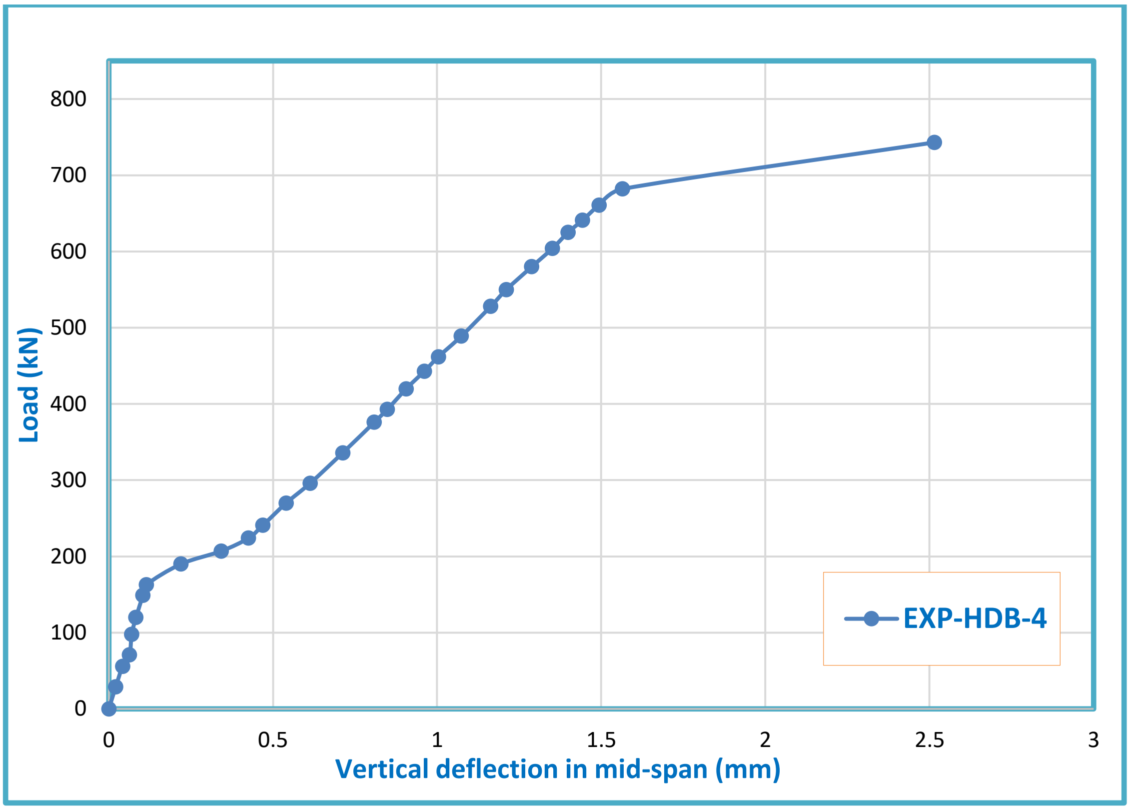

Figure (4.4) Relationship between the vertical mid-span deflection and the applied load for the hybrid deep beam HDB-4 at (a/h=1.25/3)

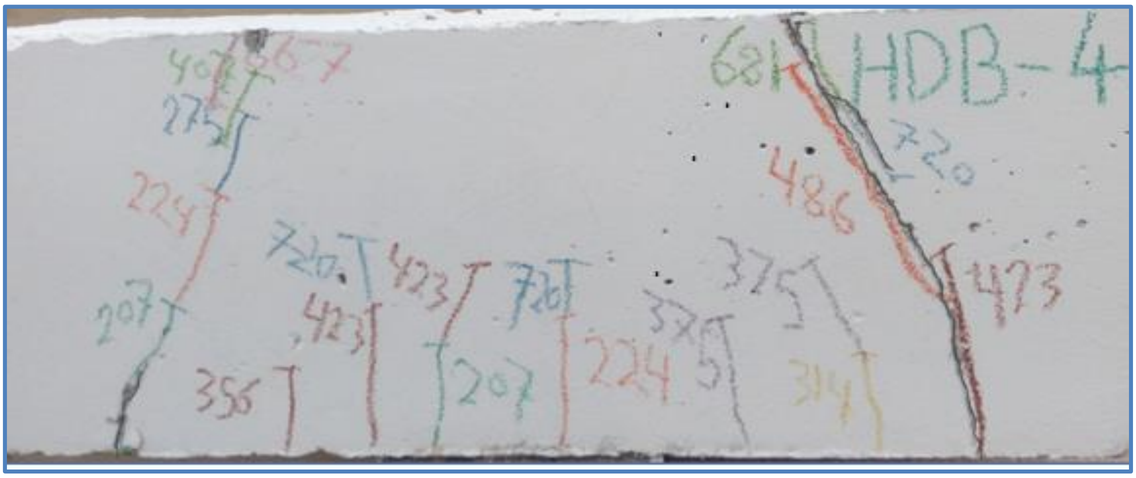

Plate (4.4) Crack pattern of hybrid deep beam HDB-4 at failure.

4.3.3.3 Hybrid Deep Beam HDB-5

This deep beam was made from two different types of concrete at the same cross-section, RPC (75 mm) in the compression zone, and NSC (225 mm) in tension zone, with a/h=2/3. At the applied load about (206 kN) the first visible shear cracks appeared near the support in the shear region, where the vertical deflection at the midspan under the effect of the first visible crack load was (0.543mm), the ($\frac{Pcr}{Pu}$) of this specimen about (37.4) %. As the load increased, the first inclined cracks were developed to the loading point and other inclined shear cracks appeared in the strut region until the bearing failure occurred above the support point at the ultimate load of (551 kN) due to high increasing in a compressive stress. The vertical deflection at the midspan under the effect of the ultimate load was (1.544 mm). The initial visible flexural cracks appeared in the mid-span region at the applied load about (223 kN). As the load increased, other flexural cracks appeared in the region between the supports, some of which evolved to the middle of the depth of beam HDB-5 which were greater than the cracks developed in beam NDB-1 and beam HDB-3 (same a/h=2/3). The load-vertical deflection of beam HDB-5 was shown in Figure (4.5). Plate (4.5) shows the formation and spread of cracks at ultimate load as well as the pattern of final failure.

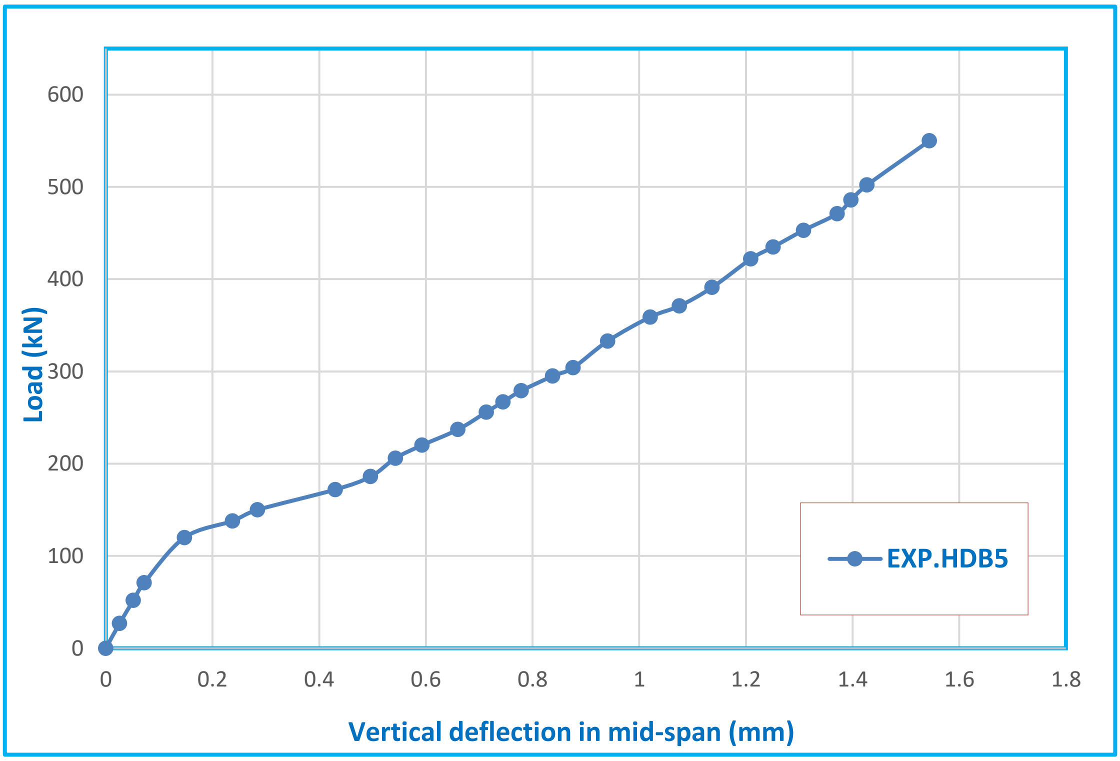

Figure (4.5) Relationship between the vertical mid-span deflection and the applied load for the hybrid deep beam HDB-5 at (a/h=2/3)

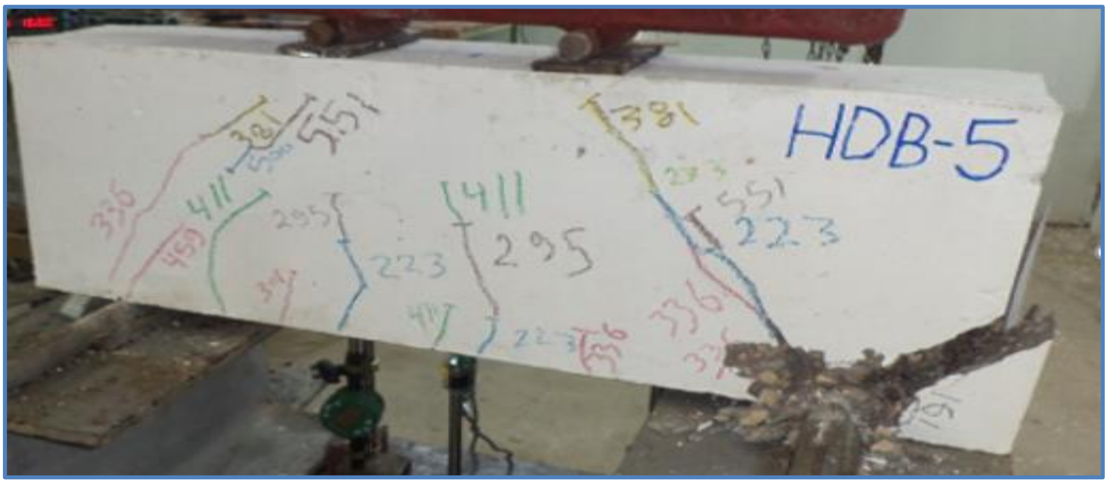

Plate (4.5) Crack pattern of hybrid deep beam HDB-5 at failure.

4.3.3.4 Hybrid Deep Beam HDB-6

The specimen HDB-6 is the same as the specimen HDB-5 but a/h=1.25/3. The diagonal shear cracks that occurred in the shear span region were the first visible cracks under the applied load about (210 kN), the vertical deflection in mid-span at the first cracking load of the beam HDB-6 was (0.36 mm), the ($\frac{Pcr}{Pu}$) of this specimen about (36.1) %, its less than HDB-5. As increasing the applied load, the diagonal shear cracks evolved in the direction of the loading points until the bearing failure occurred above the support points due to high increasing in the compressive stress at a final load of about (582 kN). The vertical deflection at the midspan under the effect of the ultimate load was (1.21mm). The first flexural cracks were visible at the midspan at load about (271 kN), with increased the applied load appeared other flexural cracks in the region between support points but less than the flexural cracks of specimen HDB-5 and evolved to the middle of the depth of specimen. Figure (4.6) shows the relationship between the vertical mid-span deflection and the applied load for the beam HDB-6. Plate (4.6) shows the formation and spread of cracks at ultimate load as well as the pattern of final failure.

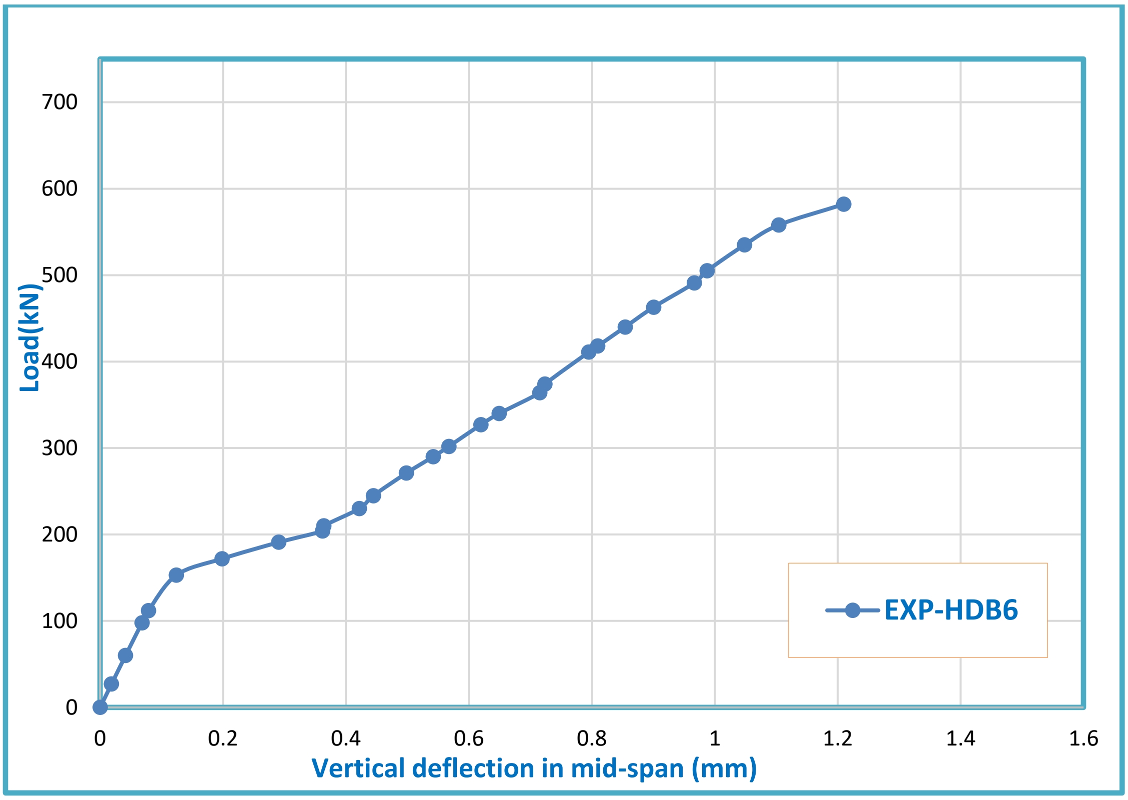

Figure (4.6) Relationship between the vertical mid-span deflection and the applied load for the hybrid deep beam HDB-6 at (a/h=1.25/3)

Plate (4.6) Crack pattern of hybrid deep beam HDB-6 at failure.

4.3.3.5 Hybrid Deep Beam HDB-7

This specimen was made from two different types of concrete at the same cross-section, the first type was RPC in tension zone at a thickness (125mm), the second type was NSC in compression zone at a thickness (175 mm), and (a/h=2/3). The applied load approximately (192 kN) caused the appearance of the first visible diagonal shear cracks in the shear span region. The first visible cracking load caused vertical deflection under the center of the mid-span of this deep beam was about (0.448 mm), the ($\frac{Pcr}{Pu}$) of this specimen about (28.9) %. While increasing the applied load, the first visible shear cracks were developed, and other inclined shear cracks appeared in the strut region until the failure of this deep beam occurred due to crushing concrete in shear span along the strut direction (strut crashing) at the ultimate load about (664 kN). The maximum vertical deflection under the effect of the ultimate load was (2.844 mm). Under the effect of the applied load of (307 kN), the initial flexural cracks in the mid-span beam region appeared. As increasing load, the propagation and development of flexural cracks increased significantly. Figure (4.7) shows the relationship between the vertical mid-span deflection and the applied load for the beam HDB-7. Plate (4.7) shows the formation and spread of cracks at ultimate load applied as well as the pattern of final failure.

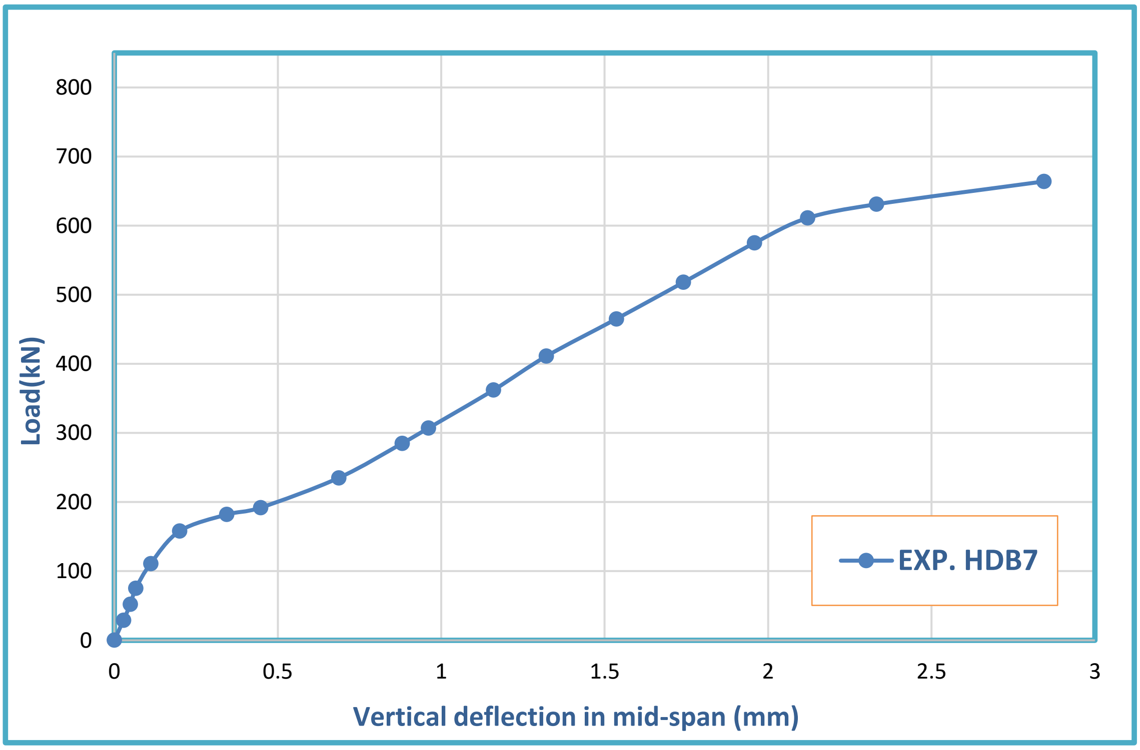

Figure (4.7) Relationship between the vertical mid-span deflection and the applied load for the hybrid deep beam HDB-7 at (a/h=2/3)

Plate (4.7) Crack pattern of hybrid deep beam HDB-7 at failure.

4.3.3.6 Hybrid Deep Beam HDB-8

The specimen HDB-8 is the same as the specimen HDB-7, but a/h=1.25/3. The visible first cracks in beam HDB-8 appeared in the shear region at the applied load about of (212 kN). The vertical mid-span deflection at first visible cracking load was (0.248 mm), the ($\frac{\mathbf{Pcr}}{\mathbf{Pu}}$) of this specimen about (26) % less than HDB-7. With increasing the applied load, the shear cracks evolved to the loading points and the other inclined shear cracks appeared in the region confined between the loading and support points (strut region). The first visible flexural cracks appeared in the mid-span beam region at the load of approximately (341 kN about) and evolved upward with increasing the applied load upward to about (to 0.6h from the base of the deep beam). The diagonal compression failure occurred at the ultimate load of (814 kN). The vertical mid-span deflection under the effect of the ultimate load was (2.262 mm). Figure (4.8) shows the load-deflection curve of the beam HDB-8. Plate (4.8) shows the formation and spread of cracks at ultimate load as well as the pattern of final failure (diagonal compression failure).

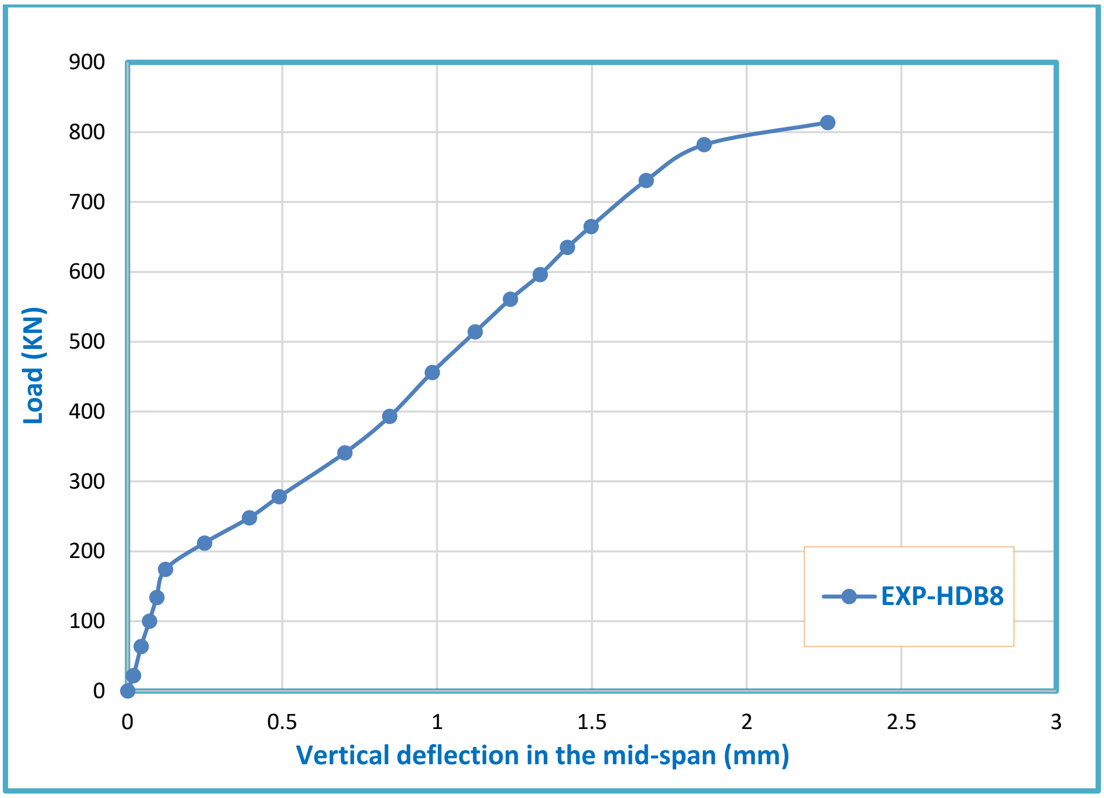

Figure (4.8) Relationship between the vertical mid-span deflection and the applied load for the hybrid deep beam HDB-8 at (a/h=1.25/3)

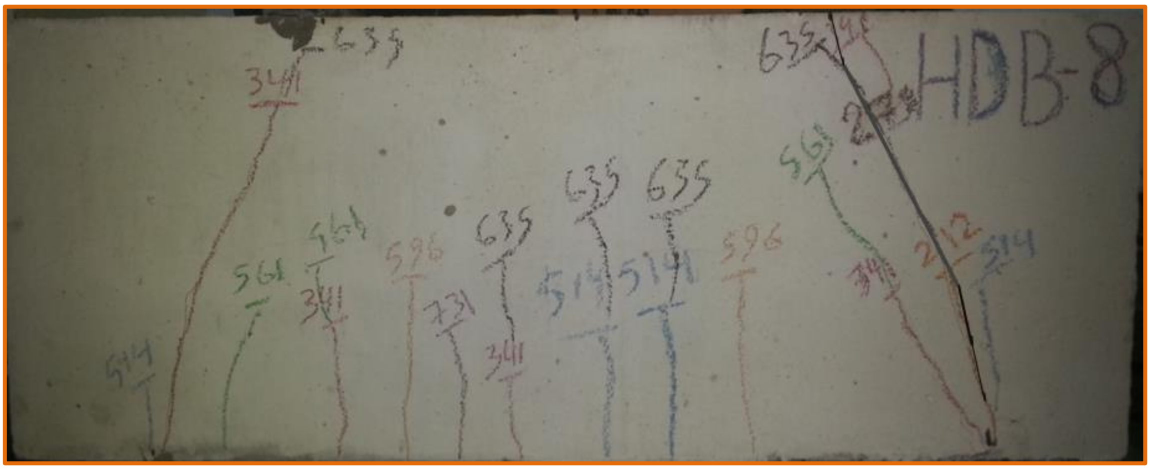

Plate (4.8) Crack pattern of hybrid deep beam HDB-8 at failure.

4.4.1 Effect of (a/h) on the Behavior of the Hybrid Specimens

The experimental program included a study of the effect (a/h = 2/3 and 1.25/3) on deep beams behavior. Generally, there was a significant improvement in the behavior of hybrid RC deep beams with the decrease (a/h). The following are the parameters that affected with the (a/h):

4.4.1.1 Effect of (a/h) on the Applied Load to the vertical Mid-Span Deflection

Generally, the deep beams were more stiff and the vertical midspan deflection amount for the same load was less with decreasing (a/h) from (2/3) to (1.25/3), as shown in Figures (4.9) to (4.12).

When the a/h was decreased that led to decrease the vertical deflection in midspan of deep beams at the initial cracking load and at the final load.

The (Δu /Δcr) ratio increased with decreasing the (a/h), the highest ductility index of (9.12) was recorded for the beam HDB-8 (with RPC (125mm) in tension zone and a/h =1.25/3), while the lowest one (2.6) was recorded for the beam NDB-1 (with a/h =2/3), as shown in Table (4.2).

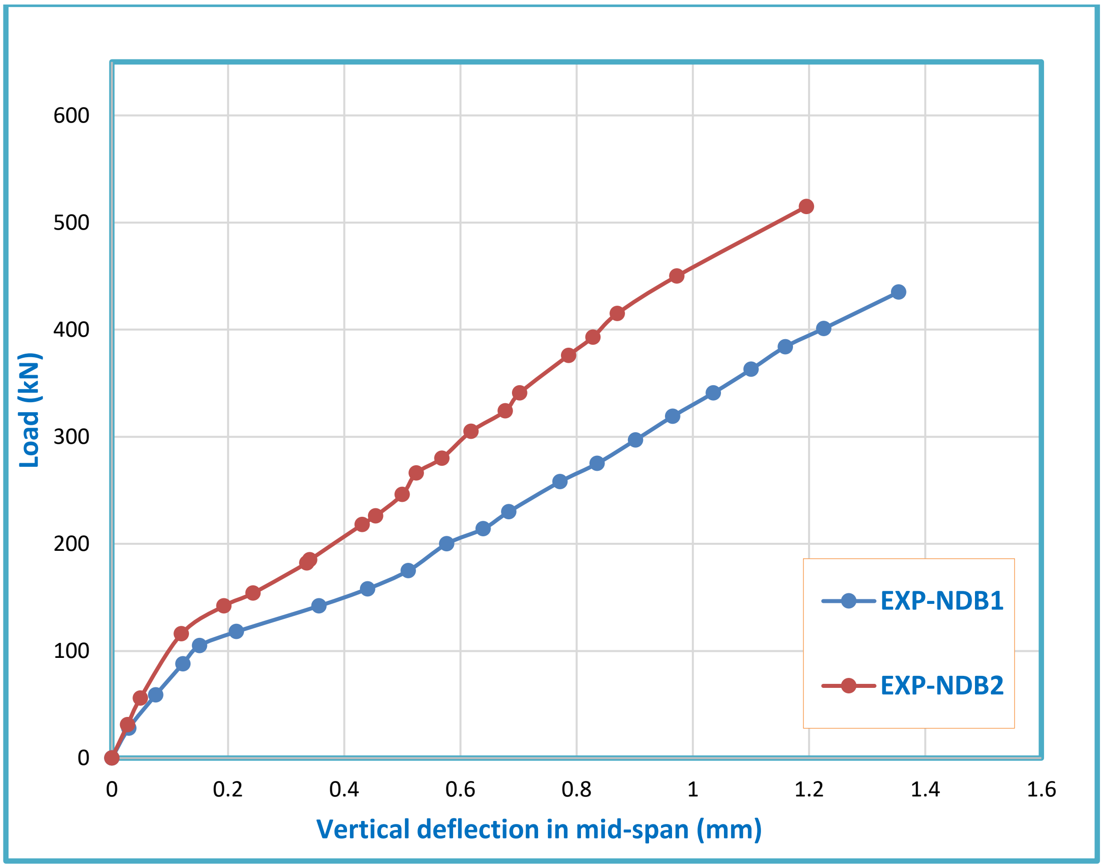

Figure (4.9) Effect of (a/h) on the load-deflection curve for group (A)

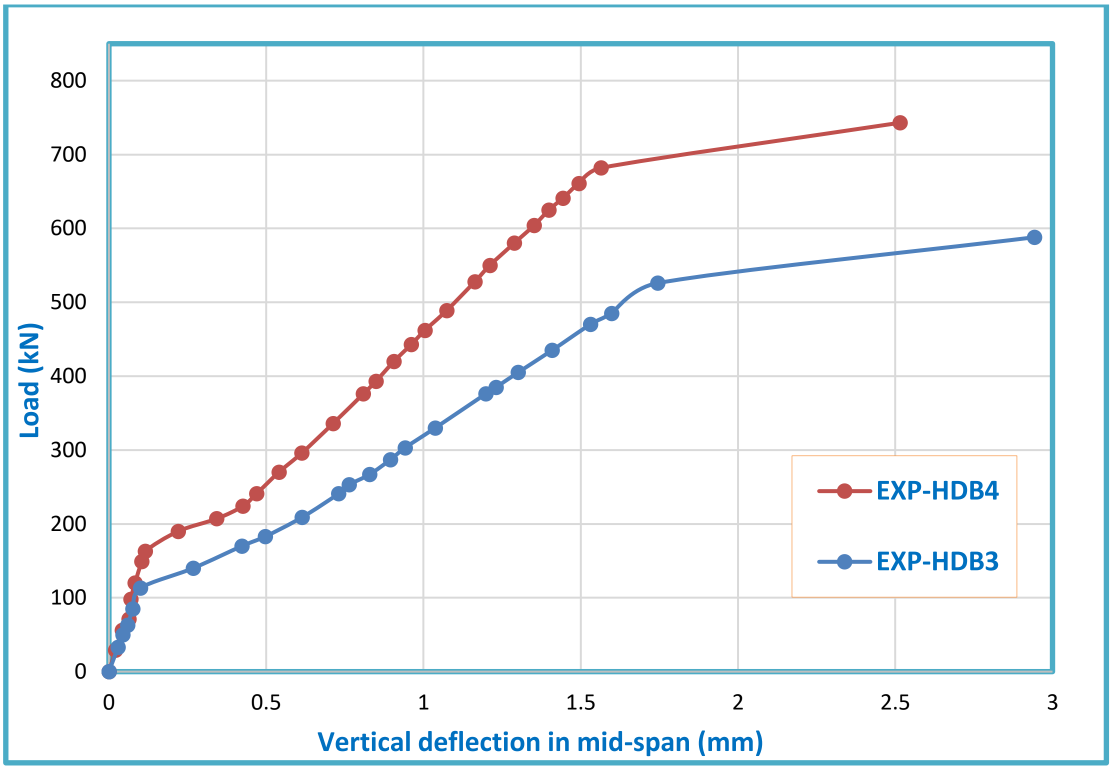

Figure (4.10) Effect of (a/h) on the load-deflection curve for group (B)

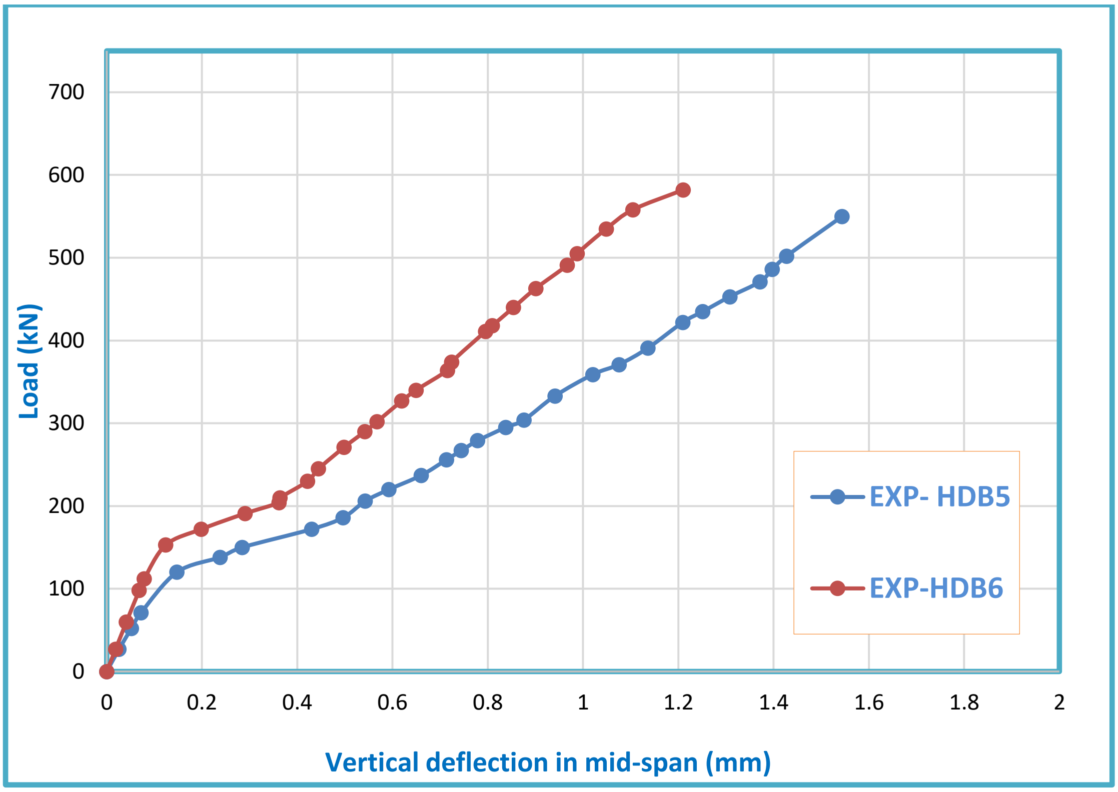

Figure (4.11) Effect of (a/h) on the load-deflection curve for group (C)

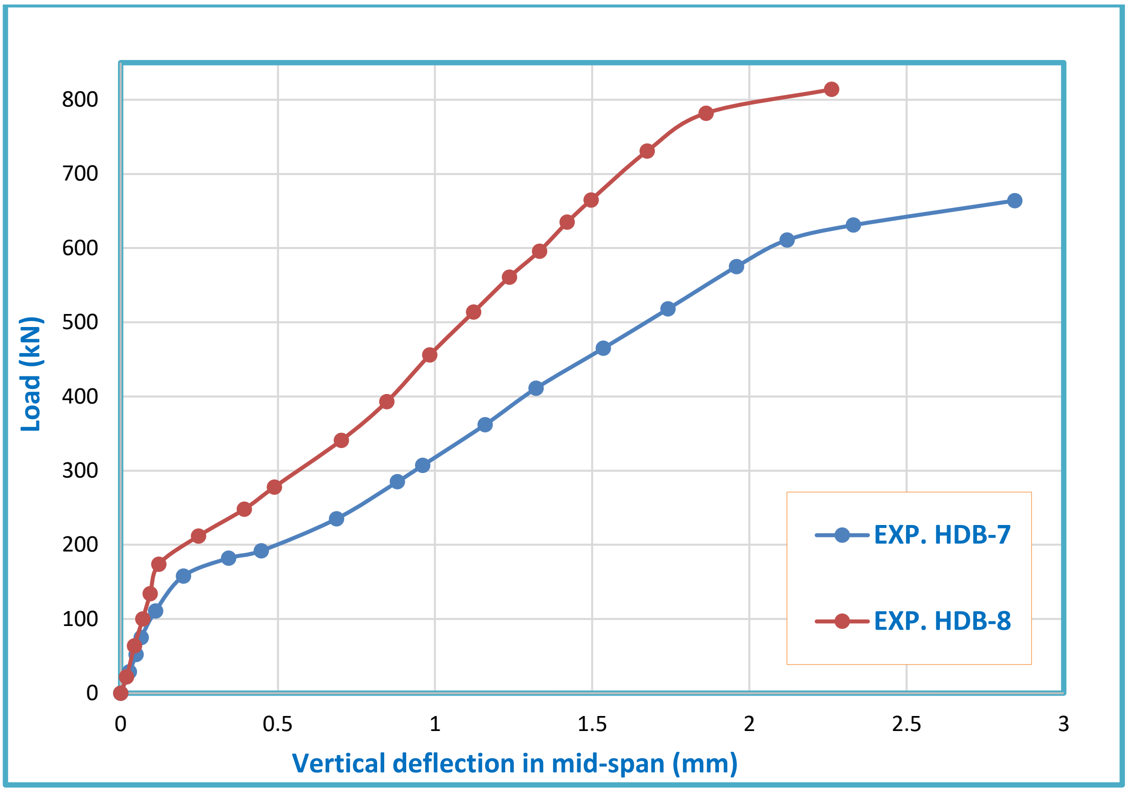

Figure (4.12) Effect of (a/h) on the load-deflection curve for group (D)

4.4.1.2 Effect of the (a/h) on the First Cracking and the Ultimate Loads

Through the experimental results, generally, the ultimate load decreased with the increasing of (a/h), due to a decrease in the effect of the tied arch action with increased (a/h). Table (4.2) includes the first cracking load as well as the failure load of the examined specimens.

The ultimate load in the normal deep beam (NDB-2) was greater than the ultimate load of the normal deep beam (NDB-1) by (21.5%), ultimate load in hybrid deep beam (HDB-4) was greater than the ultimate load of the hybrid deep beam (HDB-3) by (27.42%), and ultimate load for hybrid deep beam (HDB-6) was greater than the ultimate load of the hybrid deep beam (HDB-5) by (5.63 %), and ultimate load in hybrid deep beam (HDB-8) was greater than the ultimate load of hybrid deep beam (HDB-7) by (22.59 %).

The first cracking load in hybrid deep beams increased with decreased (a/h), the first cracking load of the (HDB-8) was greater than the load of

(HDB-7) about (10.4 %), but in the (HDB-4) if was slightly greater than the (HDB-3) about (1 %), while the (HDB-6) was slightly greater than the (HDB-5) about (1.9 %).

The ($\frac{Pcr}{Pu}$) decreased with decreasing the (a/h), where the ($\frac{Pcr}{Pu}$) of the beam (NDB-2) was less than that for beam (NDB-1) by about (17.6%), and the ($\frac{Pcr}{Pu}$) of the hybrid deep beam (HDB-4) was less than of the hybrid deep beam (HDB-3) by about (20.9%). Also the ($\frac{Pcr}{Pu}$) of the hybrid deep beam (HDB-6) was less than of the hybrid deep beam (HDB-5) by about (3.5%), finally the ($\frac{Pcr}{Pu}$) of the hybrid deep beam (HDB-8) was less than of the hybrid deep beam (HDB-7) by about (10%).

4.4.2 Effect of the Location of RPC Layer on the Behavior of Hybrid Deep Beams

The experimental program included a study of the effect location of RPC layer (tension and compression region) on the deep beams behavior. Generally, there was a significant improvement in the behavior of RC deep beams with using the RPC layer in tension or compression region. The following are the effects of location of the RPC layer:

4.4.2.1 Effect of the Location of RPC Layer on the Applied Load to the vertical Mid-Span Deflection

Generally, the load-deflection curve in the hybrid deep beams performs better than normal deep beams. The (Δu /Δcr) ratio in hybrid deep beams was greater than that for normal deep beams. The behavior of hybrid deep beams with RPC in the tension region in better than the behavior of the hybrid deep beam with RPC in compressipn region. The greater (Δu /Δcr) ratio was shown for the deep beam (HDB-7) than for all other specimens of (a/h=2/3). While (Δu /Δcr) for all specimens of (a/h=1.25/3) was calculated and the highest one is for the beam (HDB-8) which was of value (9.12).

The maximum stiffness of all deep beams tested was found for the hybrid deep beams with RPC layer in tension zone, which was greater than the other specimens as shown in Figures(4.13) and (4.14).

At (a/h =2/3), the highest vertical midspan deflection for the hybrid deep beam HDB-5 (with RPC (75 mm) in compression zone) was about (1.544 mm) which was greater than control deep beam NDB-1 (1.354 mm) but less than hybrid deep beam HDB-3 (2.942 mm) (with RPC (75 mm) in tension zone).

At (a/h =1.25/3), the highest vertical midspan deflection for the hybrid deep beam HDB-6 (with RPC (75 mm) in compression zone) was about (1.21 mm) which was greater than normal deep beam NDB-2 (1.192 mm) but less than hybrid deep beam HDB-4 (2.515 mm) (with RPC (75 mm) in tension zone).

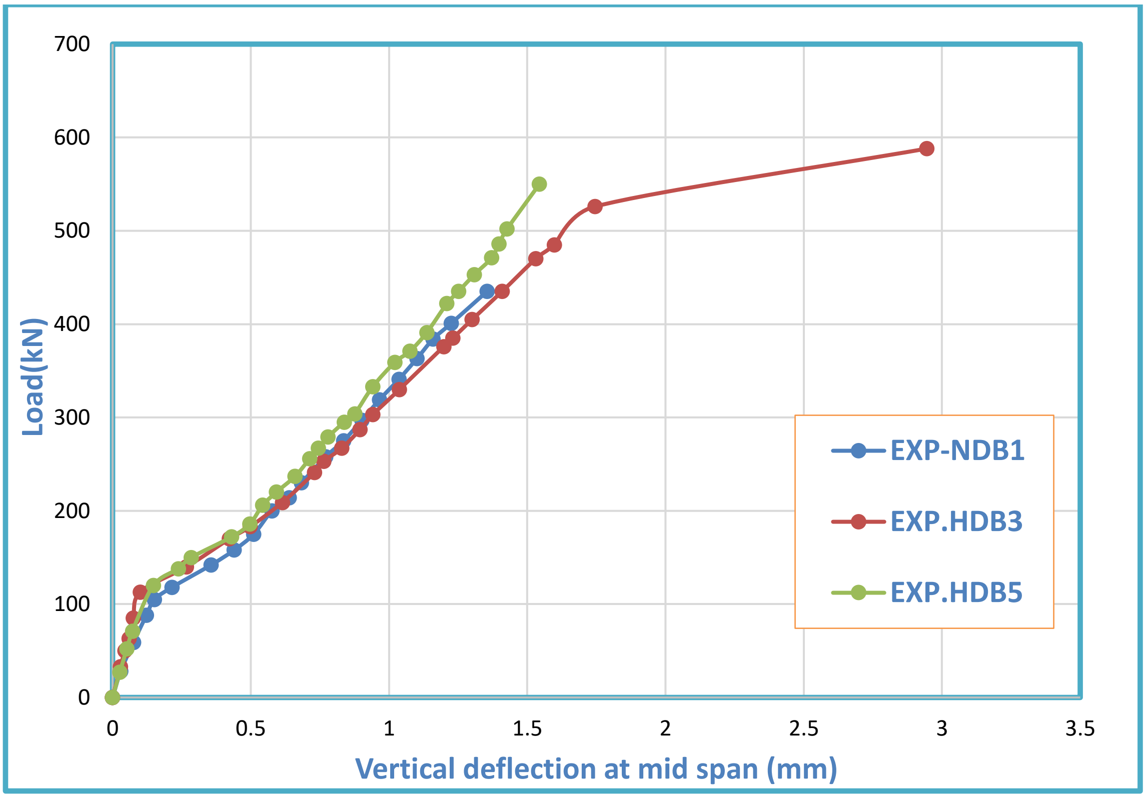

Figure (4.13) Effect of the location of the RPC layer on the load-deflection curve for (a/h = 2/3)

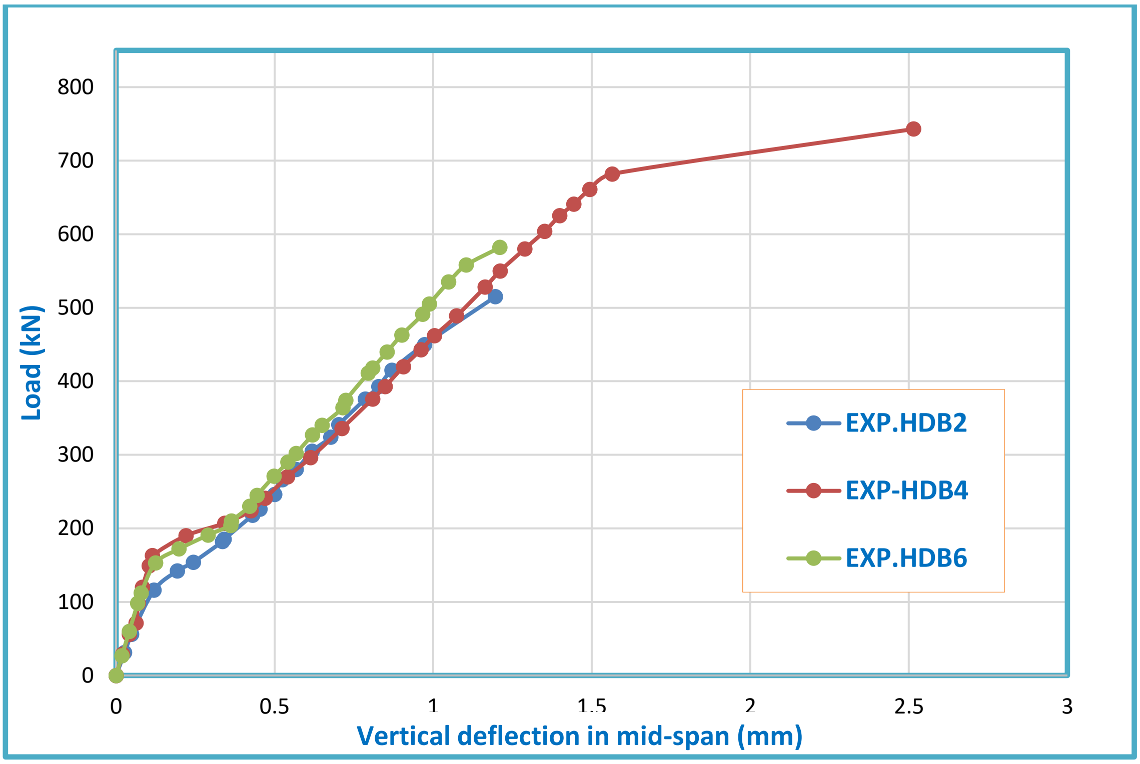

Figure (4.14) Effect of the location of the RPC layer on the load-deflection curve for (a/h = 1.25/3)

4.4.2.2 Effect of the Location of RPC layer on the First Cracking and the Ultimate Loads

Generally, the first cracking load and the final load in the hybrid deep beams were greater than that for normal deep beams.

The presence of RPC layer in the compression zone led to an increase in the moment of inertia of the cross-section, this may be the reason for the increased initial cracking load and failure load of such type of hybrid deep beams. The first cracking load and the ultimate load of beam HDB-5 were greater than that for beam NDB-1 of about (14.4% and 26.67%), respectively. While the first cracking load and the ultimate load of beam HDB-6 were greater than that for beam NDB-2 of about (16.67% and 10.12%), respectively.

The presence of RPC layer in the tension zone resulted in an increase in the ultimate load greater than its presence in the compression zone. The amount of increase in the ultimate load of the beam HDB-3 was approximately (35.17% and 6.72%) compared to beam NDB-1 and beam HDB-5, respectively. In the other hand, the amount of increase in the ultimate load of the beam HDB-4 was approximately (41.76% and 28.73%) compared to beam NDB-2 and beam HDB-6, respectively.

The first cracking load of beam HDB-3 was greater than beam NDB-1 of about (13.89%), the first cracking load of beam HDB-4 was greater than beam NDB-2 of about (15%), the first cracking load of beam HDB-7 was greater than NDB-1 of about (6.67%), the first cracking load of beam HDB-8 was greater than beam NDB-2 of about (17.78%). This enhancement was due to tensile strength and density of RPC located in the tension zone.

4.4.3 Effect of RPC Layer Thickness on the Behavior of Hybrid Deep Beams

In the experimental program, the thickness (75 mm) was adopted for RPC layer location in the tension region or the compression region, and (125 mm) thickness of RPC layer in tension region, the effect of this layer

4.4.3.1 The Effect of RPC Thickness layer on the Applied Load to the vertical Mid-Span Deflection

The behavior of hybrid deep beams in groups (B) (with RPC (75 mm) in tension zone) and (D) (with RPC (125 mm) in tension zone) were more ductile than that for group (A) at first stage of loading, as shown in Figures (4-15) and (4-16).

The ($\Delta u / \Delta cr$) ratio for the hybrid deep beams with thickness (125 mm) of RPC layer was greater than that for beams with thickness (75 mm) of RPC layer in tension zone. The highest ($\Delta u / \Delta cr$) for all specimens of (a/h=2/3) was calculated for the beam (HDB-7) which was of value (4.81). While the highest ($\Delta u / \Delta cr$) for all specimens of (a/h=1.25/3) was calculated for the beam (HDB-8) which was of value (9.12).

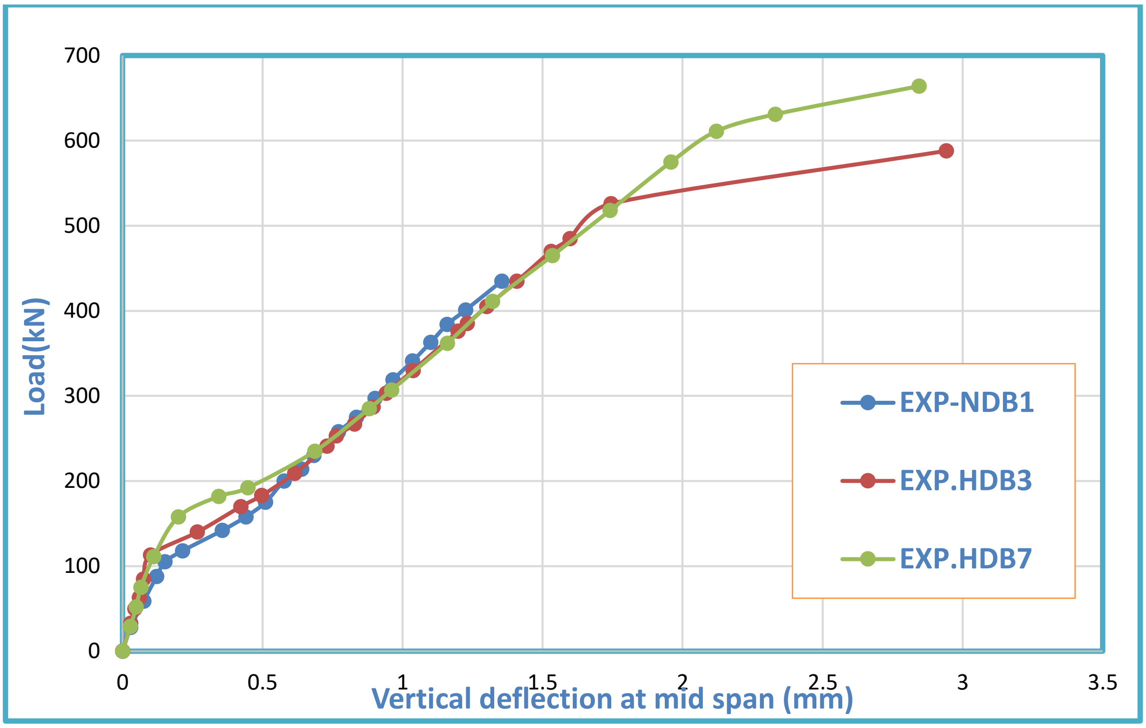

Figure (4.15) Effect thickness of the RPC layer on the load-deflection curve for (a/h = 2/3)

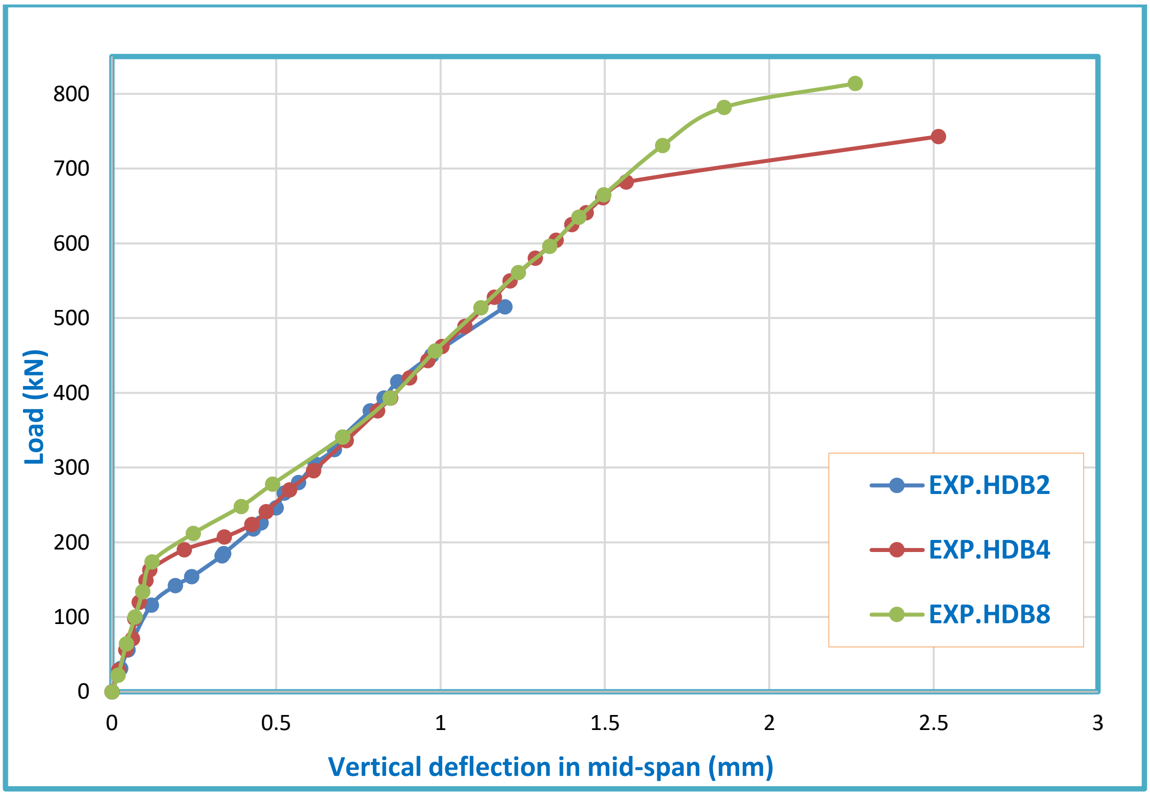

Figure (4.16) Effect thickness of the RPC layer on the load-deflection curve for (a/h = 1.25/3)

4.4.3.2 Effect of RPC layer Thickness on First Cracking and Ultimate loads

Generally, the initial cracking load and failure load of the hybrid deep beams were greater than those for the normal deep beams, the reason for this increase may be due to the presence of RPC which improved the properties of concrete (gave additional shear strength).

Experimental outcome indicated that the ultimate load of the deep beams examined was affected by the thickness of the RPC layer and the ultimate load increased with increasing thickness of RPC layer. The ultimate load for the hybrid deep beam (HDB-7) increased approximately (52.64 %) and (12.93%) with respect to control deep beam (NDB-1) and hybrid deep beam (HDB-3), Respectively. The ultimate load for the hybrid deep beam (HDB-8) increased about (54.01 %) and (8.64%) with respect to control deep beam (NDB-2) and hybrid deep beam (HDB-4), respectively. The ultimate load for the hybrid deep beam (HDB-3) increased about (35.17 %) with respect to control deep beam (NDB-1). The ultimate load for the hybrid deep beam (HDB-4) increased approximately (41.76 %) with respect to control deep beam (NDB-2).

The first cracking load in hybrid deep beams was greater than normal deep beam due to hybrid effect. The first cracking load of the hybrid beams with RPC in the compression region was greater than the normal deep beams by about (23.89% and 16.67%) at (a/h= 2/3 and 1.25/3) respectively. The first cracking load in HDB-8 (RPC 125 mm) was greater than NDB-1 and HDB-4 (RPC 75 mm) by about (17.78% and 2.4%) respectively, while the first cracking load of the hybrid deep beams with RPC (75 mm) in the tension zone greater than the normal deep beams by about (13.89 % and 15 %) at (a/h= 2/3 and 1.25/3) respectively.

4.5 Failure Mode

The pattern of failure in the normal deep beams (NDB-1 and NDB-2) was the diagonal compression in the shear zone, where the arch occurred in the beam (NDB-1) was due to increasing the a/h, as shown in Plates (1 and 2).

The diagonal compression failure in the shear zone was a failure pattern for the hybrid deep beams (HDB-3 and HDB-4), the arch occurred in the beam (HDB-3) was due to increased the a/h, as shown in Plate (3 and 4).

In the hybrid deep beams (HDB-5 and HDB-6) with RPC in compression region and NC in tension region, the bearing failure pattern occurred, as shown in Plate (5 and 6).

The diagonal compression failure in the shear zone was a failure pattern for the hybrid deep beams (HDB-7 and HDB-8), as shown in Plate (7 and 8).

Chapter Five

5

FINITE ELEMENT ANALYSIS

CHAPTER FIVE

FINITE ELEMENT ANALYSIS

5.1 Introduction

Traditional methods based on experimental data used in the analysis and design of RC structures cannot solve all practical problems of their difficulties. So, numerical methods are used to obtain approximate solutions for more complex problems. The finite element method (FEM) is one of the numerical methods used for this purpose.

FEM is a numerical technique based on the division of the member into small elements connected with each other by nodes. This method is widespread to solve engineering problems in various geometric fields such as a stress analysis, heat transfer and fluid flow.

The behavior of the concrete structures is nonlinear due to the non-linearity of the materials resulting from; yielding of the reinforcing steel, crushing the concrete, cracking the concrete member, and non-linear response to the stress-strain of concrete. Structural geometry, which has large deformations (such as slender columns, long beam, and thin plates), also causes nonlinear behavior.

The formulation of the finite element, nonlinear solution techniques, modeling, and properties of the materials are contained in appendix (B).

5.2 Modeling of Specimens (Deep beams):

The **ANSYS** (**AN**alysis **SYS**tem) version 17.2 (2016), was used for modeling the specimens. Choosing the element type and defining both the real constants and the properties of the materials for the selected element is considered an important stage before modeling the specimens.

5.2.1 Choosing Element Type

In this study. Three types of elements were chosen: SOLD65, LINK180, and SOLD185, representing, concrete (NSC and RPC), reinforcement steel bars (diameter 12 mm and 6 mm) and plat for (supports and loading), respectively.

5.2.2 Real Constant

A real constant set No. 1 was used for the SOLD65 element. While the real constants of the LINK180 element, which represent the longitudinal reinforcement steel bar and shear reinforcement steel bar, were used Link Section 510 for reinforcement steel bar diameter 6 mm, and Link Section 636 for reinforcement steel bar diameter 12 mm, as shown in Table (5.1). All specimens have the same reinforcement steel bars. The longitudinal flexural steel used was 5 Ø 12 mm, arranged in two layers. The shear reinforcement steel bars (horizontal and vertical) was 6 mm diameter and distributed every 50 mm.

Table (5.1) Real constant for reinforcement steel bar

Element type	Section name	Constant	
LINK180	510	Cross-section area (mm^2)	24.6
LINK180	636	Cross-section area (mm^2)	111.2

5.2.3 Material Properties

Each element has a behavior of the material model (material properties). Table (5.2) includes a summary of the parameters adopted in the finite element models (FEM), for the current study.

Table (5.2) Parameters for element used in (FEM) for deep beams

Concrete								
Concrete Parameter	**definition**	**Deep Beams**						
		NDB-1 NDB-2	**HDB-3 HDB-4**		**HDB-5 HDB-6**		**HDB-7 HDB-8**	
		NSC	**NSC**	**RPC**	**NSC**	**RPC**	**NSC**	**RPC**
f'c*	**Compressive Strength (N/mm^2)**	29.45	32.4	60.2	31.85	60.7	32.4	60.2
f'sp*	**Splitting Strength (N/mm^2)**	3.07	3.42	5.33	3.33	5.39	3.42	5.33
υ**	**Poisson Ratio**	0.2	0.2	0.2	0.2	0.2	0.2	0.2
E_c*	**Young Modulus (N/mm^2)**	25506	26753	32659	26525	32659	26753	32659
β_0**	**Shear Transfer Parameters**	0.56	0.56	0.3	0.56	0.3	0.56	0.3
β_1**		0.84	0.84	0.5	0.84	0.5	0.84	0.5

Reinforcing Steel			
Reinforcing Steel Parameter	**definition**	**Bar Diameter**	
		6 mm	**12mm**
E_s**	Young Modulus (N/mm^2)	200000	200000
f_y*	Stress of Yielding (N/mm^2)	510.4	636.2
υ_s**	Poisson Ratio	0.3	0.3
A*	Cross Section area (mm^2)	24.6	111.2
Steel Plate			
E_s**	Young Modulus (N/mm^2)	200000	
υ_s**	Poisson Ratio	0.3	

* From experimental tests ** Assumed

5.3 Meshing

SOLID65 was used to represent normal concrete and reactive powder concrete. SOLID185 was used to represent both; the loading plate and the supports. The dimensions of each element in SOLD 65 and SOLD185 were (12.5 × 12.5 × 25) mm. LINK180 was used to represent the reinforcing steel. All structural members were divided into smaller elements as shown in Figures (5.1), (5.2), and (5.3).

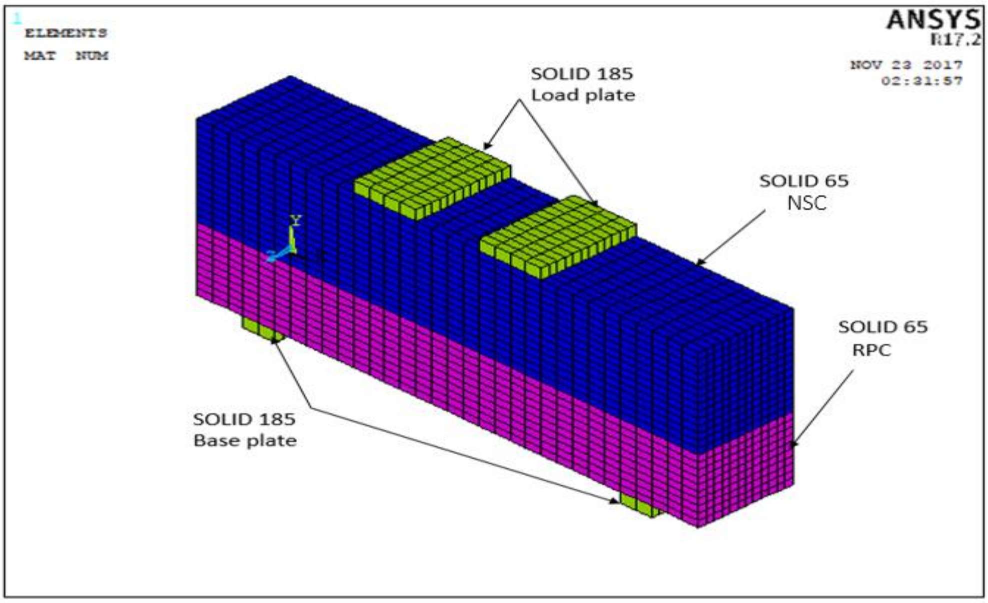

Figure (5.1) Meshing of SOLID185 and SOLID65

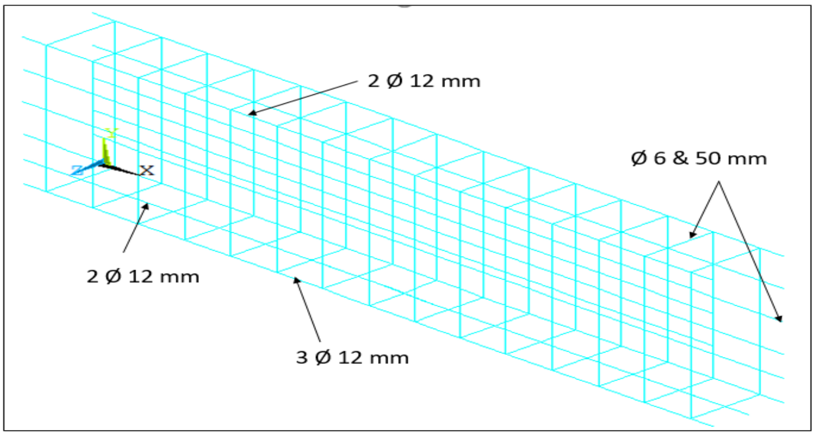

Figure (5.2) Meshing of LINK180

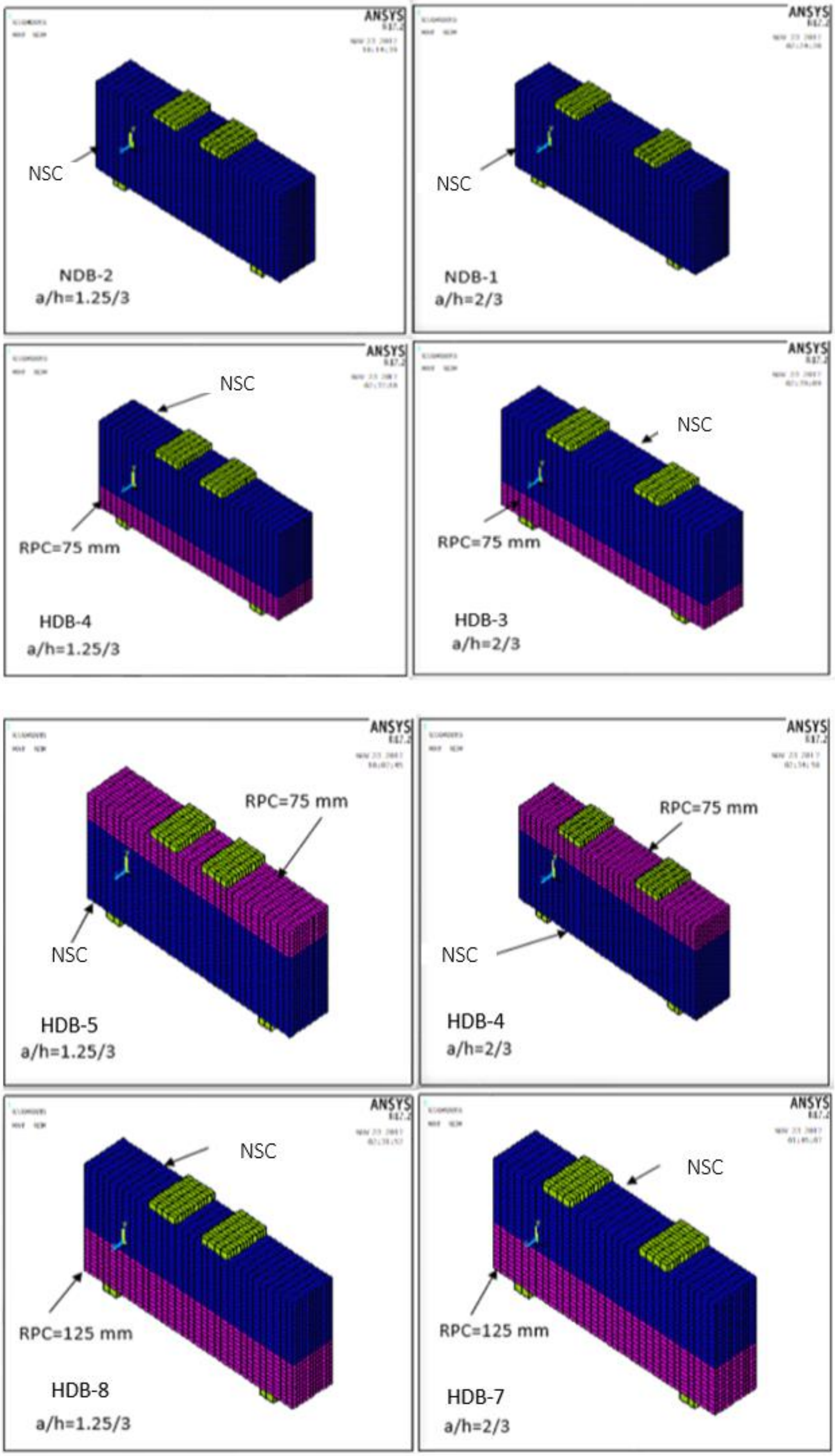

Figure (5.3) Meshing of all specimens

5.4 Loading and Boundary Conditions

For the purpose of preventing stress concentration in the contact area between the loading points and the concrete, and between concrete and support. Figures (5.4) illustrates the representation of the support application at the nods.

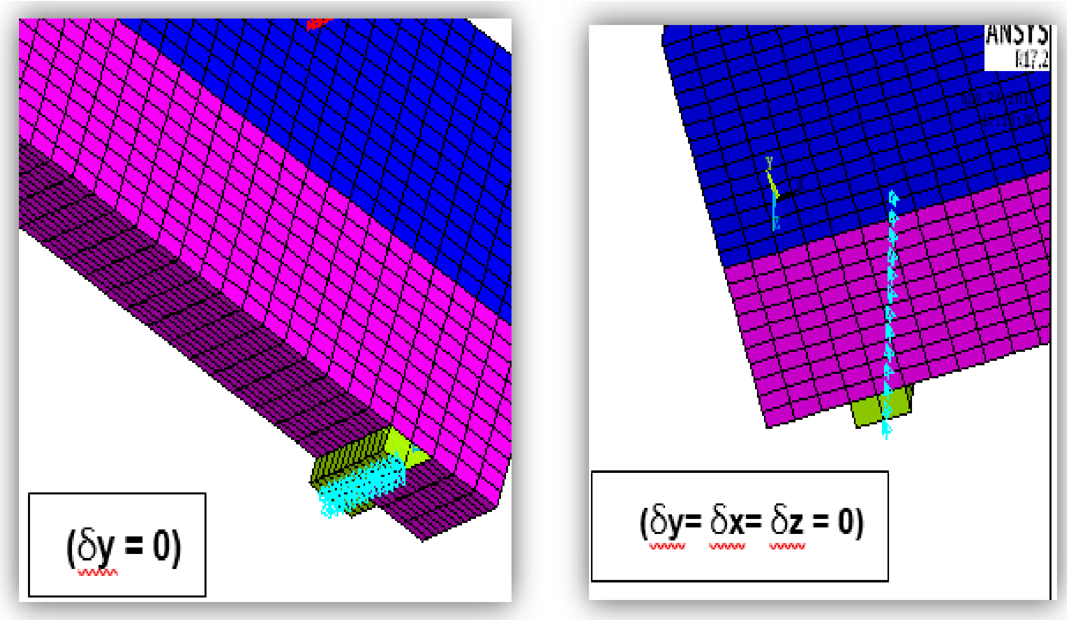

Figure (5.4) Representation of the support

5.5 Numerical analysis

5.5.1 Load- Deflection Response

In the experimental part, LVDT was placed in the center of the bottom of the deep beam for the purpose of measuring the deflection at all loading stages. In the ANSYS program, the deflection was measured at the same location (center of the lower face of the deep beam). Figure (5.5) represents the deflection shape of the ANSYS model for HDB-4. The Figures from (5.6) to (5.13) illustrate the load-deflection (at mid-span) curves obtained from the finite element method and compare them with the experimental results.

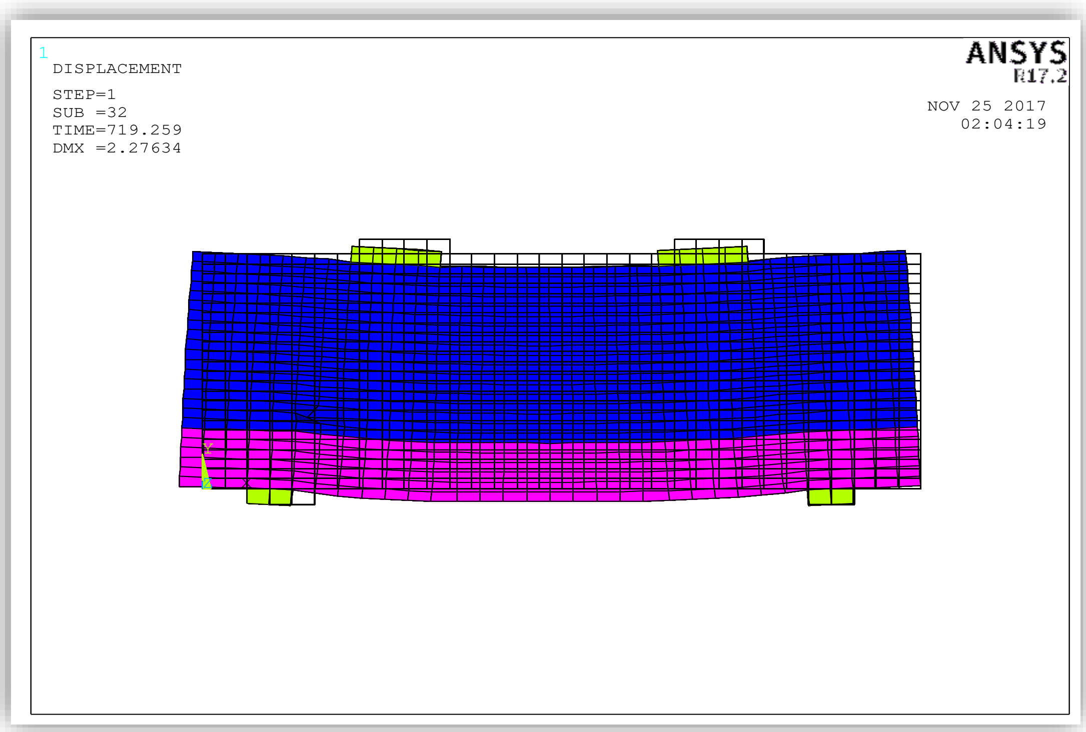

Figure (5.5) Deflection shape of the ANSYS model for HDB-4

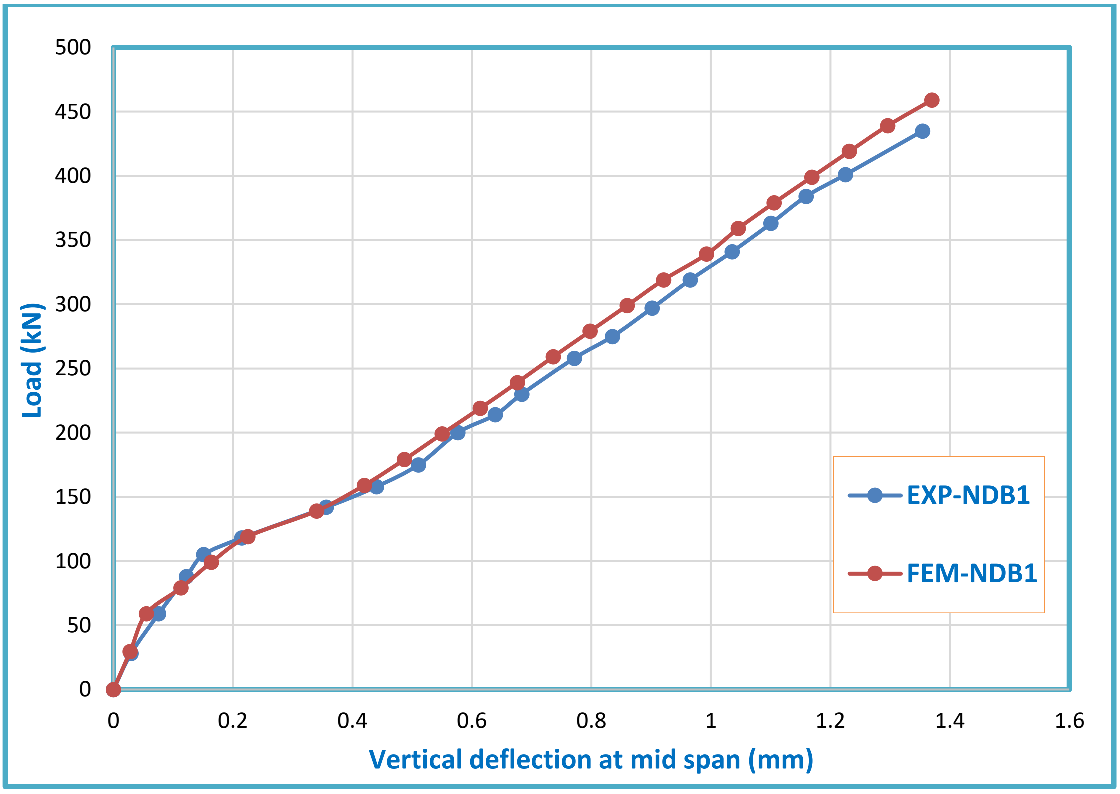

Figure (5.6) Load-vertical deflection of the beam NDB-1 at a/h=2/3 by experimental work and FEM

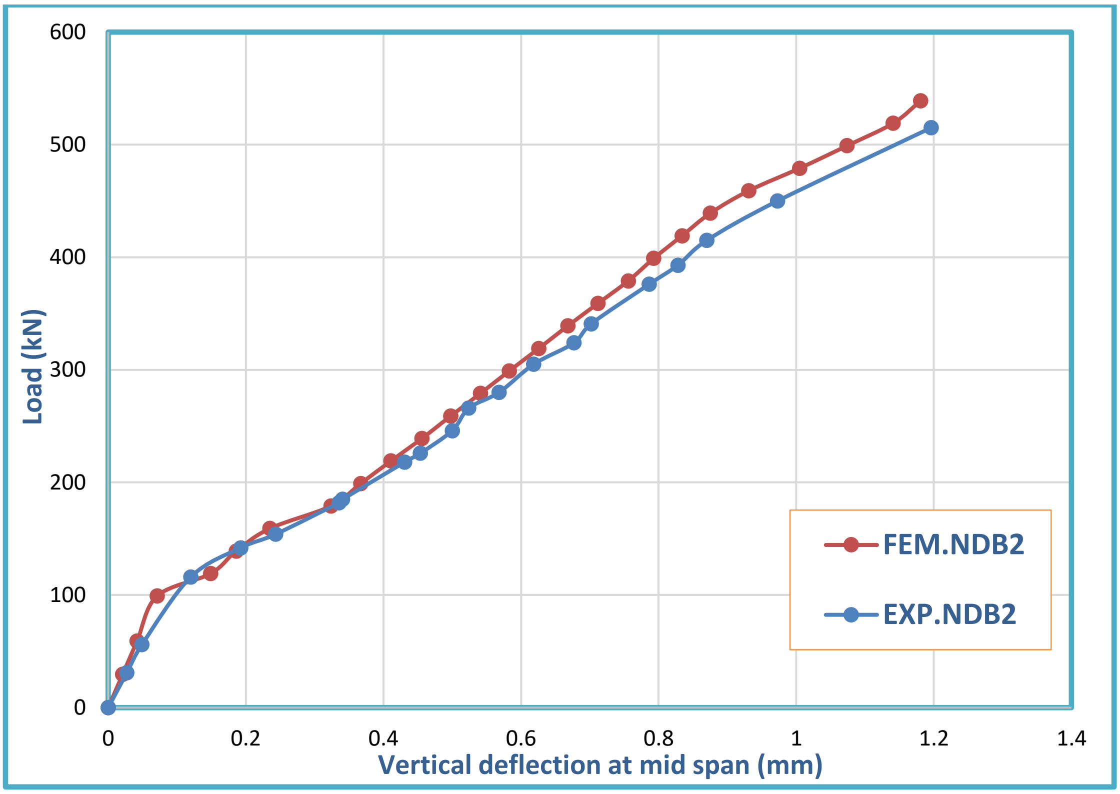

Figure (5.7) Load-vertical deflection of the beam NDB-2 at a/h=1.25/3 by experimental work and FEM

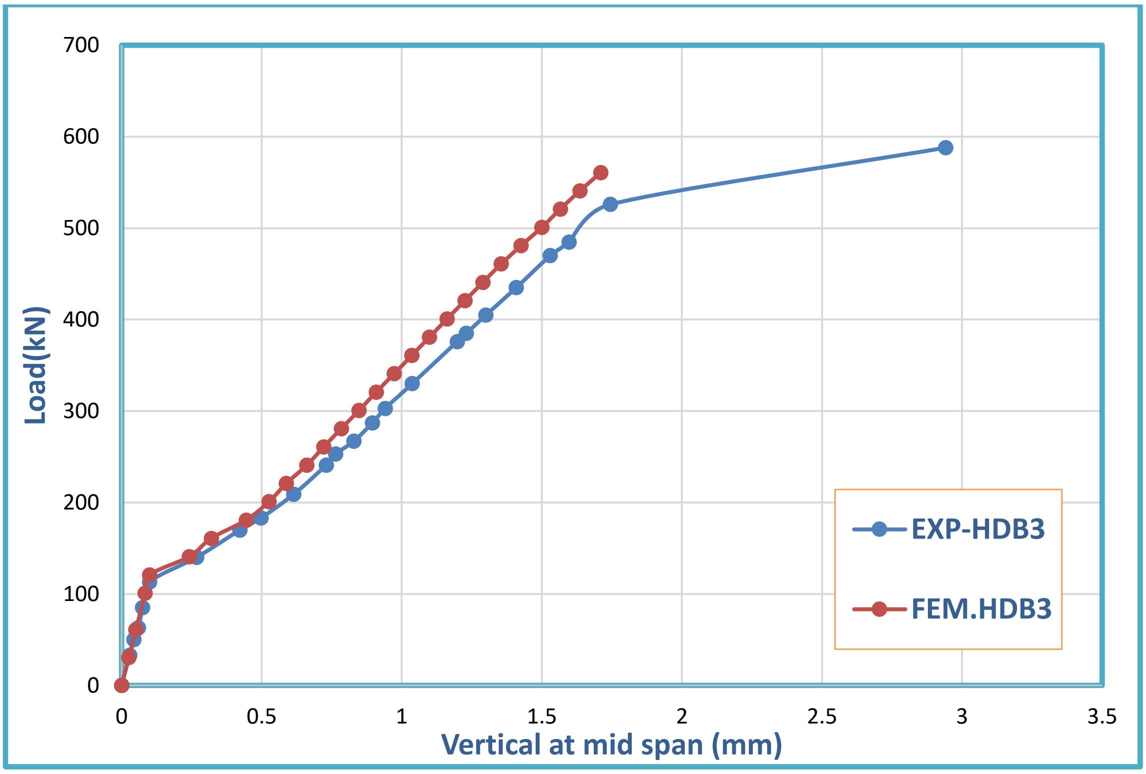

Figure (5.8) Load-vertical deflection of the beam HDB-3 at a/h=2/3 by experimental work and FEM

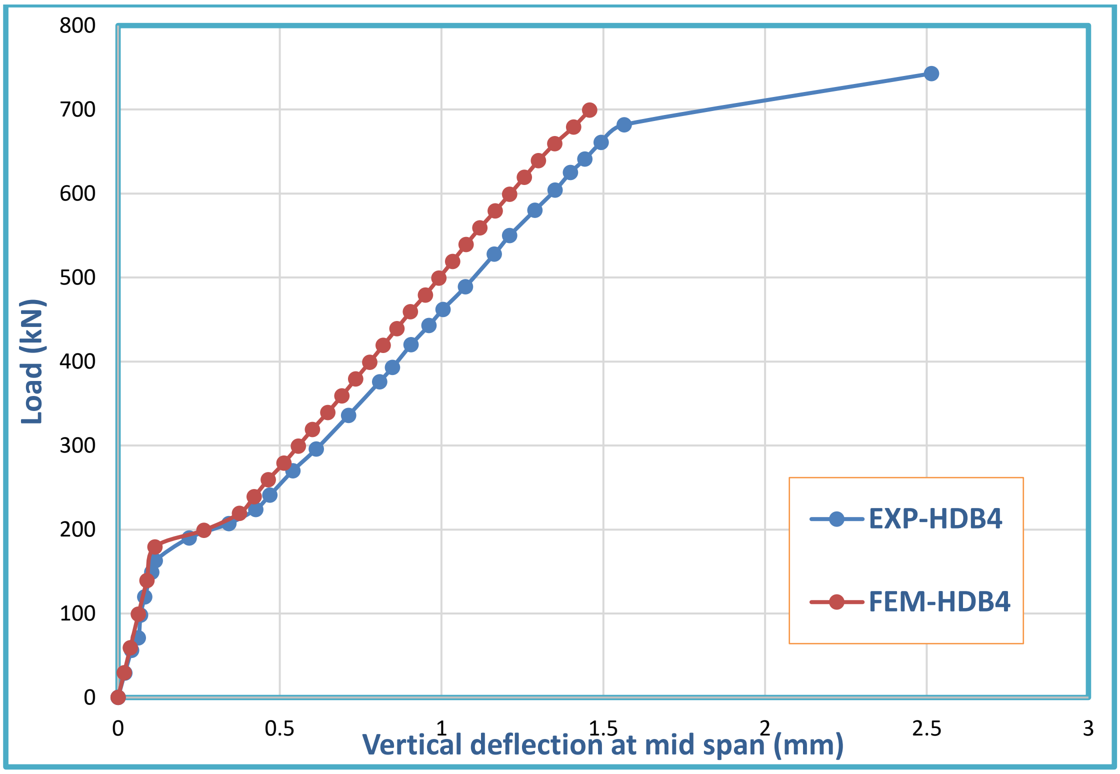

Figure (5.9) Load-vertical deflection of the beam HDB-4 at a/h=1.25/3 by experimental work and FEM

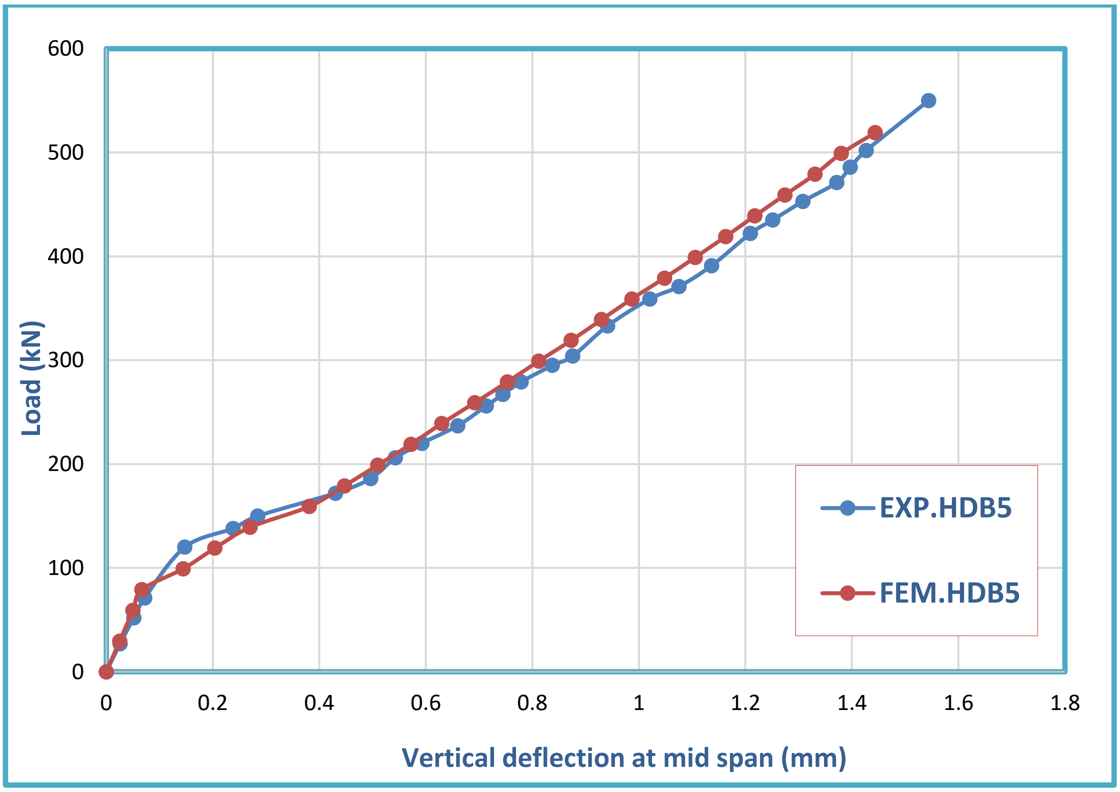

Figure (5.10) Load-vertical deflection of the beam HDB-5 at a/h=2/3 by experimental work and FEM

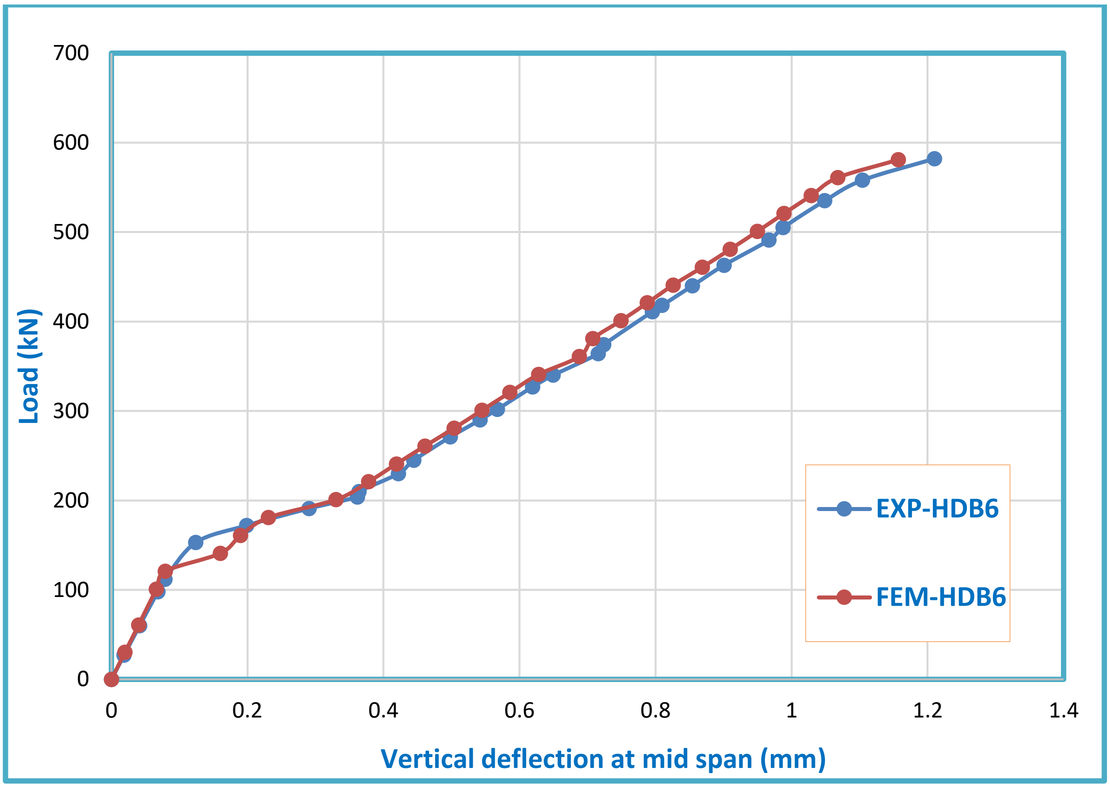

Figure (5.11) Load-vertical deflection of the beam HDB-6 at a/h=1.25/3 by experimental work and FEM

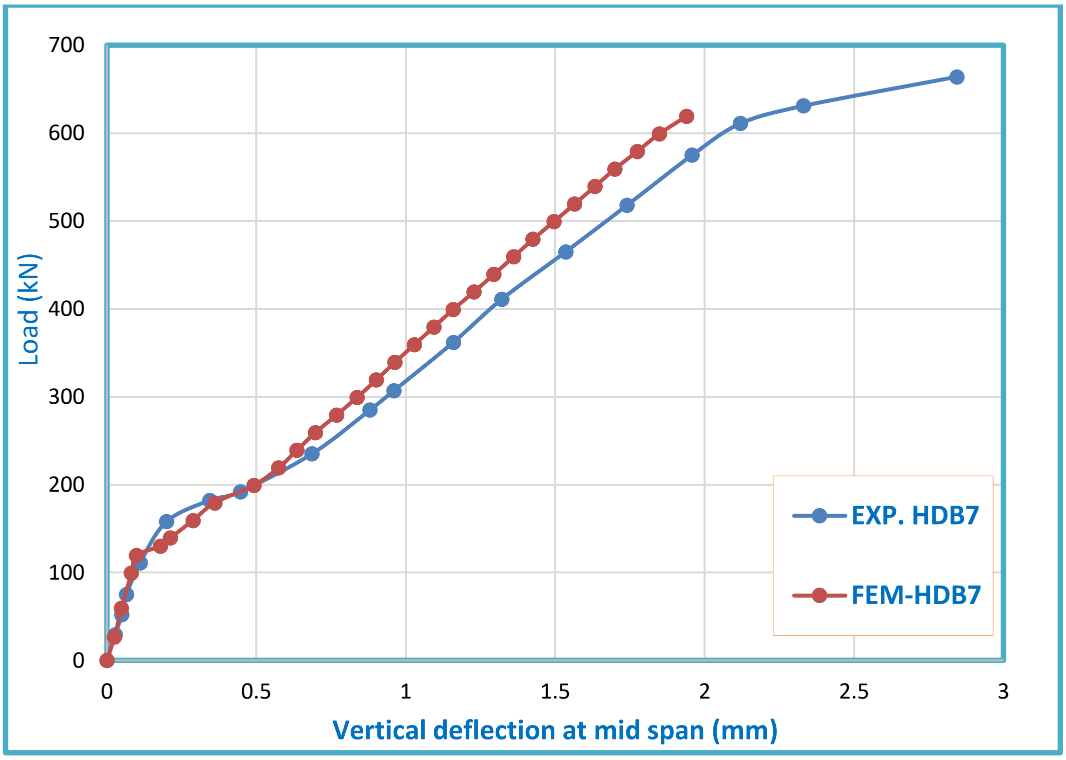

Figure (5.12) Load-vertical deflection of the beam HDB-7 at a/h=2/3 by experimental work and FEM

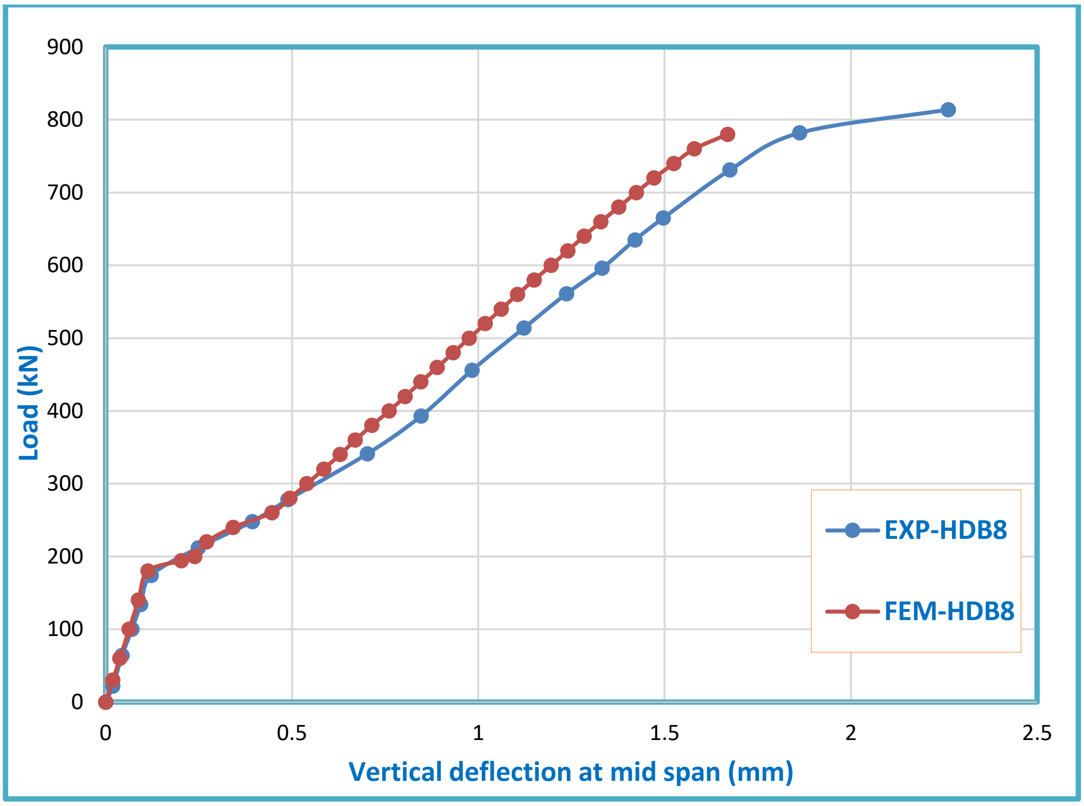

Figure (5.13) Load-vertical deflection of the beam HDB-8 at a/h=1.25/3 by experimental work and FEM

5.5.2 Ultimate Load

There was a good convergence between the experimental ultimate load and the FEM ultimate load, for all specimens. Table (5.3) contains the values of the ultimate load for the tested deep beams in a finite element method and the experimental work, with a comparison between them. The maximum difference is (6.74 %) and the minimum difference is (0.19 %).

Table (5.3) Experimental and FEM ultimate load

Deep beam	Ultimate Load (kN)		
	Experimental $Pu_{(EXP)}$	FEM $Pu_{(FEM)}$	$\frac{Pu(FEM) - Pu(EXP)}{Pu(FEM)} \times 100\%$
NDB-1	435	459.09	5.54
NDB-2	528.52	539.09	2

Table (5.3) Experimental and FEM ultimate load (Continue)

Deep beam	Ultimate Load (kN)		
	Experimental $Pu_{(EXP)}$	FEM $Pu_{(FEM)}$	$\frac{Pu(FEM) - Pu(EXP)}{Pu(FEM)} \times 100\%$
HDB-3	588	560.87	- 4.6
HDB-4	749.23	699.26	- 6.67
HDB-5	551	539.09	- 2.16
HDB-6	582	580.87	- 0.19
HDB-7	664	619.26	- 6.74
HDB-8	814	780	- 4.18

5.5.3 Cracks propagation

The Figures from (5.14) to (5.21) illustrate the spread of the cracks of deep beams analyzed by the (FEM) at the ultimate load. One of the advantages of the ANSYS program that it shows the spread of cracks in each stage of loading. The first crack is slight crack and it is symbolized by a red circle outline, second cracking is a moderate crack and it is symbolized by green circle outline, and the crack of failure is the third crack which is symbolized by a blue circle outline. The signs of cracks are as following:

Flexural crack.

Compressive crack.

Diagonal tensile crack.

Two cracks (diagonal and compressive crack).

Three cracks (Diagonal tensile and compressive crack)

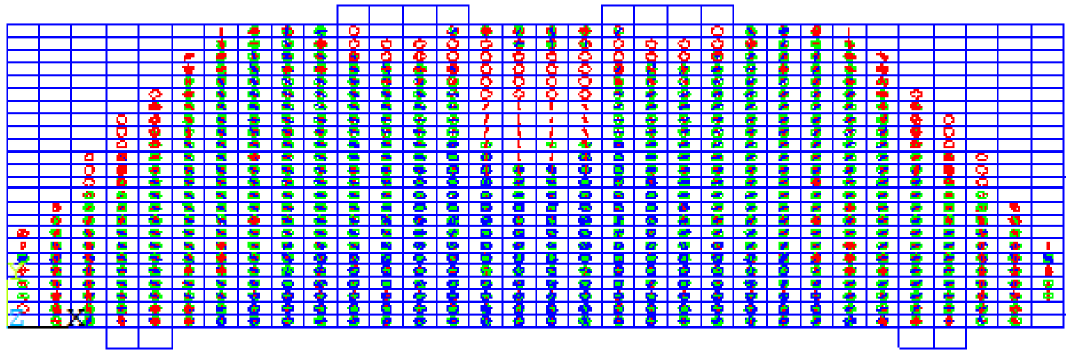

Figure (5.14) Ultimate crack propagation of deep beam (NDB-1)

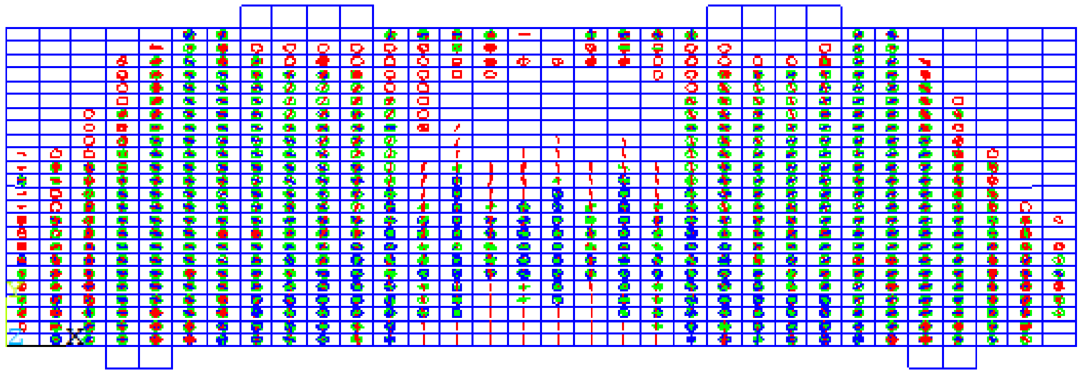

Figure (5.15) Ultimate crack propagation of deep beam (NDB-2)

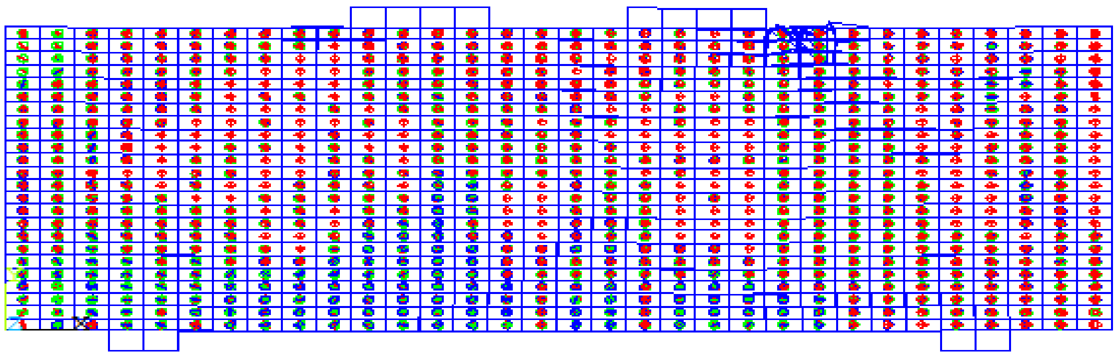

Figure (5.16) Ultimate crack propagation of deep beam (HDB-3)

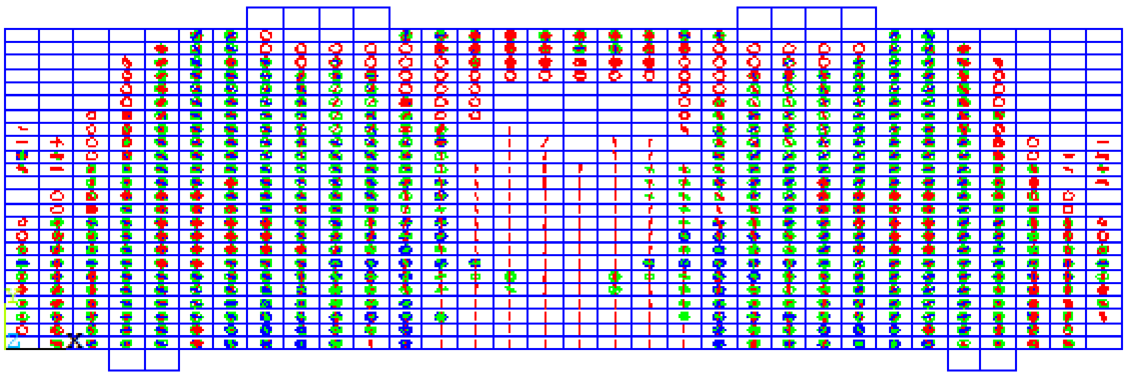

Figure (5.17) Ultimate crack propagation of deep beam (HDB-4)

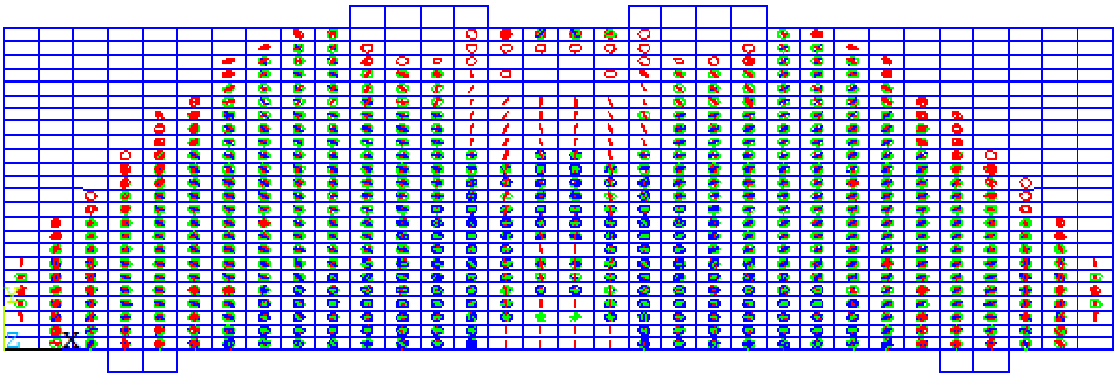

Figure (5.18) Ultimate crack propagation of deep beam (HDB-5)

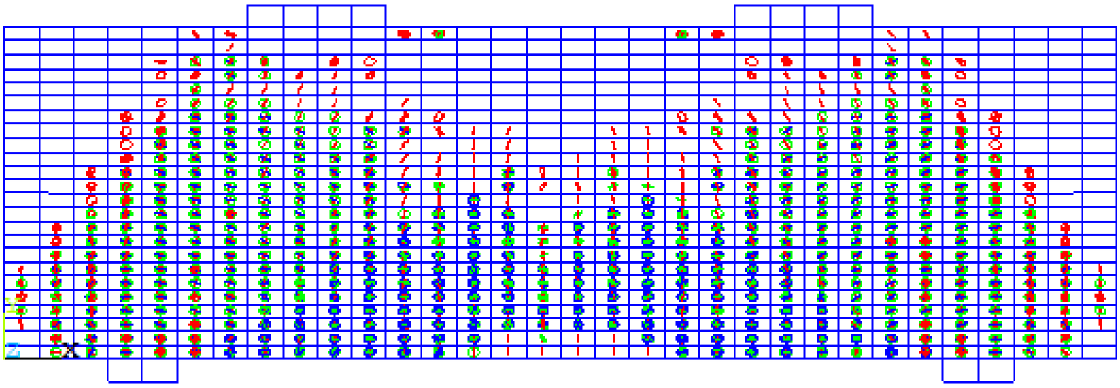

Figure (5.19) Ultimate crack propagation of deep beam (HDB-6)

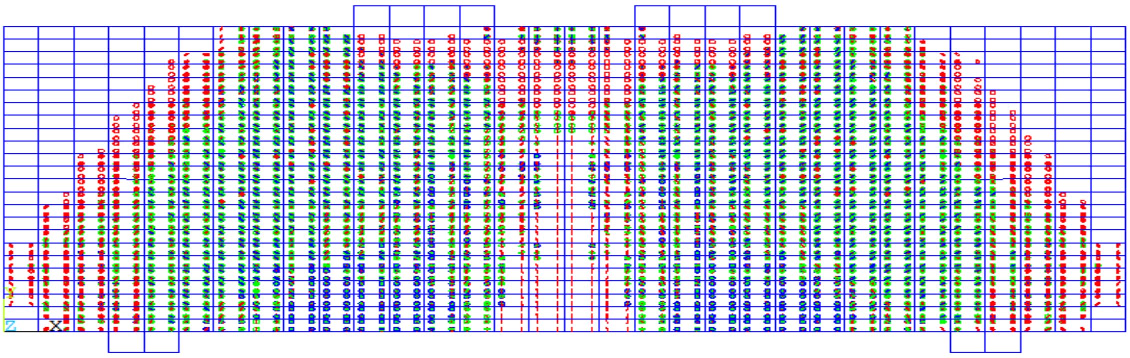

Figure (5.20) Ultimate crack propagation of deep beam (HDB-7)

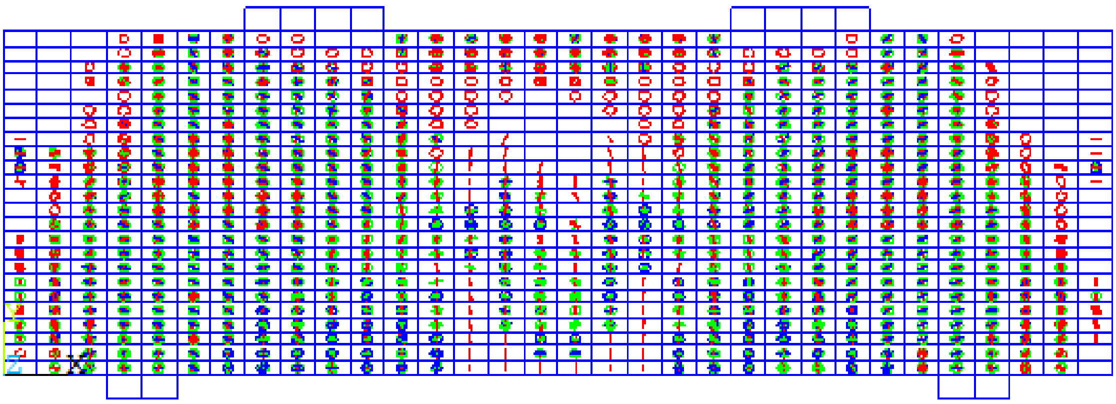

Figure (5.21) Ultimate crack propagation of deep beam (HDB-8)

5.6 Parametric Study

The purpose of the parametric study is to cover the research objectives with more detailed information. The effects of these parameters include: first cracking load, ultimate load, and load-deflection relations depending on the numerical analysis model used to represent the deep beams examined in the current study.

The studied parameters are the following:

1 -a/h= 1.5/3.

2- RPC (50 mm) layer in the tension region.

3- RPC (50 mm) layer in the compression region.

4 -RPC (50 mm) in tension region and compression region at the same cross-section.

5- RPC for overall depth

5.7 Description of the Specimens used in FEM

Twenty-four deep beams analyzed by ANSYS program under conditions similar to deep beams in the experimental program. The specimens were divided into seven groups (G-1, G-2, G-3, G-4, G-5, G-6, G-7, and G-8). Group (G-1) included normal deep beams (NDB-2/3, NDB-1.5/3, and NDB-1.25/3). Group (G-2) had hybrid cross-section RPC (50mm) in compression zone and included (HDBC50-2/3, HDBC50-1.5/3, and HDBC50-1.25/3). Group (G-3) had hybrid cross-section RPC (75mm) in compression zone and included (HDBC75-2/3, HDBC75-1.5/3, and HDBC75-1.25/3). Group (G-4) had hybrid cross-section RPC (50mm) in tension zone and included (HDBT50-2/3, HDBT50-1.5/3, and HDBT50-1.25/3). Group (G-5) had hybrid cross-section RPC (75mm) in tension zone and included (HDBT75-2/3, HDBT75-1.5/3, and HDBT75-1.25/3). Group (G-6) had hybrid cross-section RPC (125mm) in tension zone and included

(HDBT125-2/3, HDBT125-1.5/3, and HDBT125-1.25/3). Group (G-7) had hybrid cross-section RPC (50mm) in tension zone and (50 mm) in compression zone and included (HDBCT50-2/3, HDBCT50-1.5/3, and HDBCT50-1.25/3). Group (G-8) had homogenies cross-section RPC (300mm) for overall depth and included (RPC-2/3, RPC-1.5/3, and RPC-1.25/3) Table (5.4) includes the details of the specimens used in numerical analysis program FEM. Table (5.5) includes the FEM Result of the deep beams.

Table (5.4) Details the deep beams by FEM

Specimens Name	a/h	Thickness of RPC (mm)	Location of RPC	Thickness of NSC (mm)
NDB-1.5/3	1.5/3	0	/	300
HDBC50-2/3	2/3	50	Compression	250
HDBC50-1.5/3	1.5/3	50	Compression	250
HDBC50-1.25/3	1.25/3	50	Compression	250
HDBC75-2/3	2/3	75	Compression	225
HDBC75-1.5/3	1.5/3	75	Compression	225
HDBC75-1.25/3	1.25/3	75	Compression	225
HDBT50-2/3	2/3	50	Tension	250
HDBT50-1.5/3	1.5/3	50	Tension	250
HDBT50-1.25/3	1.25/3	50	Tension	250
HDBT75-2/3	2/3	75	Tension	225
HDBT75-1.5/3	1.5/3	75	Tension	225
HDBT75-1.25/3	1.25/3	75	Tension	225
HDBT125-2/3	2/3	125	Tension	175
HDBT125-1.5/3	1.5/3	125	Tension	175
HDBT125-1.25/3	1.25/3	125	Tension	175

Table (5.4) Details the deep beams by FEM **(**Continue)

Specimens Name	a/h	Thickness of RPC (mm)	Location of RPC	Thickness of NSC (mm)
HDBCT50-2/3	2/3	50	Compression & Tension	200
HDBCT50-1.5/3	1.5/3	50	Compression & Tension	200
HDBCT50-1.25/3	1.25/3	50	Compression & Tension	200
RPC-2/3	2/3	300	Overall depth	0
RPC-1.5/3	1.5/3	300	Overall depth	0
RPC-1.25/3	1.25/3	300	Overall depth	0

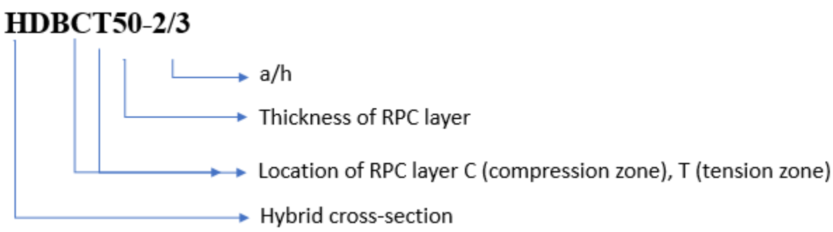

Table (5.5) FEM Result of the deep beams

Specimens Name	First Crack load (kN) P_{cr}	Vertical Deflection at First Crack load (mm) Δcr	Ultimate Load (kN) P_u	Vertical Deflection at Ultimate load (mm) Δu	$\frac{Pcr}{Pu} \times 100\%$	$\frac{\Delta u}{\Delta cr}$
NDB-2/3	79.09	0.113	459.09	1.37	17.2	12.12
NDB-1.5/3	99.09	0.126	499.09	1.216	19.9	9.65
NDB-1.25/3	119.09	0.149	539.09	1.181	22.1	7.93
HDBC50-2/3	99.09	0.146	499.09	1.386	19.9	9.49
HDBC50-1.5/3	119.09	0.16	539.09	1.229	22.1	7.68

Table (5.5) FEM Result of the deep beams (Continue**)**

Specimens Name	First Crack load (kN) P_{cr}	Vertical Deflection at First Crack load (mm) Δcr	Ultimate Load (kN) P_u	Vertical Deflection at Ultimate load (mm) Δu	$\frac{Pcr}{Pu} \times 100\%$	$\frac{\Delta u}{\Delta cr}$
HDBC50-1.25/3	142	0.17	554.4	1.05	25.6	6.18
HDBC75-2/3	99.09	0.144	519.09	1.444	19.1	10.03
HDBC75-1.5/3	121.6	0.16	559.09	1.245	21.7	7.78
HDBC75-1.25/3	160.87	0.185	580.87	1.157	27.7	6.25
HDBT50-2/3	140.87	0.252	560.87	1.699	25.1	6.74
HDBT50-1.5/3	180.9	0.259	620	1.499	29.2	5.79
HDBT50-1.25/3	200.9	0.333	680.9	1.398	29.5	4.2
HDBT75-2/3	140.87	0.242	560.87	1.711	25.1	7.07
HDBT75-1.5/3	180	0.252	660	1.652	27.3	6.56
HDBT75-1.25/3	199.26	0.266	699.26	1.458	28.5	5.48
HDBT125-2/3	130	0.179	619.26	1.94	21	10.84
HDBT125-1.5/3	179.26	0.216	739.26	1.894	24.2	7.69

Table (5.5) FEM Result of the deep beams (Continue)

Specimens Name	First Crack load (kN) P_{cr}	Vertical Deflection at First Crack load (mm) Δcr	Ultimate Load (kN) P_u	Vertical Deflection at Ultimate load (mm) Δu	$\frac{Pcr}{Pu} \times 100\%$	$\frac{\Delta u}{\Delta cr}$
HDBT125-1.25/3	200	0.239	780	1.669	25.6	6.98
HDBCT50-2/3	140.9	0.25	620.9	1.784	22.3	7.14
HDBCT50-1.5/3	160	0.278	660	1.52	24.2	5.47
HDBCT50-1.25/3	200	0.321	740	1.47	27	4.58
RPC-2/3	150	0.227	870	2.554	17.4	11.25
RPC-1.5/3	187.5	0.254	917.5	2.107	20.4	8.3
RPC-1.25/3	220	0.263	960	1.839	22.9	6.99

5.8 Effect of the (a/h)

The values of (a/h) used in this section were (2/3,1.5/3, and 1.25/3) for the purpose of investigating its effect on; load-deflection curve, first cracking load, and ultimate load.

5.8.1 Effect of the (a/h) on the Load-Deflection Response

Generally, the behavior of load-deflection curve in the deep beams was stiffer with decreased (a/h). Figures from (5.22) to (5.29) illustrate the effect of (a/h) on the relationship of the applied load/ vertical midspan deflection for all groups. The vertical midspan deflection at the first crack load increased with decreasing (a/h), but at the ultimate load the vertical midspan deflection decreased with decreasing (a/h), the vertical midspan deflection at ultimate load to the vertical midspan deflection at first crack load ratio (Δu / Δcr) decreased with decreased (a/h). Table (5.5) illustrates the vertical midspan deflection at first cracking load and ultimate load, as well as (Δu / Δcr) for all beams with different (a/h),

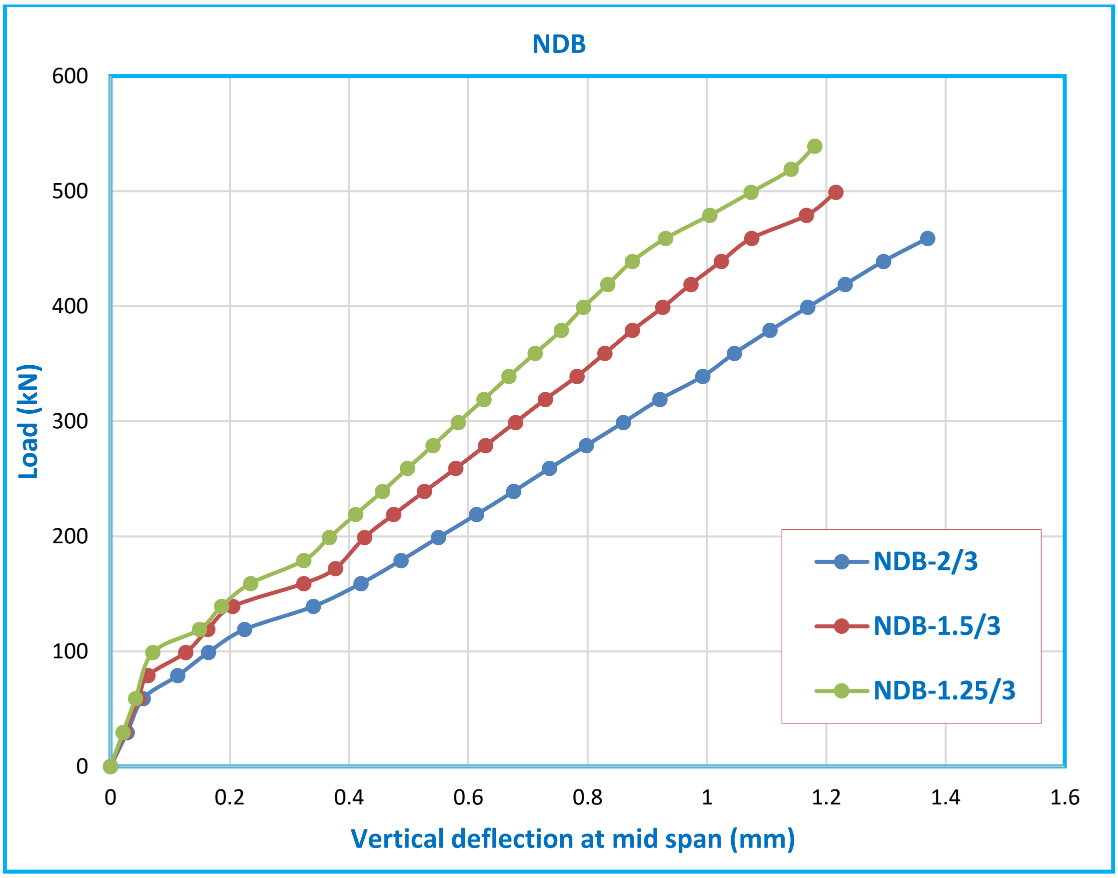

Figure (5.22) Relationship between the vertical mid-span deflection and the applied load in group (G-1)

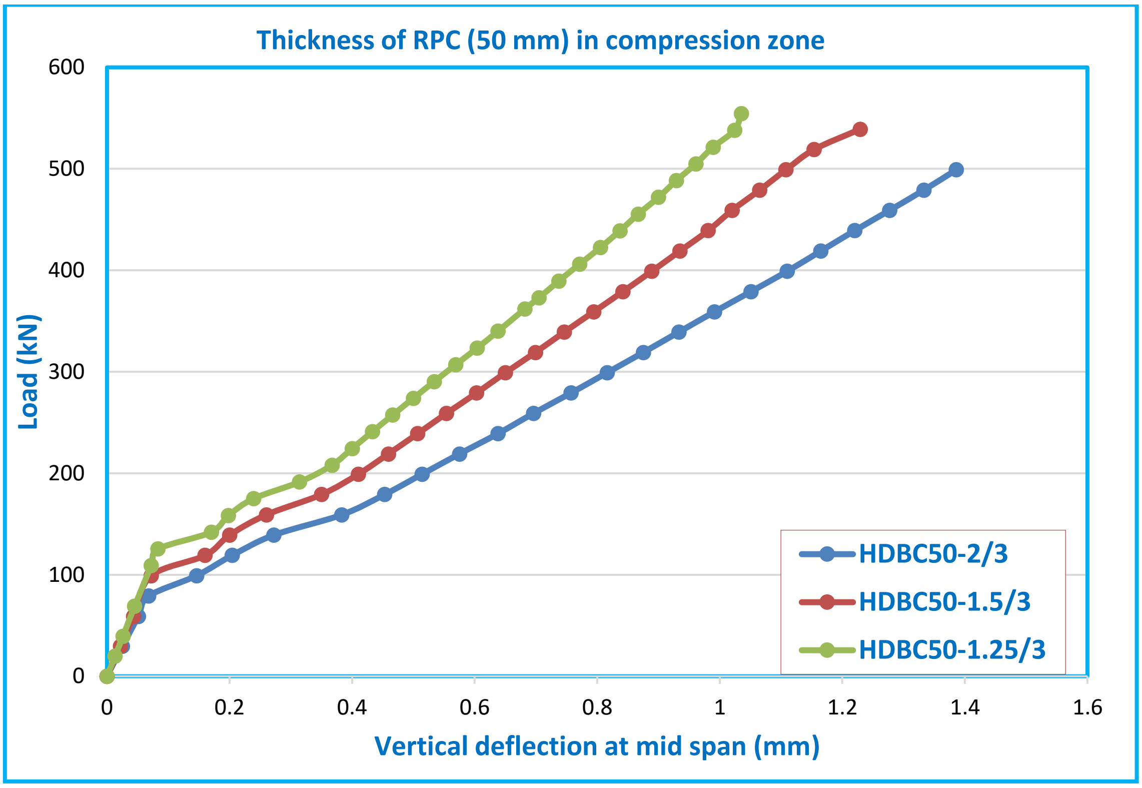

Figure (5.23) Relationship between the vertical mid-span deflection and the applied load in group (G-2)

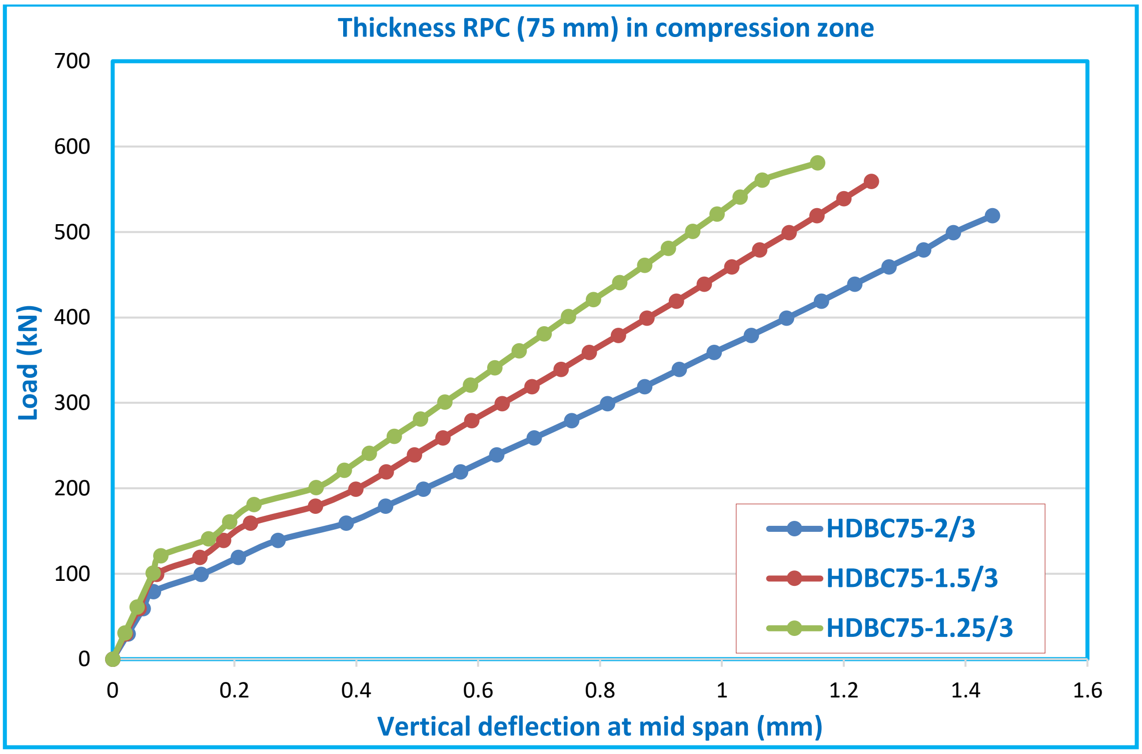

Figure (5.24) Relationship between the vertical mid-span deflection and the applied load in group (G-3)

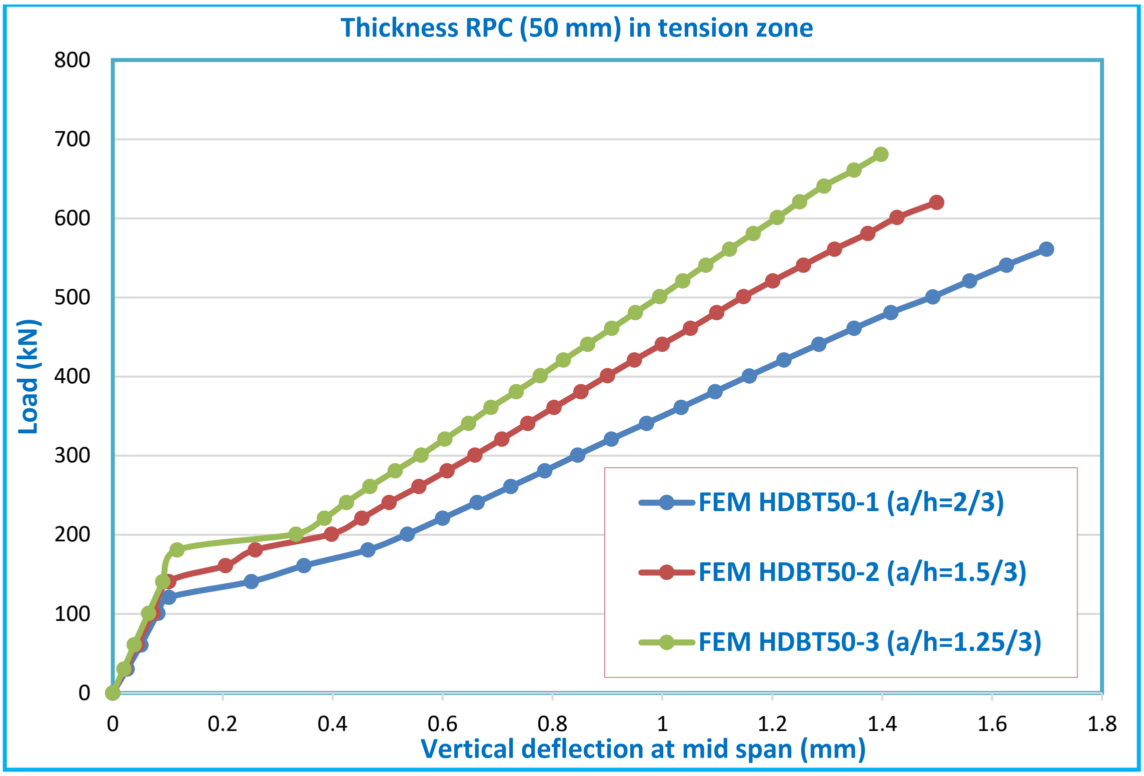

Figure (5.25) Relationship between the vertical mid-span deflection and the applied load in group (G-4)

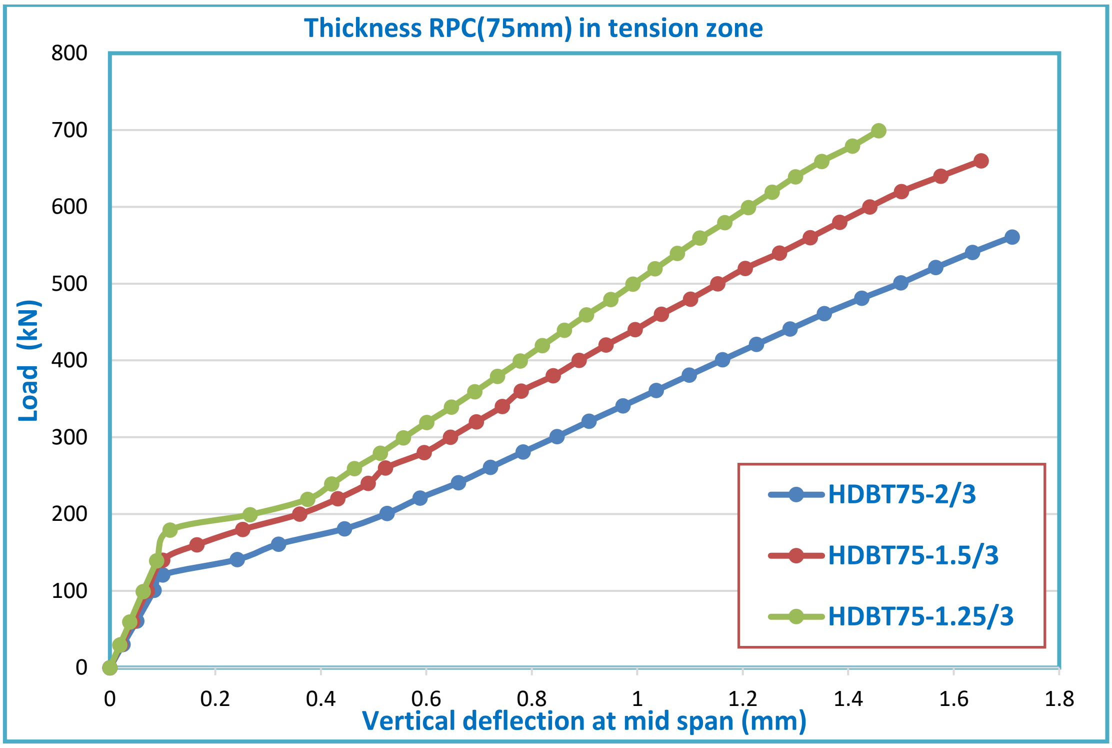

Figure (5.26) Relationship between the vertical mid-span deflection and the applied load in group (G-5)

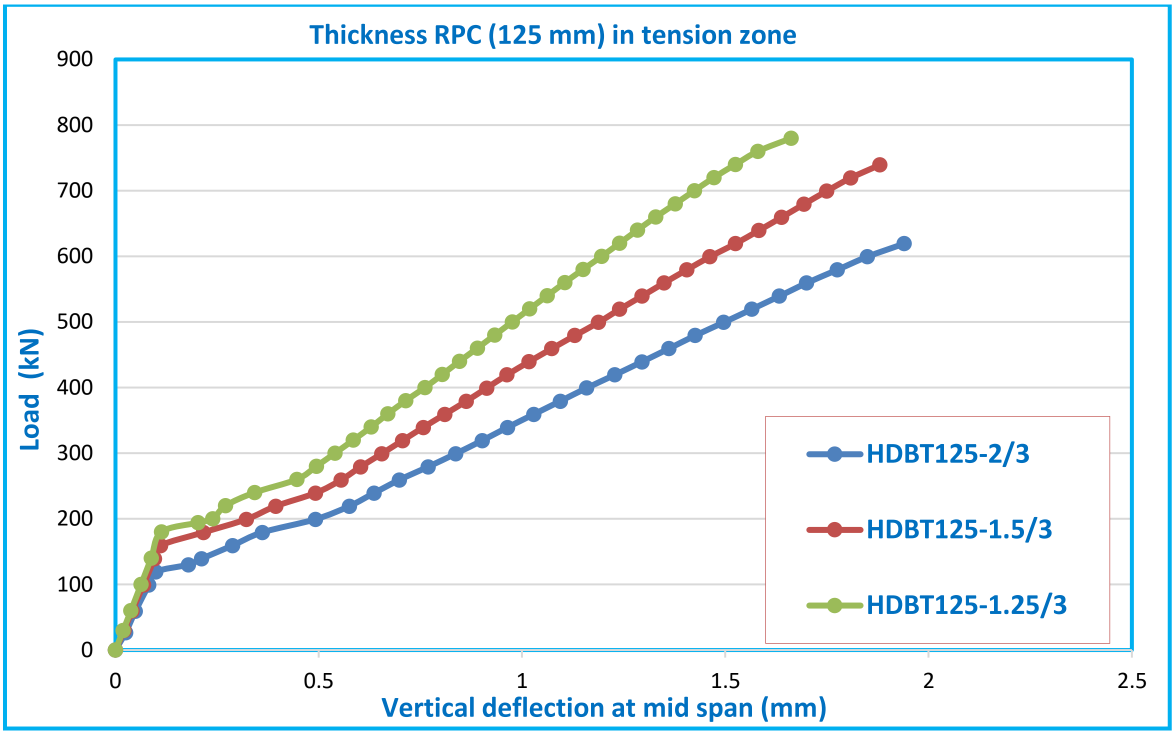

Figure (5.27) Relationship between the vertical mid-span deflection and the applied load in group (G-6)

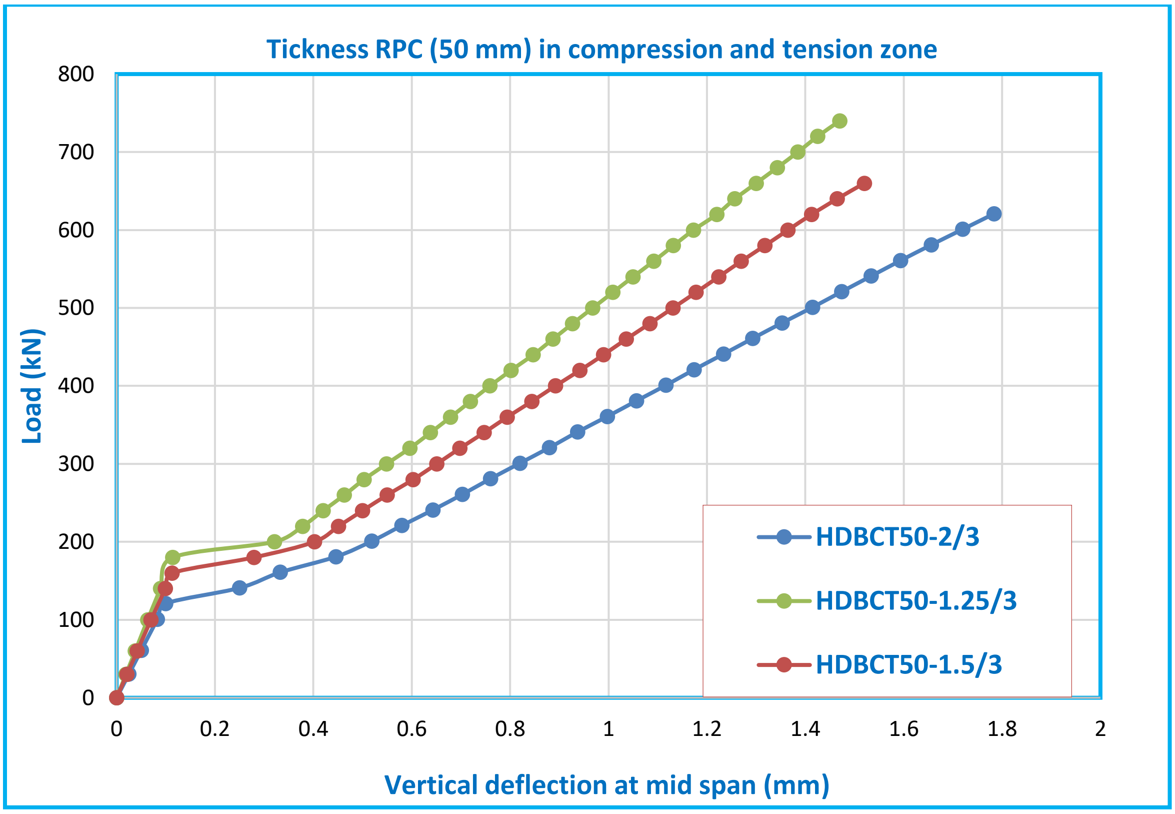

Figure (5.28) Relationship between the vertical mid-span deflection and the applied load in group (G-7)

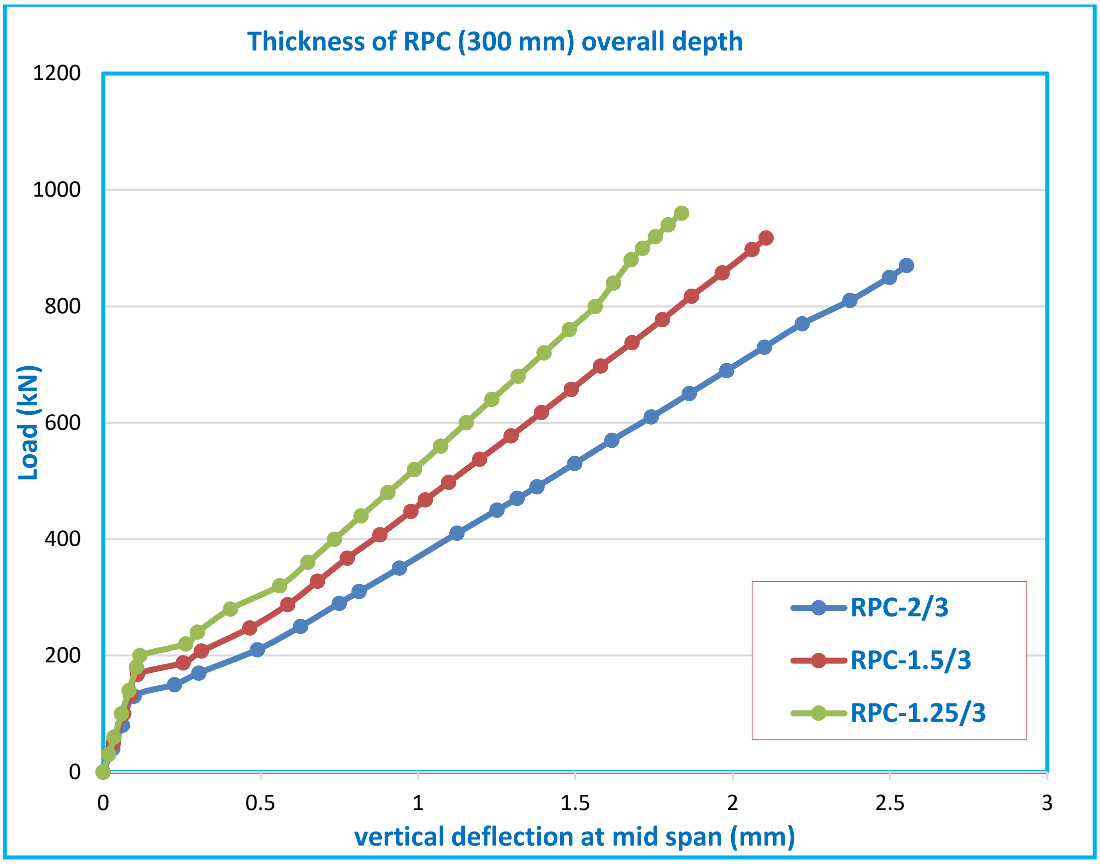

Figure (5.29) Relationship between the vertical mid-span deflection and the applied load in group (G-8)

5.8.2 Effect of the (a/h) on the First Crack and Ultimate Loads

Table (5.6) shows the results obtained from numerical analysis and it indicates the following:

1- First crack load increased with decreased (a/h) for all specimens. Table (5.6) shown the increased percentage of the first cracking loads for all deep beams. The maximum increase of the first cracking load was (62.3%) in the beam (HDBC75-1.25/3) with decreased (a/h) from (2/3) to (1.25/3),

2- The ultimate load increased with decreased (a/h). Table (5.6) shown the increased percentage of the ultimate loads for all deep beams. The maximum increase of the ultimate load was (26%) in the hybrid deep beam (HDBT125-1.25/3) with decreased (a/h) from (2/3) to (1.25/3).

3- The rate of the increasing in first cracking load was greater than the rate of the increasing in the ultimate load of all deep beams with decreased (a/h).

Table (5.6) Effect of (a/h) on the ultimate load and first cracking load for all specimens by FEM

Deep beam	First Cracking Load (P_{cr}) (kN)	Ultimate Load (P_u) (kN)	$\frac{(Pcri - Pcrr)}{Pcrr} \times 100\%$	$\frac{(Pui - Pur)}{Pur} \times 100\%$
Group (G-1)				
NDB-2/3^r	79.09	459.09	/	/
NDB-1.5/3^i	99.09	499.09	25.3	8.7
NDB-1.25/3^i	119.09	539.09	50.6	17.4
Group (G-2)				
HDBC50-2/3^r	99.09	499.09	/	/
HDBC50-1.5/3^i	119.09	539.09	20.2	8
HDBC50-1.25/3^i	142	554.4	43.3	11.1
Group (G-3)				
HDBC75-2/3^r	99.09	519.09	/	/
HDBC75-1.5/3^i	121.6	559.09	22.2	7.7
HDBC75-1.25/3^i	160.87	580.87	62.3	11.9
Group (G-4)				
HDBT50-2/3^r	140.87	560.87	/	/
HDBT50-1.5/3^i	180.9	620	28.4	10.5
HDBT50-1.25/3^i	200.9	680.9	42.6	21.4
Group (G-5)				
HDBT75-2/3^r	140.87	560.87	/	/
HDBT75-1.5/3^i	180	660	27.8	17.7
HDBT75-1.25/3^i	199.26	699.26	41.4	24.7

Table (5.6) Effect of (a/h) on the ultimate load and first cracking load for all specimens by FEM (Continue)

Deep beam	First Cracking Load (P_{cr}) (kN)	Ultimate Load (P_u) (kN)	$\frac{(Pcri - Pcrr)}{Pcrr} \times 100\%$	$\frac{(Pui - Pur)}{Pur} \times 100\%$
Group (G-6)				
HDBT125-2/3 ^{r}	130	619.26	/	/
HDBT125-1.5/3^i	179.26	739.26	37.9	19.4
HDBT125-1.25/3^i	200	780	53.8	26
Group (G-7)				
HDBCT50-1.25/3 ^{r}	140.9	620.9	/	/
HDBCT50-1. 5/3^i	160	660	13.6	6.3
HDBCT50-1.25/3^i	200	740	41.9	19.2
Group (G-8)				
RPC-2/3^r	150	870	/	/
RPC-1.5/3^i	187.5	917.5	25	5.5
RPC-1.25/3^i	220	960	46.7	10.3

i: -Considered deep beam   r: - Reference deep beam

5.9 Effect of Thickness of RPC

The thickness of RPC used in this section was (50, and 75) mm in compression region, (50, 75, and 125) mm in tension region, (50) mm in compression and tension region, and (300) mm for overall depth to investigate its effect on; load-deflection, first cracking load, and ultimate load.

5.9.1 Effect of Thickness of RPC on the Load-Deflection Response

Generally, the behavior of the load-vertical midspan deflection curves of the hybrid deep beams was symmetric with increasing thickness of the RPC layer only in the final stages of loading due to the increase of the ultimate load with increased thickness of the RPC layer, this led to increase the area under the load-deflection curves and the behavior was more ductile, as shown in Figures (5.30) to (5-35). The ($\Delta u / \Delta cr$) increased with increasing the thickness of RPC layer for all hybrid deep beams. In the hybrid deep beams (RPC in tension zone) with increased the thickness of RPC layer from (50mm) to (75 mm), (125 mm), and (300 mm for overall depth) the (Δu / Δcr) increased about (4.9, 60.8, and 66.9) %, respectively at (a/h= 2/3), and (13.3, 32.8 and 43.4) %, respectively, at (a/h= 1.5/3), and (30.5, 66.2 and 66.4) %, respectively, at (a/h= 1.25/3). For the hybrid deep beams (RPC in compression zone), when increasing the thickness of RPC layer from (50mm) to (75 mm) and (300 mm for overall depth) the (Δu / Δcr) increased about (5.7 and 18.5) %, respectively at (a/h= 2/3), and (1.3 and 8.1) %, respectively, at (a/h= 1.5/3), and (1.1 and 13.1)%, at (a/h=1.25/3), respectively.

The behavior of hybrid deep beams with RPC (50mm) in tension and compression zone was stiffer when compared with normal deep beams at same (a/h) due to the increase in the vertical mid-span deflection at ultimate load as a shown Figure (5.36).

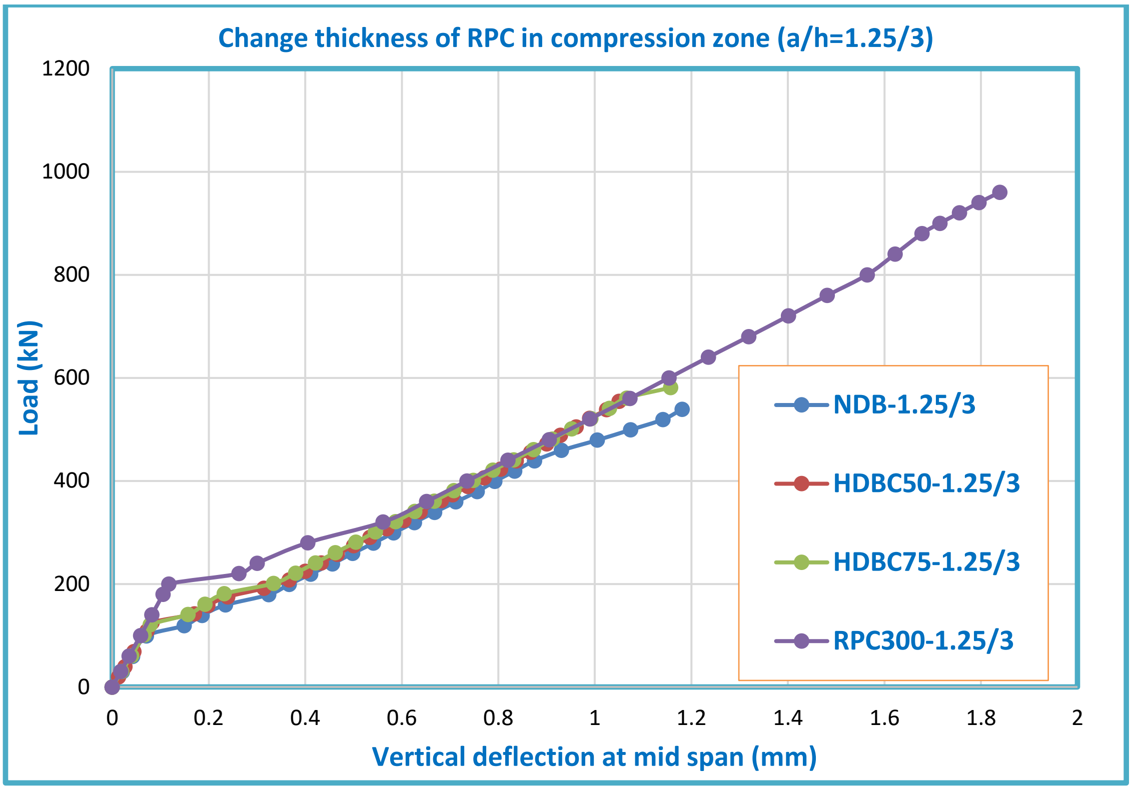

Figure (5.30) Effect RPC thickness in compression zone on the load-deflection curve at (a/h=1.25/3)

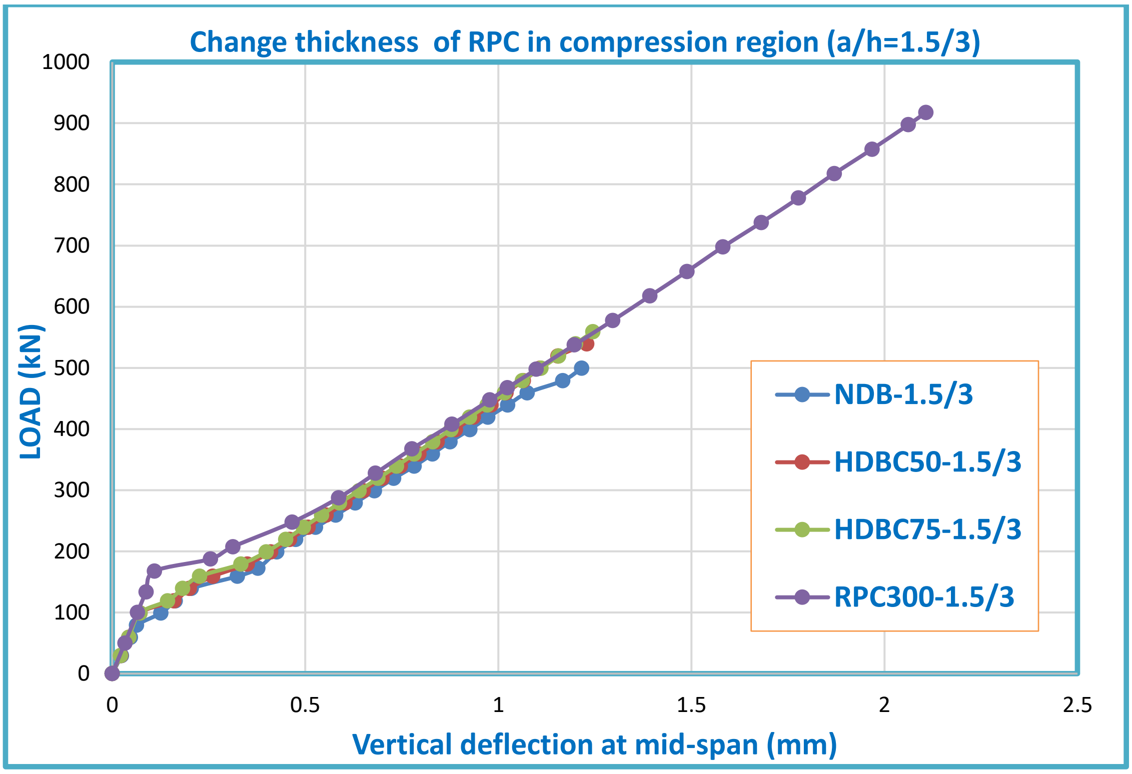

Figure (5.31) Effect RPC thickness in compression zone on the load-deflection curve at (a/h=1.5/3)

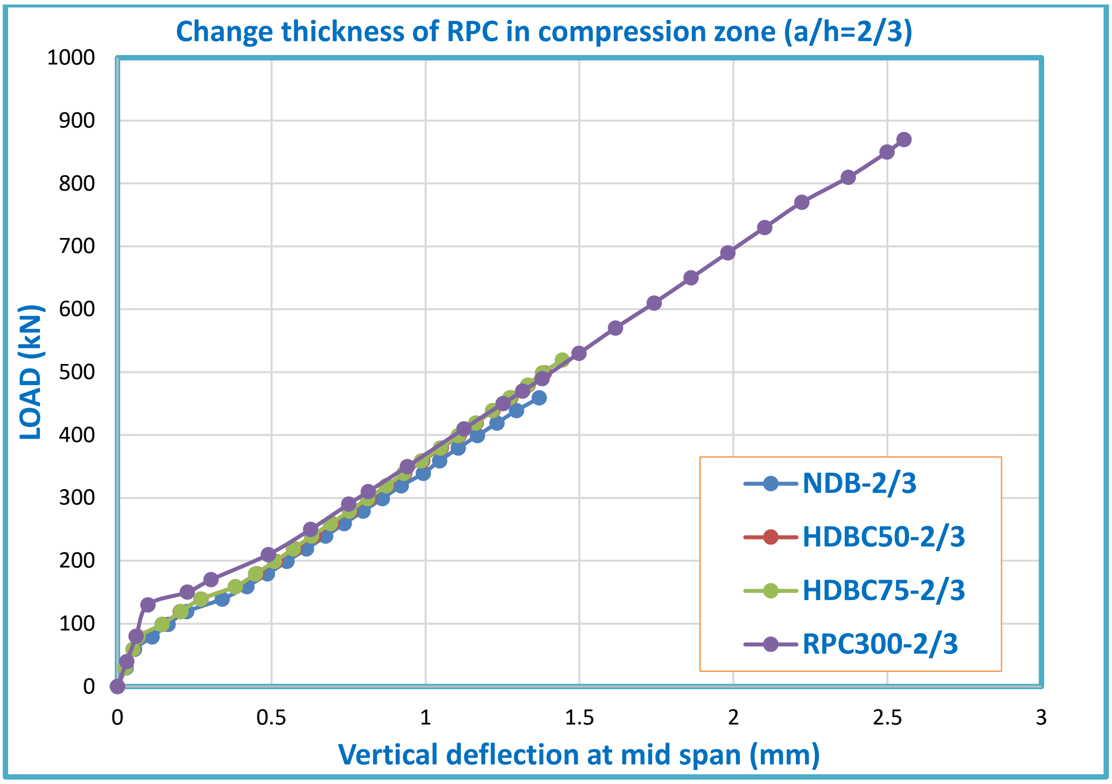

Figure (5.32) Effect RPC thickness in compression zone on the load-deflection curve at (a/h=2/3)

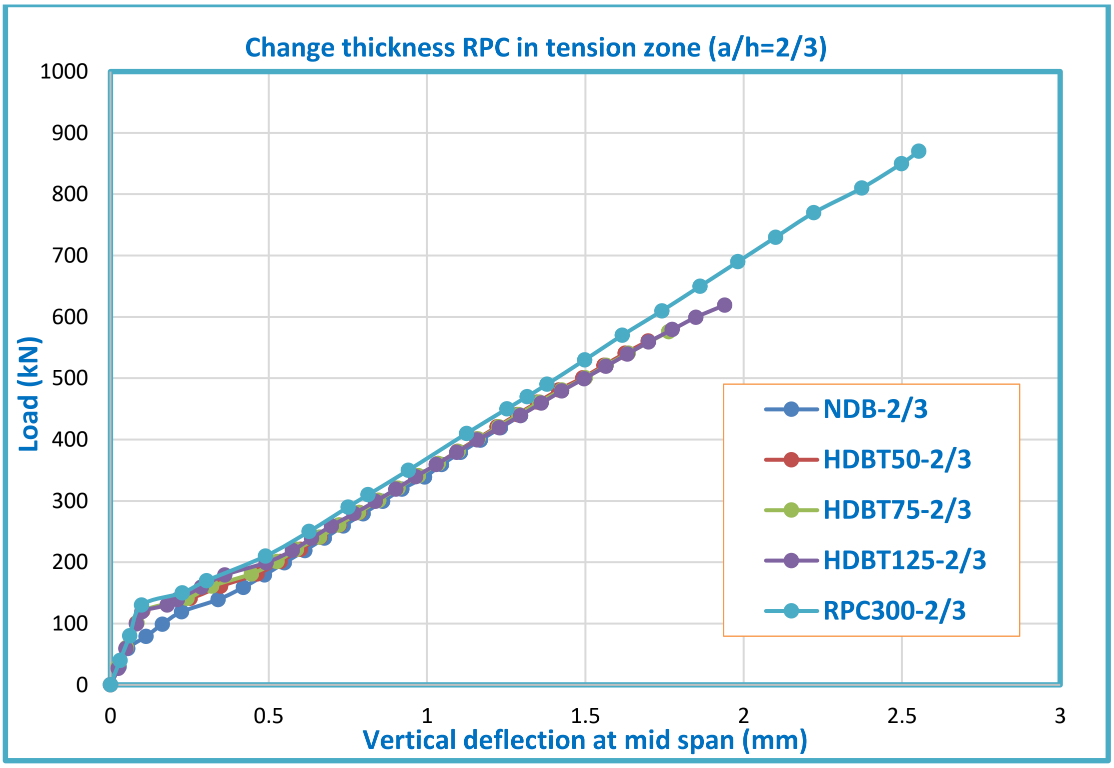

Figure (5.33) Effect RPC thickness in tension zone on the load-deflection curve at (a/h=2/3)

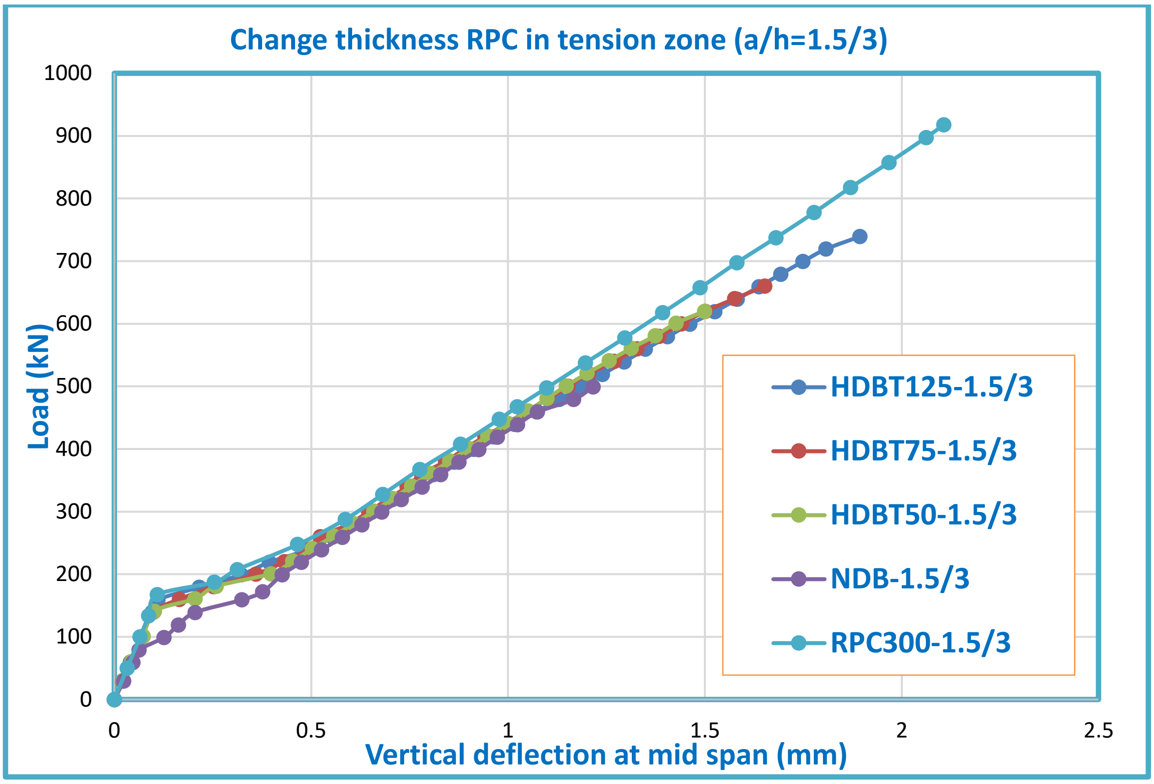

Figure (5.34) Effect RPC thickness in tension zone on the load-deflection curve at (a/h=1.5/3)

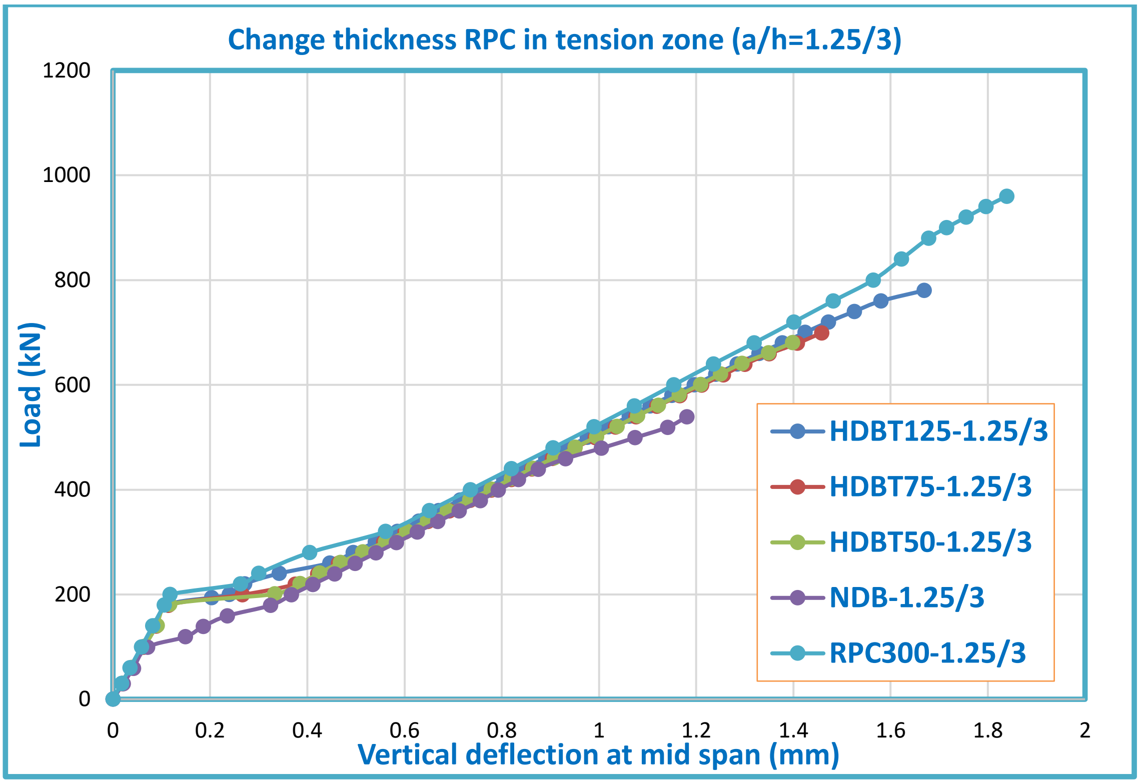

Figure (5.35) Effect RPC thickness in tension zone on the load-deflection curve at (a/h=1.25/3)

5.9.2 Effect Thickness of RPC on the First cracking and Ultimate Loads

Generally, the first cracking and ultimate loads in the hybrid deep beam were greater than those for normal deep beam due to effect the hybridization, but less than those in deep beams with RPC for overall depth. The effect of increasing the thickness of RPC in hybrid deep beams with RPC in compression zone on the first cracking load was little at a/h= 2/3 and 1.5/3, but its effect was obvious when a/h= 1.25/3. The effect of increasing the thickness of layer RPC in hybrid deep beams with RPC in the tension zone on the first cracking load was insignificant.

The ultimate load increased with increasing the thickness of RPC layer, Table (5.7) shows the increasing in the first cracking and ultimate loads for all hybrid deep beams when compared with the normal deep beams.

Table (5.7) Effect thickness of RPC layer on first cracking and ultimate loads

Deep beam	**First Cracking Load (P_{cr}) (kN)**	**Ultimate Load (P_u) (kN)**	$\frac{(Pcri - Pcrr)}{Pcrr} \times 100\%$	$\frac{(Pui - Pur)}{Pur} \times 100\%$
RPC in compression zone and a/h=2/3				
NDB-2/3 ^{r}	79.09	459.09	/	/
HDBC50-2/3^i	99.09	499.09	25.3	8.7
HDBC75-2/3^i	99.09	519.09	25.3	13.1
RPC300-2/3^i	150	870	89.7	89.5
RPC in the compression zone at a/h=1.5/3				
NDB-1.5/3 ^{r}	99.09	499.09	/	/
HDBC50-1.5/3^i	119.09	539.09	20.2	8

Table (5.7) Effect thickness of RPC layer on first cracking and ultimate loads (Continue)

Deep beam	First Cracking Load (P_{cr}) (kN)	Ultimate Load (P_u) (kN)	$\frac{(Pcri - Pcrr)}{Pcrr} \times 100\%$	$\frac{(Pui - Pur)}{Pur} \times 100\%$
HDBC75-1.5/3^i	121.6	559.09	22.7	12
RPC300-1.5/3^i	187.5	917.5	89.2	83.8
RPC in the compression zone at a/h=1.25/3				
NDB-1.25/3^r	119.09	539.09	/	/
HDBC50-1.25/3^i	142	554.4	19.2	2.8
HDBC75-1.25/3^i	160.87	580.87	34.4	7.8
RPC300-1.25/3^i	220	960	84.7	78.1
RPC in the tension zone at a/h=2/3				
NDB-2/3^r	79.09	459.09	/	/
HDBT50-2/3^i	140.87	560.87	78.1	22.2
HDBT75-2/3^i	140.87	560.87	78.1	22.2
HDBT125-2/3i	130	619.26	64.4	34.9
RPC in the tension zone at a/h=1.5/3				
NDB-1.5/3^r	99.09	499.09	/	/
HDBT50-1.5/3^i	180.9	620	81.7	24.2
HDBT75-1.5/3^i	180	660	81.6	32.2
HDBT125-1.5/3i	179.26	780	80.9	56.3
RPC in the tension zone at a/h=1.25/3				
NDB-1.25/3^r	119.09	539.09	/	/
HDBT50-1.25/3^i	200.9	680.9	68.7	26.3
HDBT75-1.25/3^i	199.26	699.26	67.3	29.7
HDBT125-1.25/3^i	200	780	67.9	44.7

Table (5.7) Effect thickness of RPC layer on first cracking and ultimate loads (Continue)

Deep beam	First Cracking Load (P_{cr}) (kN)	Ultimate Load (P_u) (kN)	$\frac{(Pcri - Pcrr)}{Pcrr} \times 100\%$	$\frac{(Pui - Pur)}{Pur} \times 100\%$
RPC in the compression zone and the tension zone at a/h=2/3				
NDB-2/3 ^{r}	79.09	459.09	/	/
HDBCT50-2/3i	140.9	620.9	78.2	35.2
RPC in the compression zone and the tension zone at a/h=1.5/3				
NDB-1.5/3 ^{r}	99.09	499.09	/	/
HDBCT50-1.5/3 ^{i}	160	660	61.5	32.2
RPC in the compression zone and the tension zone at a/h=1.25/3				
NDB-1.25/3 ^{r}	119.09	539.09	/	/
HDBCT50-1.25/3 ^{i}	200	740	67.9	37.3

i: -Considered deep beam *r: - Reference deep beam*

5.10 Effect the Location of RPC Layer

5.10.1 Effect the Location of RPC Layer on the Load-Deflection Response

Generally, the behavior of load-deflection in group G-7 (RPC 50mm in compression and tension zone) was stiffer than groups (G-1 normal deep beams, G-2 hybrid deep beams with RPC 50 mm in compression region, and G-4 hybrid deep beams with RPC 50 mm in tension region). The behavior of load-deflection in group G-2 (RPC 50 mm in compression region) was stiffer than group G-l (normal cross-section) but less than group G-4 (RPC 50mm in tension zone), as shown Figures from (5.36) to

(5.41). At (a/h=2/3), the ultimate vertical midspan deflection in group (G-7) was greater than groups (G-1, G-2, and G-4) by about (30.2, 28.7, and 5)%, respectively, and the ultimate vertical midspan deflection in group (G-4) was greater than groups (G-1, and G-2) by about (24, and 22.6)%, respectively. At (a/h=1.5/3), the ultimate vertical midspan deflection in group (G-7) was greater than groups (G-1, G-2, and G-4) by about (25, 23.7, and 1.4)%, respectively, and the ultimate vertical midspan deflection in group (G-4) was greater than groups (G-1, and G-2) by about (23.3, and 22.0)%, respectively. At (a/h=1.25/3), the ultimate vertical midspan deflection in group (G-7) was greater than groups (G-1, G-2, and G-4) by about (24.4, 40, and 5.2)%, respectively, and the ultimate vertical midspan deflection in group (G-4) was greater than groups (G-1, and G-2) by about (18.4, and 33.1)%, respectively.

The behavior of load-deflection in group G-3 (RPC 75mm in compression zone) was stiffer than that for group G-1 (normal beam) but less than group G-5 (RPC 75 mm in tension zone) as shown figures from (5-40) to (5-42). At (a/h=2/3), the ultimate vertical midspan deflection for group (G-5) was greater than groups (G-1, and G-3) by about (24.9, and 18.5)%, respectively. At (a/h=1.5/3), the ultimate vertical midspan deflection for group (G-5) was greater than groups (G-1, and G-3) by about (35.9, and 32.7)%, respectively. At (a/h=1.25/3), the ultimate vertical midspan deflection for group (G-5) was greater than groups (G-1 and G-3) by about (23.5, and 26)%, respectively.

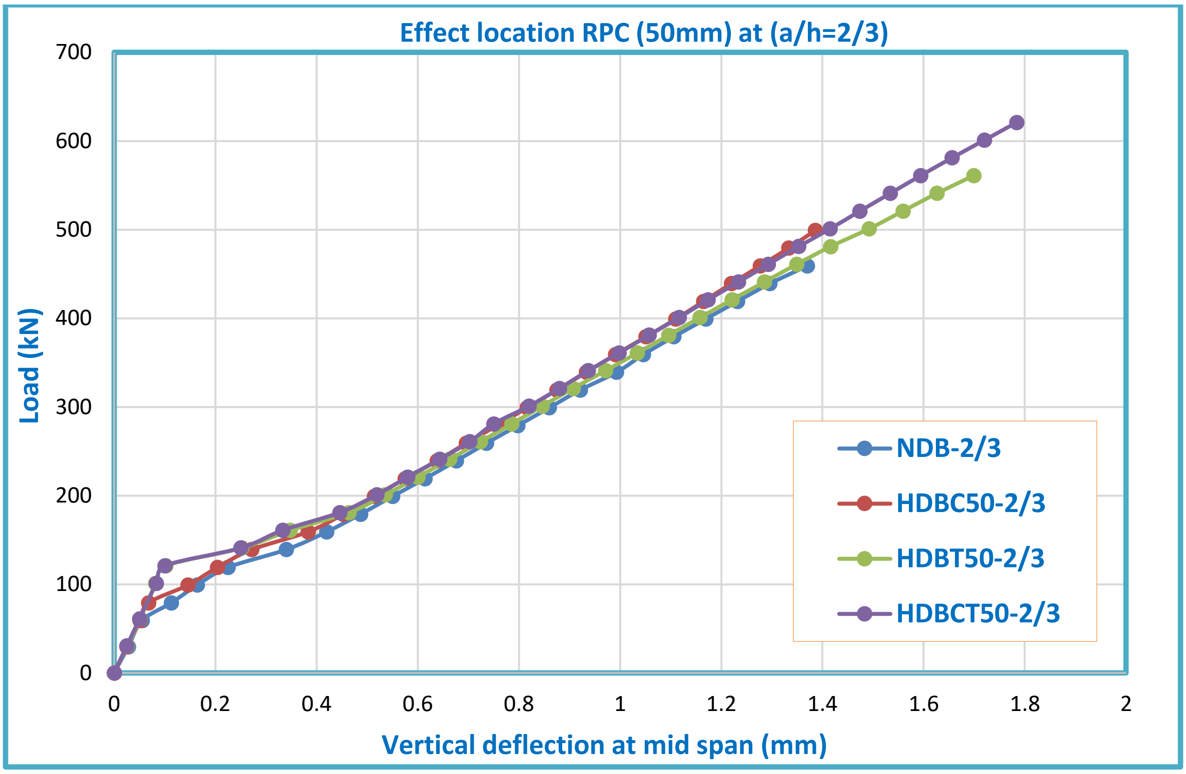

Figure (5.36) Effect location RPC (50 mm) on the load-deflection curve at (a/h=2/3)

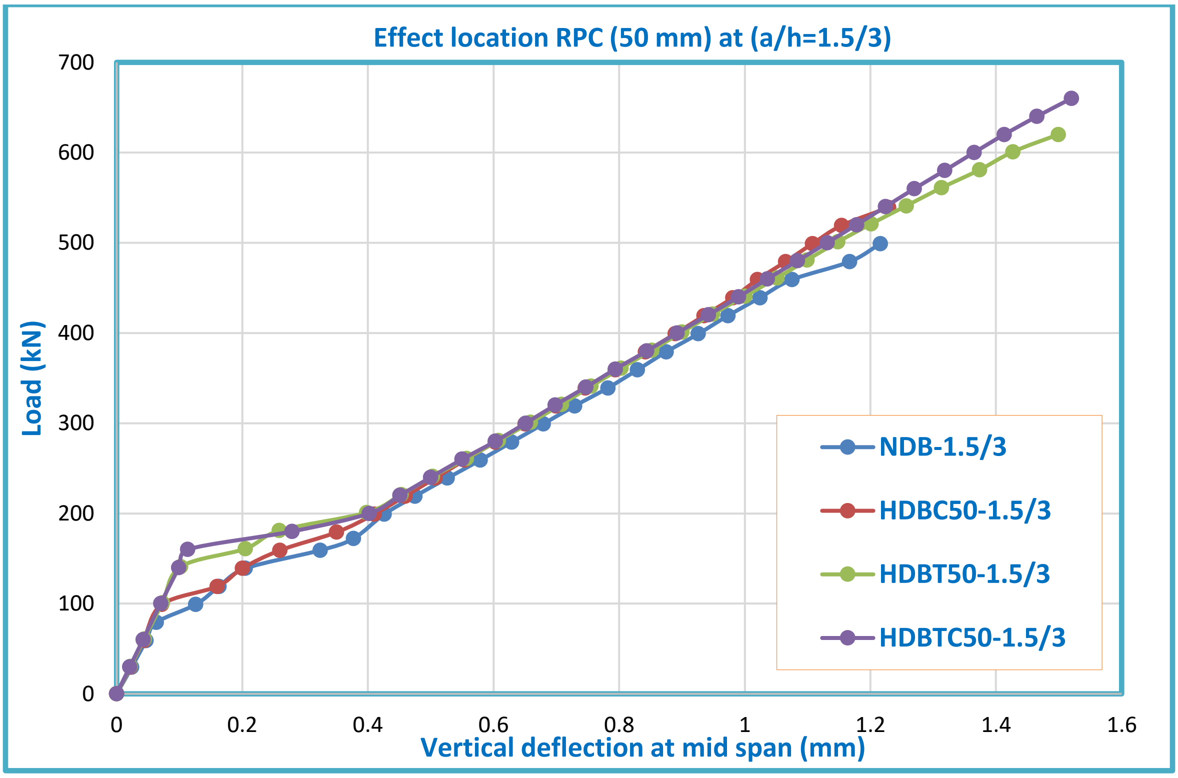

Figure (5.37) Effect location RPC (50 mm) on the load-deflection curve at (a/h=1.5/3)

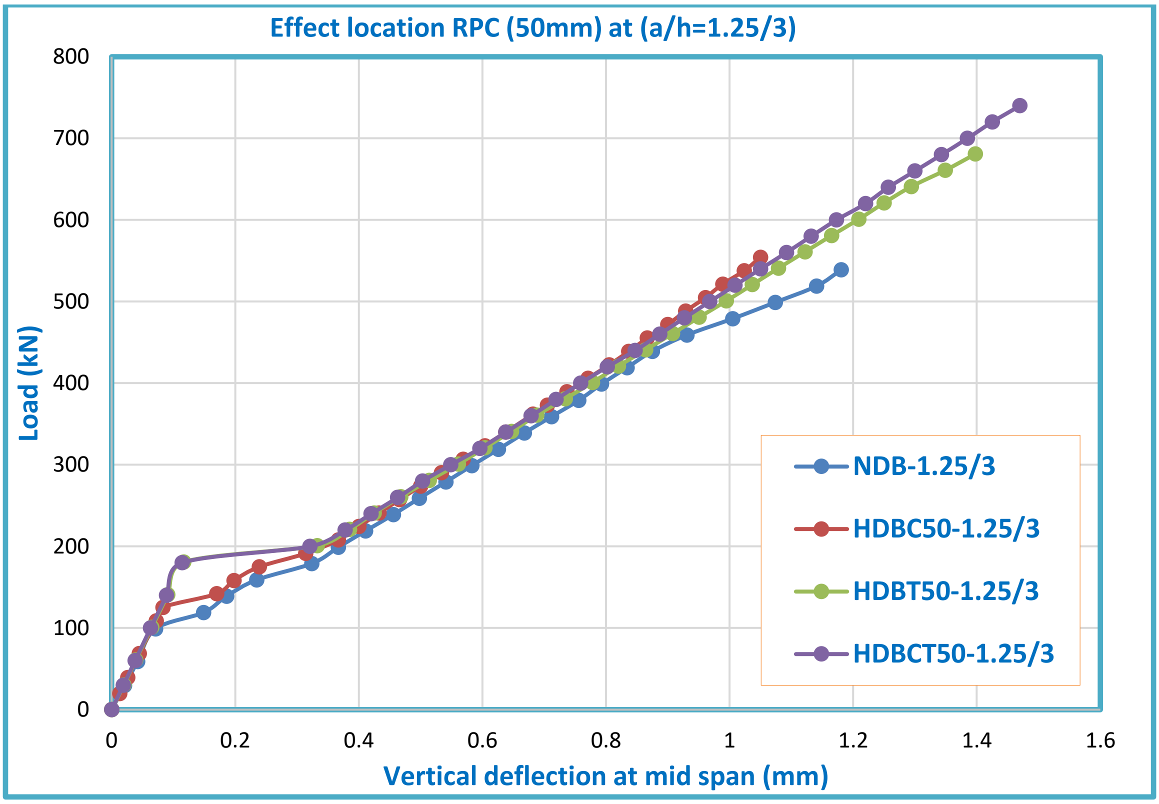

Figure (5.38) Effect location RPC (50 mm) on the load-deflection curve at (a/h=1.25/3)

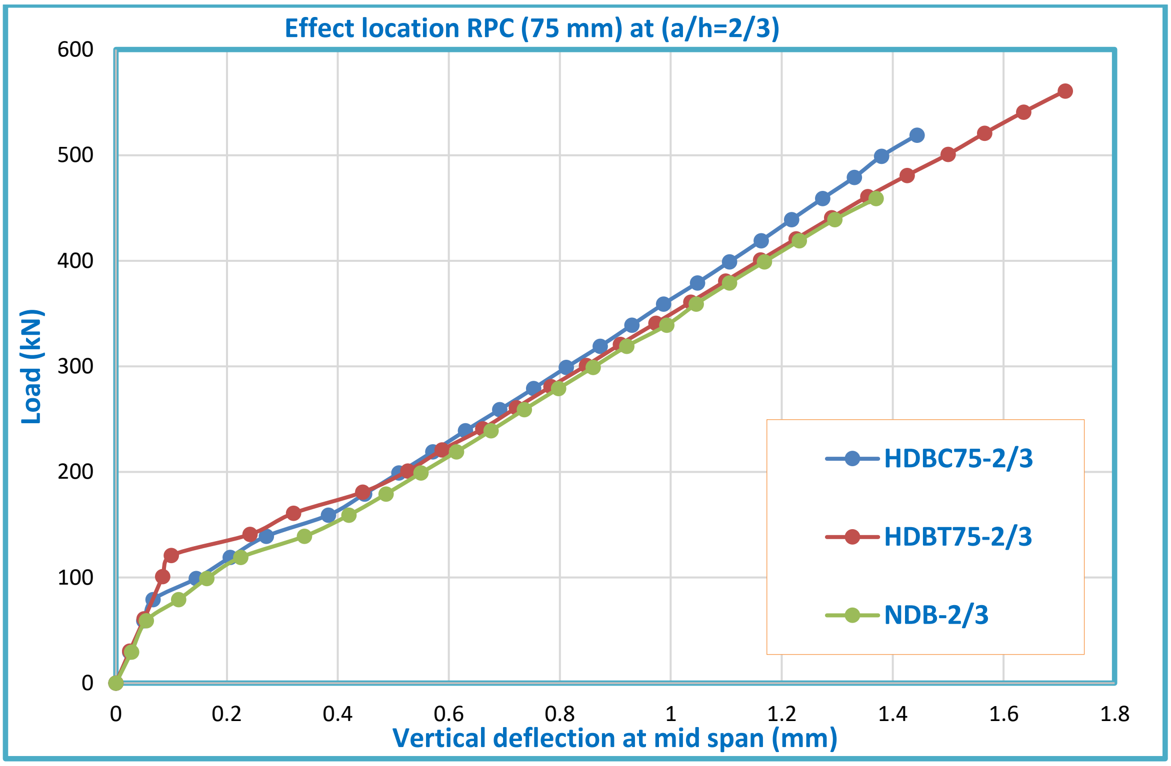

Figure (5.39) Effect location RPC (75 mm) on the load-deflection curve at (a/h=2/3)

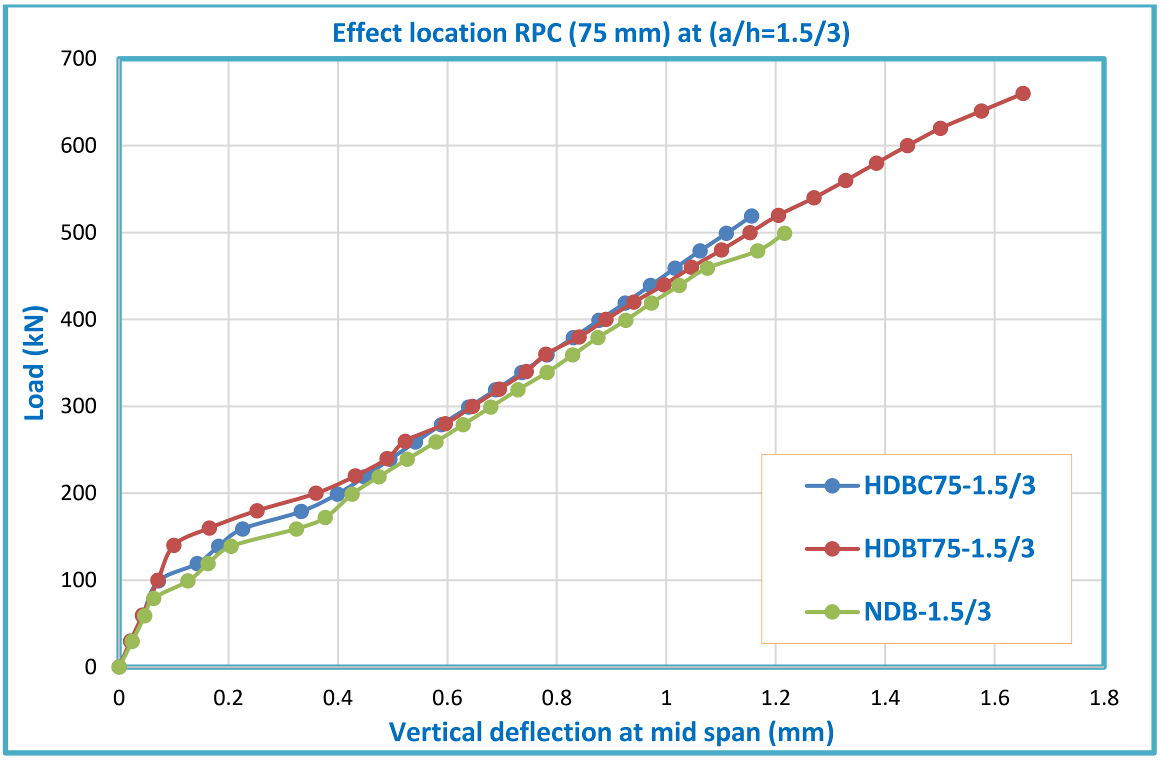

Figure (5.40) Effect location RPC (75 mm) on the load-deflection curve at (a/h=1.5/3)

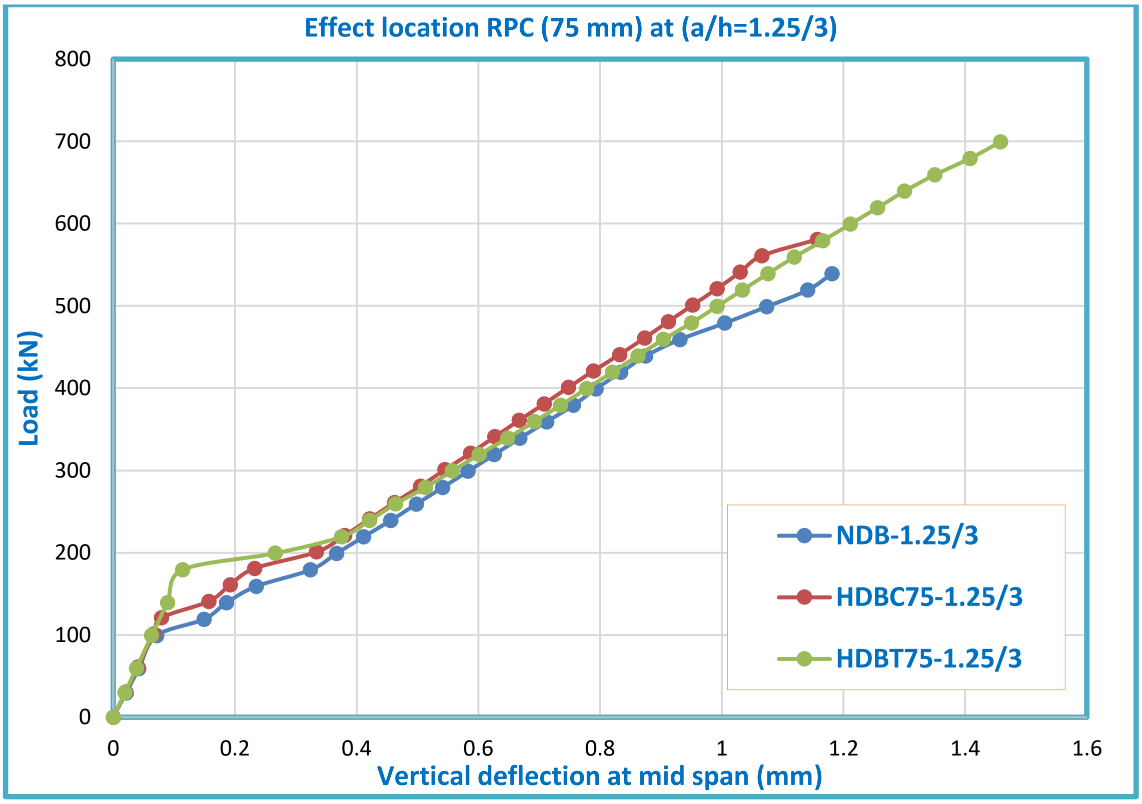

Figure (5.41) Effect location RPC (75 mm) on the load-deflection curve at (a/h=1.25/3)

5.10.2 Effect the Location of RPC Layer on the First Cracking and Ultimate Loads

Generally, the first crack load in hybrid deep beams with RPC in tension region was greater than the first crack load in hybrid deep beams with RPC in compression region. The ultimate load in hybrid deeb beams with RPC layer in the tension and compression region was greater than the ultimate load in hybrid deep beams with RPC layer in the compression region or in the tension region, the ultimate load in beam (HDBCT50-2/3) was greater than the ultimate load in beams (NDB-2/3, HDBC50-2/3, and HDBT50-2/3) by about (35.2, 24.4, and 10.7)%, respectivily, the ultimate load in beam (HDBCT50-1.5/3) was greater than the ultimate load in beams (NDB-1.5/3, HDBC50-1.5/3, and HDBT50-1.5/3) by about (32.2, 22.4, and 6.5)%, respectivily, the ultimate load in beam (HDBCT50-1.25/3) was greater than the ultimate load in beams (NDB-1.25/3, HDBC50-1.25/3, and HDBT50-1.25/3) by about (37.3, 33.5, and 8.7)%, respectivily . The first cracking load in the hybrid deep beam with RPC in the tension region was greater than the hybrid deep beam with RPC in the compression region, the first cracking load in the beam (HDBT50-2/3) was greater than (HDBC50-2/3) by (42.2%), the first cracking load in the beam (HDBT50-1.5/3) was greater than (HDBC50-1.5/3) by (51.9%), the first cracking load in the beam (HDBT50-1.25/3) was greater than (HDBC50-1.25/3) by (41.5%). The first cracking load in the beam (HDBT75-2/3) was greater than (HDBC75-2/3) by (42.2%), the first cracking load in the beam (HDBT75-1.5/3) was greater than (HDBC75-1.5/3) by (48%), and the first cracking load in the beam (HDBT75-1.25/3) was greater than (HDBC75-1.25/3) by (23.9%). The ultimate load in the hybrid deep beam with RPC in the tension region was greater than the hybrid deep beam with RPC in the compression region, the ultimate load in the beam (HDBT50-2/3) was greater than (HDBC50-2/3) by (12.4%), the ultimate load in the beam

(HDBT50-1.5/3) was greater than (HDBC50-1.5/3) by (15%), the ultimate load in the beam (HDBT50-1.25/3) was greater than (HDBC50-1.25/3) by (22.8%), the ultimate load in the beam (HDBT75-2/3) was greater than (HDBC75-2/3) by (8 %). The ultimate load in the beam (HDBT75-1.5/3) was greater than (HDBC75-1.5/3) by (18%), and the ultimate load in the beam (HDBT75-1.25/3) was greater than (HDBC75-1.25/3) by (20.4%). Table (5.8) shows the increasing in the ultimate load and the first crack load for all hybrid deep beams when compared with the normal deep beams.

Table (5.8) Effect the Location of RPC Layer on the First Cracking and Ultimate Loads

Deep beam	**First Crack Load (P_{cr}) (kN)**	**Ultimate Load (P_u) (kN)**	$\frac{(Pcri - Pcr}{Pcrr} \times 100\%$	$\frac{(Pui - Pur}{Pur} \times 100\%$
Thickness of RPC layer (50 mm) at (a/h=2/3)				
NDB-2/3 ^{r}	79.09	459.09	/	/
HDBC50-2/3 ^{i}	99.09	499.09	25.3	8.7
HDBT50-2/3 ^{i}	140.87	560.87	78.1	22.2
HSBTC50-2/3 ^{i}	140.9	620.9	78.1	32.2
Thickness of RPC layer (50 mm) at (a/h=1.5/3)				
NDB-1.5/3 ^{r}	99.09	499.09	/	/
HDBC50-1.5/3 ^{i}	119.09	539.09	20.2	8
HDBT50-1.5/3 ^{i}	180.9	620	82.6	24.2
HDBTC50-1.5/3 ^{i}	160	660	61.5	32.2
Thickness of RPC layer (50 mm) at (a/h=1.25/3)				
NDB-1.25/3 ^{r}	119.09	539.09	/	/
HDBC50-1.25/3 ^{i}	142	554.4	19.2	2.8
HDBT50-1.25/3 ^{i}	200.9	680.9	68.7	26.3

Table (5.8) Effect the Location of RPC Layer on the First Cracking and Ultimate Loads (Continue)

Deep beam	First Crack Load (P_{cr}) (kN)	Ultimate Load (P_u) (kN)	$\frac{(Pcri - Pcrr)}{Pcrr} \times 100\%$	$\frac{(Pui - Pur)}{Pur} \times 100\%$
HDBTC50-1.25/3^{i}	200	740	67.9	37.3
Thickness of RPC layer (75 mm) at (a/h=2/3)				
NDB-2/3^{r}	79.09	459.09	/	/
HDBC75-2/3^{i}	99.09	519.09	25.3	13.1
HDBT75-2/3^{i}	140.87	560.87	78.1	22.2
Thickness of RPC layer (75 mm) at (a/h=1.5/3)				
NDB-1.5/3^{r}	99.09	499.09	/	/
HDBC75-1.5/3^{i}	121.6	559.09	22.7	12
HDBT75-1.5/3^{i}	180	660	81.7	32.2
Thickness of RPC layer (75 mm) at (a/h=1.25/3)				
NDB-1.25/3^{r}	119.09	539.09	/	/
HDBC75-1.25/3^{i}	160.87	580.87	35.1	7.8
HDBT75-1.25/3^{i}	199.26	699.26	67.3	29.7

i: -Considered deep beam *r: - Reference deep beam*

Chapter Six

6

CONCLUSIONS AND RECOMMENDATIONS

CHAPTER SIX

CONCLUSIONS AND RECOMMENDATIONS

6.1 General

The results obtained from the experimental part and the numerical analysis showed that the hybrid reinforcement concrete deep beams possessed better behavior than normal reinforcement concrete deep beams.

This chapter presents the conclusions obtained from the present study with some recommendations for the expansion of current work in the future.

6.2 Conclusions

The conclusions obtained included the results of the experimental work and the results of the numerical analysis using the ANSYS program (version 17.2).

6.2.1 Experimental conclusions

1- The ultimate and the first cracking loads of the hybrid beam were greater than those for the normal beams.

2- The ultimate load of the hybrid deep beams with RPC (75 mm) in compression region was greater than those of normal deep beam by about (26.9 %) and (9.4%) at (a/h=2/3, and 1.25/3), respectively.

3- The ultimate load of the hybrid deep beams with RPC (75 mm) in tension region was greater than those for normal deep beam by about (33.8 %) and (41.8%) at (a/h= 2/3 and 1.25/3), respectively.

4- The ultimate load of the hybrid deep beams with RPC (125 mm) in tension region was greater than those for normal deep beam by about (52.2%) and (54%) at (a/h= 2/3 and 1.25/3), respectively.

5- The ultimate load of the hybrid deep beams increased with the increasing of the thickness of RPC layer, the ultimate load of hybrid deep beams RPC (125 mm) in tension region was greater than those for normal deep beams and hybrid deep beams with RPC (75 mm) in tension region by about (52.2%) and (13.8%)

at (a/h=2/3), respectively, and about (54%) and (8.6%) at (a/h=1.25/3), respectively.

6- The ultimate load of the hybrid deep beams with RPC (75 mm) in tension region was greater than the hybrid deep beams with RPC (75 mm) in compression region about (5.4%) and (29.5%) at (a/h=2/3 and 1.25/3), respectively.

7- The ultimate load increased with decreasing the (a/h), the ultimate load in the beam NDB-2 greater than the beam NDB-1 by about (21.7%), the ultimate load in the beam HDB-4 was greater than the beam HDB-3 by about (29%), the ultimate load in the beam HDB-6 was greater than the beam HDB-5 by about (5%), the ultimate load in the beam HDB-8 was greater than the beam HDB-7 by about (23.1%).

8- The first cracking load in the hybrid deep beams with RPC (125 mm) in tension region greater than the normal deep beam by about (6.7%) and (17.8%) at (a/h=2/3 and 1.25/3), respectively, the first cracking load in the hybrid deep beams with RPC (125 mm) in tension region greater than the hybrid deep beams with RPC(75 mm) in tension region by about (2.4%) at (a/h=1.25/3), the first cracking load in the hybrid deep beams with RPC (75 mm) in tension region greater than the normal deep beam by about (13.9%) and (15%) at (a/h=2/3 and 1.25/3), respectively, the first cracking load in the hybrid deep beams with RPC (75 mm) in compression region greater than the normal deep beam by about (14.4%) and (16.7%%) at (a/h=2/3 and 1.25/3), respectively.

9- First crack load in hybrid deep beams increased with decreased the (a/h), the first crack load in the beam (HDB-4) greater than beam (HDB-3) about (1%), the first crack load in the beam (HDB-6) greater than the beam (HDB-5) about (10%), the first cracking load in beam (HDB-8) greater than the beam (HDB-7) about (10.4%).

10- The load-deflection curves indicated that the behavior of the normal and hybrid deep beams became stiffer with decreasing (a/h).

11- Hybrid deep beams with RPC in compression zone were stiffer than the normal deep beams.

12- The hybrid deep beams with RPC in tension region were toughness than the hybrid deep beams in the initial stages of loading.

13- Hybrid deep beams with RPC in compression zone were stiffer than the hybrid deep beam with RPC in compression region.

6.2.2 Numerical conclusions

1- There was an acceptable agreement in the general behavior of deep beams between the experimental program and the analytical program through the load-deflection curves, the increased in the deflection at the ultimate load in the experimental program was about (13.66%) as average.

2- The ultimate loads of the deep beams recorded by the experimental program were close to the results given by the numerical program, where the largest difference was (7.22%).

3- The behavior of deep beams was more ductile with increasing a / h.

4- The ultimate load of deep beams increased with decreased a/h. When (a/h) decreased from (2/3) to (1.5/3) and (1.25/3), the ultimate load of normal deep beams increased by about (25.28%) and (50.57%), respectively. Also ultimate load in the hybrid deep beams with RPC (50 mm) in compression region increased by about (20.18%) and (43.3%) respectively, moreover ultimate load in the hybrid deep beams with RPC (50 mm) in tension region increased by about (13.58%) and (28.58%) respectively, finally ultimate load in the hybrid deep beams with RPC (50 mm) in tension and compression region increased by about (27.75%) and (41.94%) respectively.

5- The first cracking load of deep beams increased with decreased (a/h). When (a/h) decreased from (2/3) to (1.5/3) and (1.25/3), the first crack load in the normal deep beams increased by about (8.71%) and (17.43%), respectively. Also first crack load in the hybrid deep beams with RPC (50 mm) in compression region increased by about (8.01%) and (11.08%), respectively, moreover first crack load in the hybrid deep beams with RPC (50 mm) in tension region increased by about (10.7%) and (21.4%), respectively, finally first crack load in the hybrid deep beams with RPC (50 mm) in tension and compression region increased by about (3.08%) and (19.18%), respectively.

6- The location of the RPC layer in the tension and compression region led to get the best behavior of the load-deflection curve as well as the ultimate load in this deep beam was greater than all deep beams.
7- The ultimate load in the hybrid deep beams with RPC in tension region was greater than those for the hybrid deep beams with RPC in compression region.
8- The first crack load in the hybrid deep beams with RPC in compression region was greater than the normal deep beam, but less than the hybrid deep beams with RPC in tension region.
9- The first crack load of the hybrid deep beams increased with the increase of the RPC thickness.

6.3 Recommendations

1- It is possible to use the experimental program in the current study for other beams with different cross-sections such as (I, and T).

2- The hybridization technology can be used to study the behavior of hybrid members such as slabs, columns, and concrete walls.

3- It is possible to extend the current work by studying more parameters such as increasing the compression strength of RPC, cancel the horizontal and/or vertical shearing bars, and change the ratios of the longitudinal tension bars.

4- The same experimental work can be done for hybrid deep beams with openings in the web.

5- It is possible to extend the current work by changing the type of load (e.g. distributed load, cyclic loading, impact and dynamic load).

6- The hybrid concept can be applied to slender beams.

7- For the same experimental work of the current study can be used to the investigation of the effect of the bending, torsion and axial force on the behavior of deep beams and shallow beams.

REFRENCESS

Abolfazl A., Reza A., and Ali R. R., " ***Investigation of Experimental and Analytical Shear Strength of Reinforced Concrete Deep Beams,***" International Journal of Civil Engineering, Vol. 9, 2011, pp 207-2015.

ACI Committee 318, (2014). "***Building Code Requirements for Structural Concrete and Commentary,***'' Reported by ACI Committee 318M, 2014.

ACI Committee-363, "***State of the Art Report on High Strength Concrete (ACI 363R-92),***" American Concrete Institute, Detroit, 1997.

Ammar Yaser Ali and Maha Ghazi Zghair. "***Experimental Investigation and Nonlinear Analysis of Hybrid Reinforced Concrete Deep Beams***," Al-Qadisiyah Journal for Engineering Sciences, Vol. 8, 2015, pp. 99-119.

Ansys, "***ANSYS Manual***," Version 7.0, USA, 2002.

ASTM A496-02, "***Standard Specification for Steel Wire, Deformed, for Concrete Reinforcement,***" ASTM Committee A-1 on Steel, Stainless Steel, and Related Alloys, West Conshohocken, PA 19428-2959, United States, 2002, p5.

ASTM A615/A615M-05a., "***Standard Specification for Deformed and Plain Carbon-Steel Bars for Concrete Reinforcement,***" 2005 Annual Book of ASTM Standards, Vol.01, ASTM, Philadelphia, PA.

ASTM C494-86," ***Chemical Admixture for Concrete***," Annual book of ASTM Standards American Society for Testing and Materials, vol.04-02, 1988.

ASTM C496/C496M-04, "***Standard Test Method for Splitting Tensile Strength of Cylindrical Concrete Specimens,***" Vol. 04.02, 2004, p5.

ASTM C1240-04, "***Standard Specification for the Use of Silica Fume as a Mineral Admixture in Hydraulic Cement Concrete, Mortar and Grout***," Vol. 4.2, 2004, p6.

Attarde P. M., and Barbat D. K., "***Behavior and Strength of RC Deep Beams using High Performance Concrete-A Literature Revie***," International Journal of Modern Trends in Engineering and Research (IJMTER) Volume 02, Issue 02, [February - 2015] e-ISSN: 2349-9745, p-ISSN: 2393-8161, pp. 147-150.

Bashandy A.A., Meleka N.N., and Arab M.A., "***Behavior and Analysis of Economically Reactive Powder RC beams,***" ASIAN journal of civil engineering (BHRC) Vol. 15, 2014, pp. 721-739.

Bernard, O., Mivelaz, P., and Brühwiler, E., "***Investigation of the Long-Term Behavior of Hybrid Concrete Structures,***" 2nd International Ph. D Symposium in Civil Engineering, Budapest, 1998, pp. 1-8.

B.S. 1881, part 116, "***Method of determination of compressive strength of concrete cubes,***" British Standards Institution, 1989, p3.

BS-8110(1985), "***Structural Use of Concrete,***" British Standards Institution, London.

Burke, B. T., "***Residual Strength of Ultra High-Performance Concrete after Exposure to Elevated Temperatures,*** "M.SC. Thesis, University of Connecticut, 2008, p74.

Chen, W.F., and Saleeb, A.F., "***Constitutive Equations for Engineering Materials,***" Johen Wiley & Sons Inc., USA, 1981, p580.

Dauriac, C., "***Special Concrete May Give Steel Stiff Competition,*** " The Seattle Daily Journal of Commerce {online}, May 9, 1997, pp. 1-5.

De Paiva, H. A. R., and Siess, C. P., "***Strength and Behavior of Deep Beams in Shear***," Journal of the Structural Division, 1965, Vol. 91, pp. 19-41.

De-Xin Xiong, and Xiao-Xiong Zha, "***A numerical Investigation on the Behavior of Concrete Filled Steel Tubular Columns under Initial Stresses,***" Journal of Construction Steel Research, Vol. 63, 2007, pp 599-611.

Desayi, P., and Krishnan, S., "***Equation for the Stress-Strain Curve of Concrete,***" Journal of the American Concrete Institute, Vol.61, 1964, pp. 345-350, [Cited by Ref. (Kachlakev,2005)].

Fenner, R.T., "***Finite Element Methods for Engineers,***" Department of Mechanical Engineering, Imperial College of Science, Technology and Medicine, London, 1996. [Cited by Ref. (Naser ,2013)].

Hani M. Fahmi, Abdullah Sinan Ahmed, and Ihsan A.S Al-Shaarbaf " ***Behavior of Reactive Powder Concrete Deep Beams,***" AL- Mansour Journal / No.20/ Special Issue.12th Scientific Conference 4-5, 2013.

Hassan Falah Hassan." ***Behavior of Hybrid Deep Beams Containing Ultra High Performance and Conventional Concretes***," Eng. & Tech- Journal, Vol.33, Part (A), 2015, pp. 30-51.

IQS No. 5/1984, "***Portland Cement***," Central Agency for Standardization and Quality Control, Planning Council, Baghdad, *Iraq, (in Arabic).*
Iraqi Specification No.45, "***Natural Sources for Gravel that is used in concrete and construction***," Baghdad, 1984.

Jasim Al-Khafaji, Ihsan Al-Shaarbaf, and Wisam Hulail Sultan, " ***Shear Behavior of Self Compacting Concrete Deep Beams***," Journal of Engineering and Development, Vol. 18, 2014, ISSN 1813- 7822.

Kamaran Sulaiman Ismail," ***Shear Behaviour of Reinforced Concrete Deep Beams***," A thesis submitted for the degree of Doctor of Philosophy in the Faculty of Engineering of The University of Sheffield, 2016.

Kang-Hai, T., Fung-Kew K., Shi T., and Lingwei G., "***High-Strength Concrete Deep Beams with Effective Span and Shear Span Variations***," ACI Structural J., 92(4), (1995). pp. 395-405.

Kupfer, H., and Grestle, K., "***Behavior of Concrete under Biaxial Stress,***" ASCE-Journal of the Engineering Mechanics, Vol.104, No. EM4, 1973, [Cited by Ref. (Aziz, 2006)].

Leet, K., and Bernal, D., "***Reinforced Concrete Design***," 3rdEdition, McGraw- Hill International Edition, Singapore 1997, p546.

Londhe R.S., "***Shear Strength Analysis and Prediction of Reinforced Concrete Transfer Beams in High-Rise Buildings***," Structural Engineering and Mechanics, Vol. 37, 2011, pp 39-59.

Manuel, R. F., Slight, B. W., and Suter, G. T., "***Deep Beam Behavior affected by Length and Shear Span Variation***," ACI Journal, V. 68, No. 12, 1971, pp. 954-958.

Mariano Valle and Oral Buyukozturk, "***Behavior of Fiber Reinforced High Strength Concrete under Direct Shear***," ACI Materials Journal, Vol. 90, 1993, pp. 122-133.

McGuire, W., Gallagher, R.H., and Ziemian, R.D., "***Matrix Structural Analysis***," Second Edition, John Wiley & Sons, Inc., 2000.

Mottram, J.T. and Show, C.T., "***Using Finite Elements in Mechanical Design***," 1st Edition, McGraw-Hill Company, UK 1996, p276.

Nabeel Abdul-Majeed Jaddou Al-Bayati," ***Behavior of Porcelanite Reinforced Concrete Deep Beams***," A thesis submitted to the building and construction engineering department of the University of Technology for the degree of doctor of philosophy in Structural engineering, 2012.

Neville, A.M., and Brooks, J.J., "***Concrete Technology***," Longman Scientific and Technical, U. K., 1987.

Oh, J. K., and Shin, S. W., "***Shear Strength of Reinforced High Strength Concrete Deep Beams***," ACI Structural Journal, V. 98, 2001, pp. 164-173.

O'Neil, E.F. and Dowd, W.H., "***Reactive Powder Concrete: A New Material for the Construction Industry***," Third National Concrete and Masonry Engineering Conference, June 15-17, 1995, San Francisco, CA, pp. 43-50.

Omar Q. Aziz & Msheer H. Ali, " ***Shear Strength and Behavior of Ultra-high-performance Fiber Reinforced Concrete (UHPC) Deep Beams without Web***," International Journal of Civil Engineering (IJCE), Vol. 2, 2013, pp. 85-96.

Pandurang S. P., and Girish V. J., "***Experimental Study of Behavior of R.C.C. Deep Beams***," International Journal of Emerging Technology and Advanced Engineering, Vol. 4, 2014, pp. 801-805.

Prach Amornpinnyo and Jaruek Teerawong, "***Shear Behavior of Reinforced Concrete Deep Beams with Various Horizontal to Vertical***

Reinforcements and Shear Span-to-Effective Depth Ratios," Advanced Materials Research Vols. 931-932, 2014, pp 473-477.

Ramachandran, V.S., "***Concrete Admixtures Handbook–Properties, Science, and Technology***, "2nd Edition, William Andrew Publishing, ISBN 0-8155-1373-9 ,1995, p121.

Ramakrishnan, V., and Ananthanarayana, Y., "***Ultimate Strength of Deep Beams in Shear***," ACI Journal, V. 65, No. 2, 1968, pp. 87-98.

Ramon L. Carrasquillo, Arthur H. Nilson, and Floyd O. Slate, "***Properties of High Strength Concrete Subject to Short Term-Loads***," ACI Journal, Proceedings, Vol. 78, 1981, pp. 171-178.

Richard, P., and Cheyrezy, M., "***Composition of Reactive Powder Concrete,***" Cement and Concrete Research, Vol. 25, No. 7, 1995, pp. 1501-1511.

Salamy M.R., Kobayashi H., and Unjoh Sh., "***Experimental and Analytical Study on RC Deep Beams***," ASIAN journal of civil engineering (BUILDING AND HOUSING) VOL. 6, 2005, pp. 487-499.

Sawsan Akram Hassan and Ghsoon Ali Faroun, "***Behavior of Hybrid Reinforced Concrete Deep Beams under Repeated Loading***," Civil and Environmental Research, Vol.8, No.10, 2016, pp.14-37.

Shengbing LIU, and Lihua XU, "***Experimental Study on Shear Behavior of Hybrid Fiber Reinforced High Performance Concrete Deep Beams***," Applied Mechanics and Materials Vols. 166-169, 2012, pp. 664-669.

Sinan Abdulhkaleq Yaseen, "***An Experimental Study on the Shear Strength of High-performance Reinforced Concrete Deep Beams without Stirrups***," Eng. &Tech. Journal, Vol.34, Part (A), No.11, 2016, pp. 2123-2139.

Smith, K.N., and Vantsiotis, A.S.," ***Shear Strength of Deep Beams***," ACI Journal, V. 68, 1982, pp.201-213.

Soroushian, P., and Lee, C.D., "***Constitutive Modeling of Steel Fiber Reinforced Concrete under Direct Tension and Compression in Recent Developments in Fiber Reinforced Cements and Concrete***," Elsevier

Science Publishers Ltd. Essex, 1989, pp. 363-377, [Cited by Ref. (Aziz, 2006)].

Subedi, N.K., Vardy, A.E. and Kubota, N., "***Reinforced Concrete Deep Beams- Some Test Results***," Magazine of Concrete Research, Vol.38, No.137, 1986, pp. 206-215.

Suresh G.S., and Kulkarni S., "***Experimental study on behavior of RC deep beams***," International Research Journal of Engineering and Technology (IRJET), Vol. 03, 2016, pp 676-680.

U.S. Department of Transportation, "***Silica Fume User's Manual,***" Federal Highway Administration, 2005.

Willam, K.J. and Warnke, E.P., "***Constitutive Model for Triaxial Behavior of Concrete***," Seminar on Concrete Structures Subjected to Triaxial Stresses, International Association of Bridge and Structural Engineering Conference, Bergamo, Italy, 1974, p.174.

Wille, K., Naaman, A.E., and El-Tawil, S., "***Optimizing Ultra-High-Performance Fiber-Reinforced Concrete***," Concrete International, 2011, pp.35-41.

Yam, LCP., "***Design of Composite Steel-Concrete Structures,***" University of Surrey Press, London, England, 1981, p 168.

Zienkiweicz, O.C., "***The Finite Element Method***," Third Edition, Mc Graw. Hill, London, 1977.

APPENDIX (A)
&
APPENDIX (B)

APPENDIX (A)

DESIGN OF DEEP BEAMS

According to the design equations of ACI-Code 318-99 (and adopted by **ACI-Code 318-08),** the design calculations are induced, as follows:

Design for flexural

$M_u = \varnothing A_s f_y jd$ $\qquad jd=0.2(L + 2h)$

Design for shear

$$V_c = \left(3.5-2.5\frac{Mu}{Vu\,d}\right)\left(0.16\sqrt{f'_c}+17\rho_w\frac{Vu\,d}{Mu}\right) b_w d \le 0.5\sqrt{f'_c}\, b_w d \ldots\ldots \text{(A-1)}$$

$$V_s = \left[\frac{A_v}{s}\left(\frac{1+\frac{ln}{d}}{12}\right) + \frac{A_{vh}}{s_2}\left(\frac{11-\frac{ln}{d}}{12}\right)\right] f_y d \qquad \ldots\ldots\ldots\ldots \text{(A-2)}$$

$$Z = 0.5 \times a \ldots\ldots\ldots\ldots \text{(A- 3)}$$

$$V_u = V_{C\ (eq.(A-1))} + V_{S(eq.(A-2))}$$

Where:

$(3.5 - 2.5\frac{Mu}{Vu\,d})$ is to be kept less than or equal to 2.5; and

f'_c= specified compressive strength of concrete, MPa;

b_w= web width, mm;

d = effective depth (distance from extreme compression fiber to centroid of longitudinal tension reinforcement), mm;

Vu = factored shear force at the critical section, N;

Mu = factored moment occurring simultaneously with Vu at the critical section, N.mm.

ln = clear span measured face to face of supports, mm;

a = shear span (distance between concentrated load and face of support), mm;

ρ_w= As /b_wd

As = area of non-prestressed tension reinforcement, mm^2;

A_v= area of shear reinforcement perpendicular to flexural tension reinforcement within a distance s, mm^2; and

A_{vh} = area of shear reinforcement parallel to flexural tension reinforcement within a distance s_2, mm^2.

Z= Critical section located at distance Z from face of support. mm

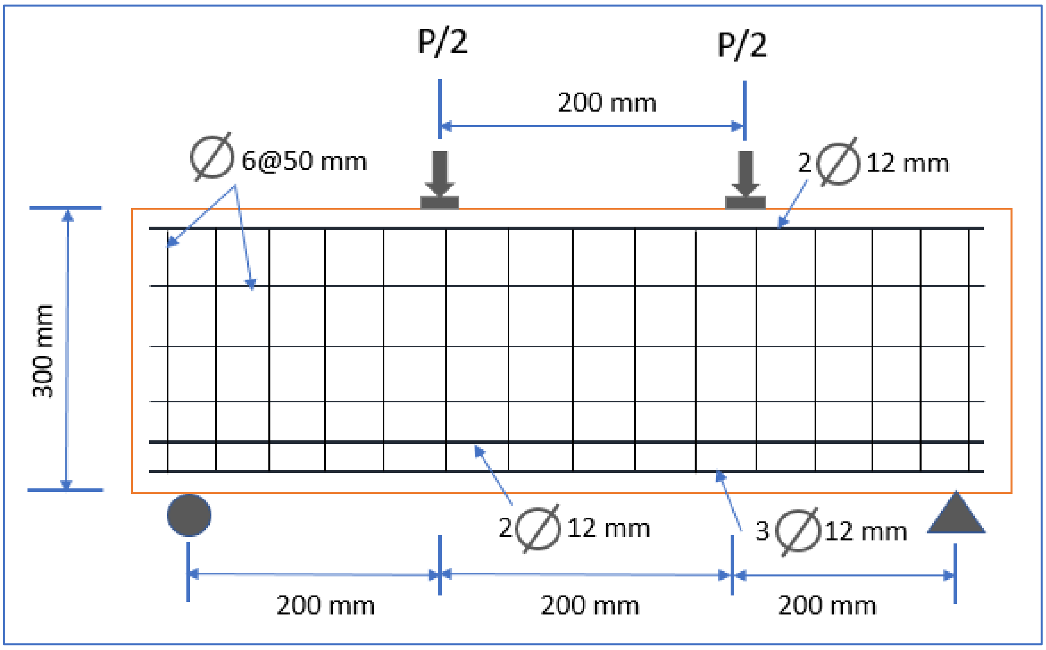

Figure A.1 Details of the dimensions of the deep beams with reinforcing steel

ρ_w = 0.01483, b=150 mm, d=250 mm

A_v= A_{vh}= 2 × 24.6= 49.2 mm^2, S1=S2= 50 mm

f_y = 636.2 MPa for bar diameter 12mm and 510.4 MPa for bar diameter 6mm

<u>Normal strength deep beam</u>

f'_c= 29.45MPa

At a/h= 2/3

jd=0.2(600 + 2×300) = 240 mm

Mu = 0.9×5×111.2×636.2×240 = 76.4 kN.m $\longrightarrow$ $P_{(flexure)}$= 1528 kN

Z= 0.5 × a = 0.1

$$3.5\text{-}2.5\,\frac{\text{Mu}}{\text{Vu d}} = 3.5\text{-}2.5\,\frac{\left(\frac{P}{2}\right)\times 0.1}{\frac{P}{2}\times 0.25} = 2.5$$

$\frac{\text{Vu d}}{\text{Mu}} = \frac{\frac{p}{2}\times 0.25}{\frac{p}{2}\times 0.1} = 2.5 > 1$ use 1

Vc = 2.5 × (0.16 × $\sqrt{29.45}$ + 17 × 0.01483 × 1) × 150 × 0.25 = 105 kN.

$V_s = \left[\frac{49.2}{50}\left(\frac{1+\frac{600}{250}}{12}\right) + \frac{49.2}{50}\left(\frac{11-\frac{600}{250}}{12}\right)\right]$ 510.4 × 250= 126 kN.

P = (Vc + Vs) × 2 = 462 kN < 1528 kN …………… ok

At a/h= 1.25/3

jd=0.2(600 + 2×300) = 240 mm

Mu = 76.4 kN.m $\longrightarrow$ $P_{(flexure)}$= (76.4 / 0.175) × 2 = 873 kN

Z= 0.5 × a = 0.0625

3.5-2.5 $\frac{\text{Mu}}{\text{Vu d}}$ = 3.5-2.5 $\frac{\left(\frac{p}{2}\right)\times 0.0625}{\frac{p}{2}\times 0.25}$ = 2.875 > 2.5 use 2.5

Vc = 2.5 × (0.16 × $\sqrt{29.45}$ + 17 × 0.01483 × 1) × 150 × 0.25 = 105 kN.

Vs = 126 kN.

P = (Vc + Vs) × 2 = 462 kN < 873 kN …………… ok.

<u>Hybrid deep beam with (RPC=125 mm) in tension region</u>

$f'_{c(NSC)}$= 32.4MPa, $f'_{c(RPC)}$= 60.2MPa.

$f'_{c(Avarege)}$= 40.74MPa

At a/h= 2/3

jd=0.2(600 + 2×300) = **240 mm**

Mu = 0.9×5×111.2×636.2×240 = 76.4 kN.m $\longrightarrow$ $P_{(flexure)}$= 1528 kN

Z= 0.5 × a = 0.1

3.5-2.5 $\frac{\text{Mu}}{\text{Vu d}}$ = 3.5-2.5 $\frac{\left(\frac{p}{2}\right)\times 0.1}{\frac{p}{2}\times 0.25}$ = 2.5

$\frac{\text{Vu d}}{\text{Mu}} = \frac{\frac{p}{2}\times 0.25}{\frac{p}{2}\times 0.1} = 2.5 > 1$ use 1

Vc = 2.5 × (0.16 × $\sqrt{40.74}$ + 17 × 0.01483 × 1) × 150 × 0.25 = 113.4 kN.

Vs = 126 kN.

P = (Vc + Vs) × 2 = 479 kN < 1528 kN …………… ok

At a/h= 1.25/3

jd=0.2(600 + 2×300) = **240 mm**

Mu = 76.4 kN.m $\longrightarrow$ $P_{(flexure)}$= (76.4 / 0.175) × 2 = 873 kN

Z= 0.5 × a = 0.0625

$3.5-2.5\,\frac{Mu}{Vu\,d} = 3.5-2.5\,\frac{\left(\frac{p}{2}\right)\times 0.0625}{\frac{p}{2}\times 0.25} = 2.875 > 2.5$ use 2.5

Vc = 2.5 × (0.16 × $\sqrt{40.74}$ + 17 × 0.01483 × 1) × 150 × 0.25 = 113.4 kN.

Vs = 126 kN.

P = (Vc + Vs) × 2 = 479 kN < 873 kN …………… ok.

APPENDIX (B)

FINITE ELEMENT METHOD

B.1 Derivation of Structural Matrices

The three-dimensional body in the finite element analysis is represented by a finite number of elements and a finite number of nodes that are identified on each element, where the finite elements are to be joined. Following is a summary of the general approach used in the finite element analysis.

To form the element equations, the principle of virtual work is sually used. This principle states that “a virtual change of the internal strain energy must be equal to an identical virtual change in external work due to the applied loads **(Mottram et. al, 1996).**

Wint. = Wext. --- (B.1)

Where:

Wint. = internal work (strain energy),

Wext. = external work (by applied force)

The virtual internal work is :

$W_{int.} = \int_v \{\partial\varepsilon\}^T \{\sigma\}.dv$ --------------------------------------(B.2)

Where:

$\{\varepsilon\}$= elements of virtual strain vector= $[\partial\varepsilon x \ \ \partial\varepsilon y \ \ \partial\varepsilon z \ \ \partial\varepsilon xy \ \ \partial\varepsilon yz \ \ \partial\varepsilon xz]^T$

$\{\delta\}$= elements of real stress vector = $[\delta\ x \ \ \delta\ y \ \ \delta\ z \ \ \delta\ xy \ \ \delta\ yz \ \ \delta\ xz]^T$

V = volume of the element

By using the general stress-strain relationship, stresses { δ }, can be determined from the corresponding strains { ε } as:

{ δ }= [D]× { ε }--(B.3)

Where:

[D] is the constitutive matrix

After substituting Equation (B.3) in (B.2), the virtual internal work can be written as:

$W_{int.}= \int_v \{\partial\varepsilon\}^T$ [D] $\{\varepsilon\}. dv$ -------------------------------- (B.4)

The displacements {U} within the element are related by interpolation to nodal displacements by:

{U}=[N] ×{a} --(B.5)

Where [N] is the shape function matrix, and {a} is the nodal displacement vector.

By differentiating equation (B.5) the strains for an element can be related to its nodal displacements by:

{ ε }= [B] ×(a)---(B.6)

where: [B]= strain-nodal displacement matrix, based on the element shape functions.

Assuming that all effects are in the global Cartesian system, then combining Equation (B.6) with Equation (B.4) yields:

$W_{int.}= \{\partial a\}^T \int_v [B]^T$ [D]$[B]\, dv\ \{a\}$ ---------------------------(B.7)

The external work, which is caused by the nodal forces applied to the element can be accounted for by:

$W_{ext.} = \{a\}^T . \{F\}$---(B.8)

Where:

{F}= nodal forces applied to the element

Finally, Equations (B.1), (B.7) and (B.8) may be combined to give:

$\{\partial a\}^T . \int_v [B]^T$ [D]$[B]\, dv\ .\{a\}$=$\{\partial a\}^T\ \{F\}$ -----------------(B.9)

Noting that $\{\partial a\}^T$ vector is a set of arbitrary virtual displacements, the condition required to satisfy Equation (B.9) can be reduced to (168):

$[K^e] . \{a\} = \{F\}$---(B-10)

Where:

$[K^e] = \int_v [B]^T$ [D]$[B]\, dv$ ----------------------------------(B.10)

$[K^e]$= element stiffness matrix

dv = dx. dy. dz.

Equation (B.10) represents the equilibrium equation on a one-element basis. For all elements, the overall stiffness matrix of the structure [K] is built up by adding the element stiffness matrices, after transforming from the local to the global coordinates, this equation can be written as:

$[K] \{a\}= \{F^a\}$ ---(B-11)

Where:

$[K]= \sum_n [K^e]$= overall structural stiffness matrix

$\{F^a\}= \{F\}$= vector of applied loads (total external force vector)

n = total number of elements.

B.2 Materials Idealization

All deep beams were analyzed by the ANSYS program (version 17.2). Table (B.1) The representation of components includes structural elements in the present study.

Table B-1 Finite Element Representation of Structural Components

Structural Components	Elements Specification in ANSYS
Concrete (NSC and RPC)	Solid 65
Bearing Plate and Support	Solid 185
Reinforcement Bars	Link 180

B.2.1 Finite Element Model of Concrete

In the current study, three-dimensional 8-node solid elements are used to model the concrete **(ANSYS Help, 2004).** The element has eight corner nodes (Solid 65), and each node has three degrees of freedom “u, v and w” in the “x, y and z “directions respectively, as shown in Figure (B.1).

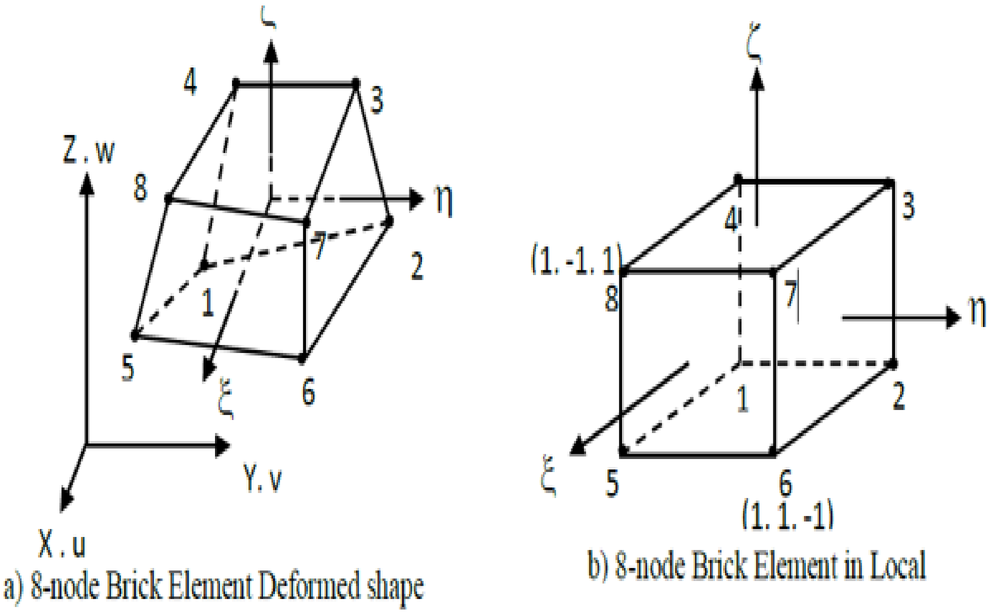

Figure (B.1) Three-dimensional 8-node brick element **(ANSYS Help, 2004)**

B.2.2 Finite Element Model of Reinforcement Bars

In the ANSYS program, element (Link 180) is used to represent all types of reinforcing steel (shear bars, longitudinal tensile bars, and compressive bars) and all diameters (6mm and 12 mm). It was assumed that reinforcing steel was capable of transmitting only an axial force. The bond between reinforcing steel and concrete was perfect by sharing at the same nodes. Figure (B.2) shows the locations of the contract to represent reinforcing steel

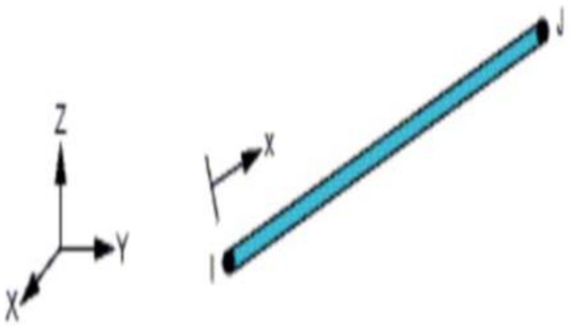

Figure (B-2) Link180 **(ANSYS Help, 2004).**

B.2.3 Finite Element Model of Bearing Plate and Support

The loading and support plates were used to avoid concentration of loads in small areas, thus preventing concrete crushing at the loading and support points. The element (Solid 185) used to represent the loading and support panels in ANSYS program. Figure (B.3) shows the geometric and node locations of this element.

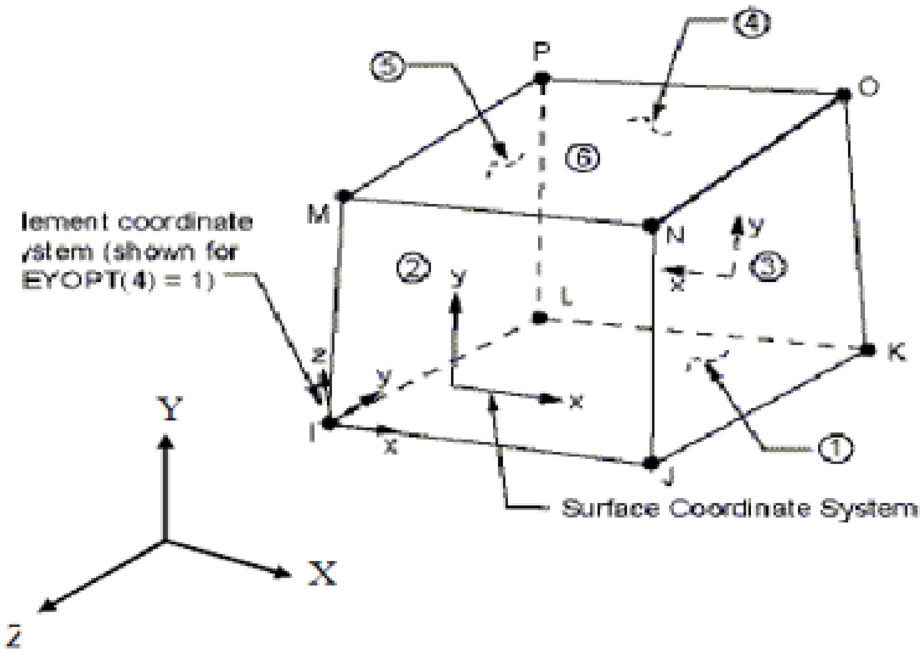

Figure (B.3) Solid 185 **(ANSYS Help, 2004).**

B.3 Modeling of Material Properties

Concrete structures consist of reinforcing steel and concrete, the behavior of each material is different from the other. The behavior of the stress - strain in reinforcing steel is similar. While the internal structure of the concrete is not homogeneous because of the different properties of the material (cement, sand, and gravel) and also because of air voids.

In the three-dimensional analysis of any structural member in a finite element method, concrete is combined with reinforcing steel to act as a composite system.

B.3.1 Modeling of Concrete

In general, concrete behavior is complex. It can behave as a linear or nonlinear material depending on the nature and level of induced stresses. Concrete is a heterogeneous material for the different properties of its constituent materials. Thus, the mechanical properties of the concrete are scattered. To ease the analysis and design can be considered as a homogeneous material in the microscopic sense **(Zienkiweicz, 1977)**

The non-linear behavior of the concrete under additional load is due to the development of the micro–cracks in the interface between aggregate and the cement mortar, this micro–cracks present prior to loading **(Neville and Brooks, 1987)**. The concrete behavior is described according to stress situations in the following:

B.3.1.1 Uniaxial Compression Behavior of Concrete

» Uniaxial Compression Behavior for NSC

Figure (B.4) illustrates the stress-strain relationship of the concrete under (uniaxial) compression. The curve consists of three stages. The first stage is linear from the beginning of the loading to about (30%) of the ultimate compressive strength of concrete (f'_c). The second stage shows the curve gradually increasing the bending to about ($0.75f'_c$ to $0.9f'_c$) and then the curve is greater until it reaches the peak point at (f'_c) and thus begins the final stage where the curve descends until the failure occurs as a result of crushing the concrete at the ultimate strain (ε_{cu}) **(Leet and Bernal, 1997)**.

According to **(ACI-318R, 2008)** Code, ultimate compressive strength occurs at a strain ($\varepsilon_\circ$) of approximately (0.002). Also, the code specifies that the ultimate strain (ε_{cu}) be taken as (0.003).

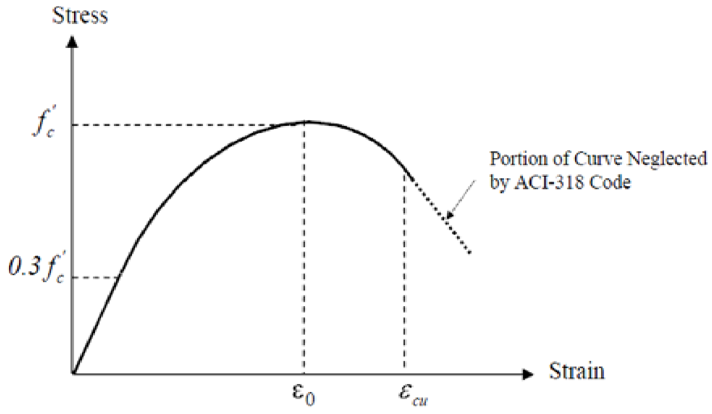

Figure (B.4) Uniaxial compressive stress-strain curve for NSC **(Leet and Bernal, 1997).**

» Uniaxial compression behavior for HSC

In the high strength concrete the ascending part of the stress-strain curve under the axial compression is more linear and slope in the normal concrete as well as the strain at the maximum stress than the normal concrete **(Ramon et. al, 1991**). In addition, the descending part of the curve in high strength concrete is steeper than normal concrete. Figure (B.5) shows the typical curve of stress-strain of high-strength concrete axial compression.

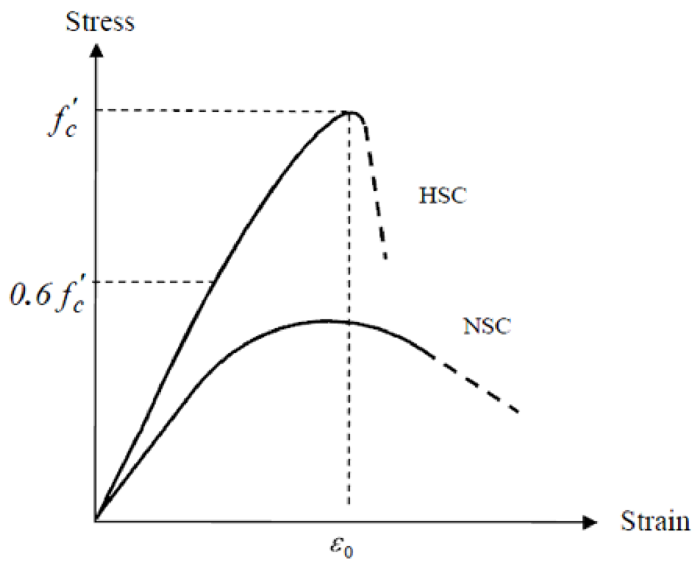

Figure (B.5) Uniaxial compressive stress-strain curve for HSC **(Ramon et. al, 1991)**

From the figure above, the curve is linear to about (60%) of the maximum compressive strength (f'_c), and a slight nonlinearity curve begins between (0.6 f'_c) and (0.7f'_c), After that, a further increase in curvature appears until (0.8f'_c). For compressive stress above this value, the curve curves sharply until the peak stress level is reached. Apart from peak stress, the lower part of the curve becomes more acute due to the rapid failure of high-strength concrete.

» Modulus of elasticity (Ec) and Poisson's ratio (υ)

In the modeling of finite element, the empirical equations below were adopted to calculate the modulus of the elasticity of RPC and NSC, that is adopted by **ACI-318** and **ACI-363.**

$Ec_{(HSC)}$ =3320 $\sqrt{f'c}$ +6900-------------------------------------(B-12)

$Ec_{(NSC)}$ = 4700$\sqrt{f'c}$ ---(B-13)

ACI committee 363 submitted a value to Poisson's ratio (υ), for NSC is (0.15 to 0.22), and (0.2-10.32) for RPC. In the normal study, the value of Poisson's ratio (0.2) was adopted for both concrete types

B.3.1.2 Uniaxial Tension Behavior of Concrete

Figure (B.6) illustrates the typical stress-strain curve of the concrete under uniaxial tensile stress. It is clear from the figure that the curve is linear "for approximately ($0.6f_t$). after that, and because of the generation and spread of the micro-crack prior to formation of continuous crack system at peak stress, the curve tends to be nonlinear. The unstable micron-crack system then grows under tensile stress bringing the material to its post-peak region **(Soroushian and Lee, 1989).**

In the current study, the split cylinder strength (f_t) was adopted as an approximation tensile strength of concrete, as in chapter four.

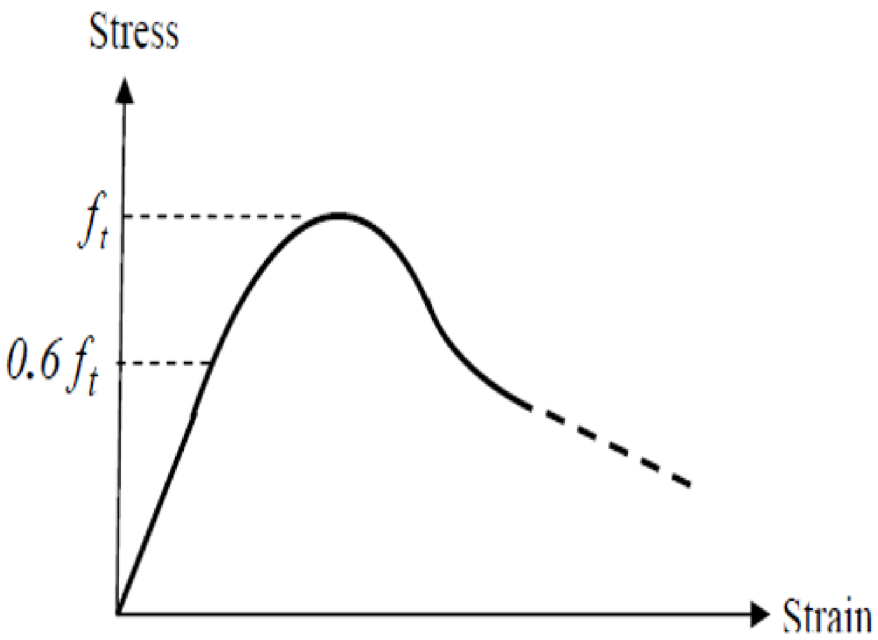

Figure (B.6) Typical uniaxial tensile stress-strain curve for concrete **(Soroushian and Lee, 1989).**

B.3.1.3 Biaxial Behavior of Concrete

The behavior of NSC and HSC under biaxial state differs from their behavior under uniaxial state. In order to understand the mechanism of failure of concrete, it is necessary to know its behavior when exposed to multiaxial states of stress.

(Kupfer et. al, 1973), concluded the ultimate strength of the concrete under biaxial compression is greater than uniaxial compression and depends on the principal stress ratio. As shown figure (B.7)

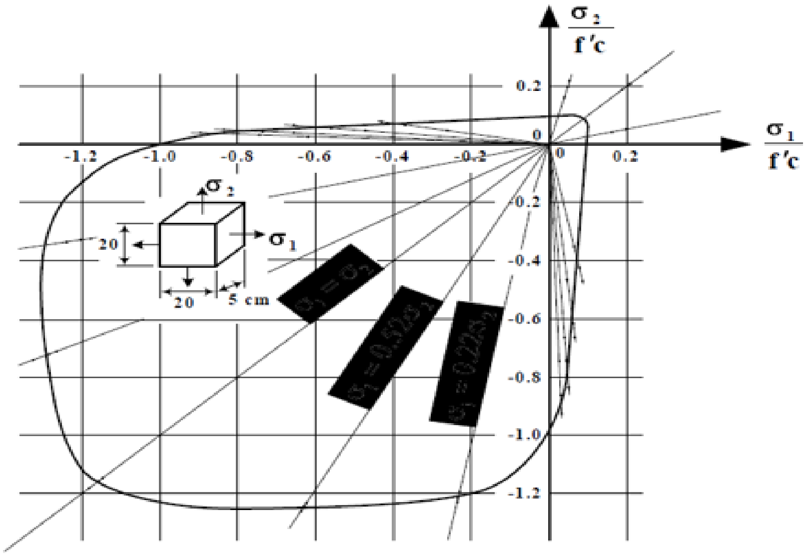

Figure (B.7) Biaxial state of loading **(Kupfer and Grestle, 1973).**

Under biaxial compression stresses, the compressive strength increased approximately (25% and 16%) than the uniaxial strength when the stress ratio (σ_2=0.5σ_1) and (σ_2=σ_1) respectively. The compressive strength decreases almost linearly with increased applied tensile stress under the biaxial tension-compression. The strength of the concrete is approximately equal to the uniaxial tensile strength when the concrete is under the biaxial tension.

B.2.1.4 Triaxial Behavior of Concrete

Under a triaxial stress state the failure surface of concrete is a function of the three principal stresses, **(Chen and Saleeb, 1981)**. Because isotropy for concrete is assumed, the elastic limit, the onset of unstable crack propagation and the failure limit all can be represented as surfaces in three-dimensional principal stress space. Figure (B.8) shows schematically the elastic-limit surface and failure surface. For increasing hydrostatic compressions along the (σ_1=σ_2=σ_3) axis, the deviatoric sections (planes perpendicular to the axis (σ_1=σ_2=σ_3)) of the failure surface are more or less circular, which indicates that the failure in this region is independent of the third stress invariant. For smaller hydrostatic pressure, these deviatoric cross sections are convex and noncircular. The failure surface can be represented by three stress invariants.

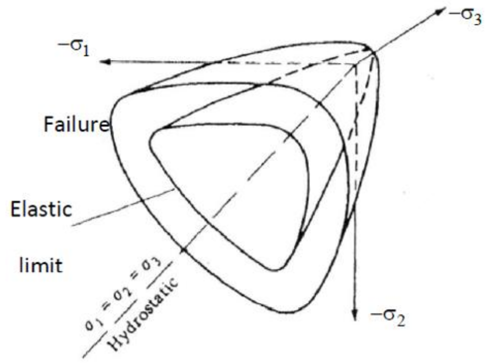

Figure (B.8) Failure surface of concrete in 3-D stress space **(Chen and Saleeb, 1981).**

B.2.1.5 Stress-Strain Relationship Models

The current study includes two types of stress-strain models

Stress-strain model for normal concrete

Figure (B.9) represents the relationship of stress - strain to normal concrete prepared by **(Desayi, and Krishnan, 1964).**

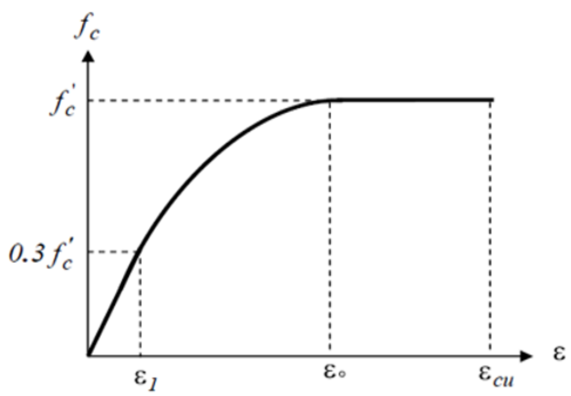

Figure (B.9) Stress-strain to normal concrete prepared by **(Desayi, and Krishnan, 1964)**

The following equations, proposed by **(Willam and Warnke, 1974),** were used to calculate the stress-strain curve of the normal strength concrete under compressive uniaxial.

$f_c = \varepsilon\, E_c$ for $0 \leq \varepsilon \leq \varepsilon_1$-------------------------(B-14)

$f_c = \frac{\varepsilon\, E_c}{1+\left(\frac{\varepsilon}{\varepsilon_\circ}\right)^2}$ for $\varepsilon_1 \leq \varepsilon \leq \varepsilon_\circ$ ---------------------------(B-15)

$f_c = f'_c$ for $\varepsilon_\circ \leq \varepsilon \leq \varepsilon_{cu}$ -------------(B-16)

And

$\varepsilon_1 = \frac{0.3 f'_c}{E_c}$ (Hooke's law) ---------------------------------(B-17)

$\varepsilon_\circ = \frac{2 f'_c}{E_c}$ ---------------------------------(B-18)

Where

ε_1= strain corresponding to ($0.3f'_c$). $\varepsilon_\circ$= strain at peak point.

ε_{cu}= ultimate compressive strain.

Stress-strain model for High Strength Concrete

For high strength concrete, the compressive uniaxial stress-strain relationship for concrete is described by a multilinear isotropic stress-strain curve, Figure (B.10), using the following expressions:

$f_c = \varepsilon\, E_c$ for $0 \leq \varepsilon \leq \varepsilon_1$-------------------------(B-18)

$f_c = 0.6f'_c + \frac{0.4 f'_c}{(\varepsilon_\circ - \varepsilon_1)}(\varepsilon - \varepsilon_1)$ for $\varepsilon_1 \leq \varepsilon \leq \varepsilon_\circ$ -------------(B-19)

$f_c = f'_c$ for $\varepsilon_\circ \leq \varepsilon \leq \varepsilon_{cu}$ ----------------------------(B-20) where;

ε_1 =strain corresponding to ($0.6f'_c$), defined by: -

$\varepsilon_1=\frac{0.6f'_c}{E_c}$ (Hooke's law) ----------------------------------(B-22)

(Mariano and Büyükoztürk, 1993) suggested peak strain ($\varepsilon_\circ$) for HSC as:

- $\varepsilon_\circ = 0.0025$ --(B-23)

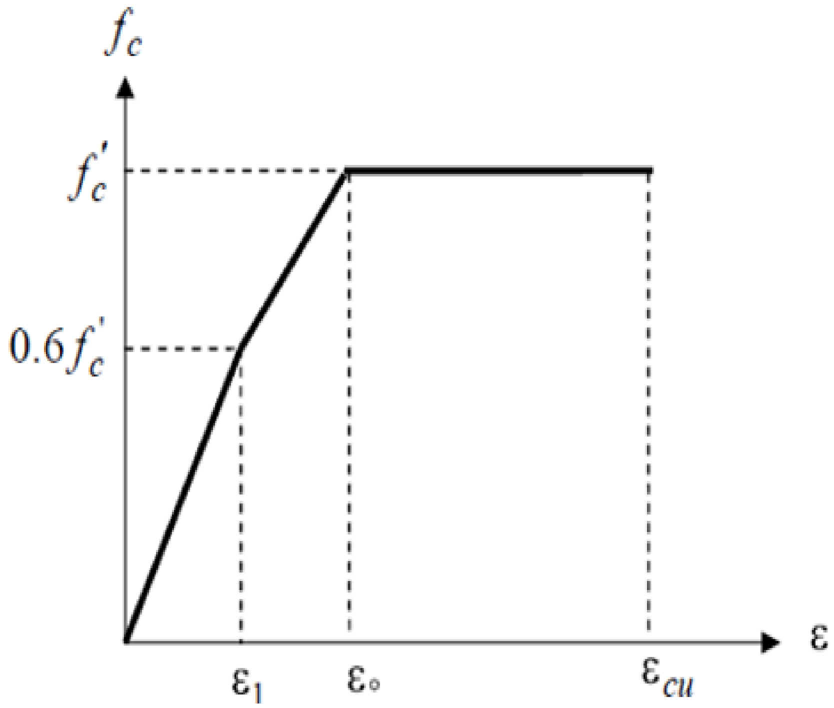

Figure (B.10) Stress-strain relationship model for HSC.

B.2.2 Modeling of Crushing

Crushing is defined as a complete deterioration in the structural integrity of the material. Under conditions where the crushing occurs, the strength of the material is assumed to have deteriorated to such an extent that the contribution of the element hardness can be ignored at the point of integration **(ANSYS Help, 2004).**

B.2.3 Modeling of Cracking

The following methods are used to model cracking in the analysis of finite elements of concrete structures **(Chen and Saleeb, 1981).**

1-Smeared cracking model,

2-Discrete cracking model, and

3-Fracture mechanics model.

The particular cracking model to be selected from the three alternatives depends upon the purpose of the analysis. The smeared cracking model is adopted when the purpose of the analysis is to know the behavior of the deflection versus load as shown in Figure (B.11). The breaking a discontinuous model is preferred if the purpose of the analysis is to identify the detailed local behavior as shown in Figure (B.12). While a fracture mechanics mode is used if the fracture mechanism is required. In general, the smeared cracking modeling is used for most structural engineering applications, (**Chen and Saleeb, 1981).**

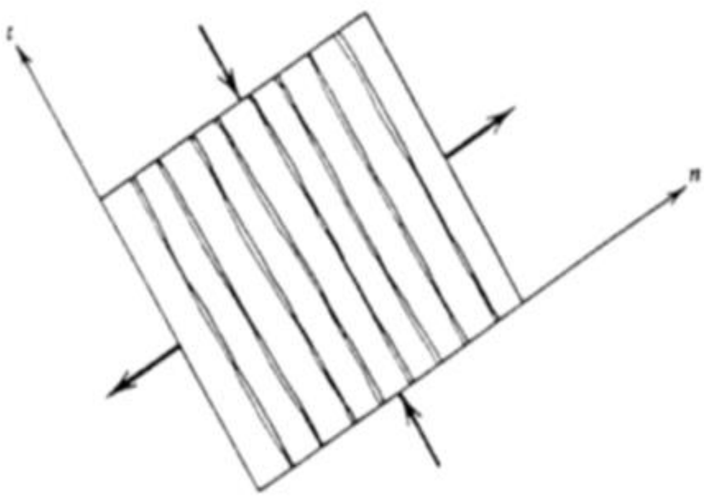

Figure (B.11) Single crack representation in the smeared cracking modeling **(Chen and Saleeb,1981).**

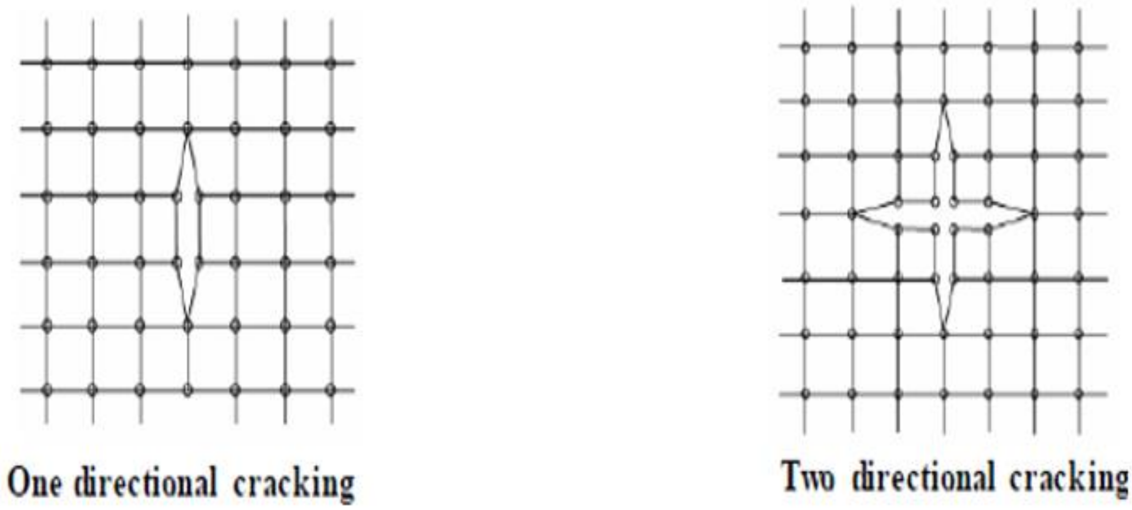

Figure (B.12) Cracking representation in discrete cracking modeling **(Chen and Saleeb, 1981).**

B.2.4 Modeling of Shear Transfer

Stress – strain curve of concrete in tension assumed to be linearly elastic up to the ultimate tensile strength. After that, the concrete cracks develop, some of the shear can be transmit through these cracks due to dowel action of the crossing reinforcement and aggregate interlock. In the current model, the strength of the untracked concrete was reduced on the shear transfer across the cracks. Use of the reduction coefficients to calculate the strength of the concrete on the shear transfer across the cracking interface. The coefficient (β_c) and β_o in the case of closed and open cracks, respectively. The range ($1> \beta_c> \beta_o> 0$) **(ANSYS Manual, 2002).**

B.2.5 Modeling of Reinforcing Steel

Figure (B.13) shows the stress-strain curve for reinforcing steel identical in tension and compression.

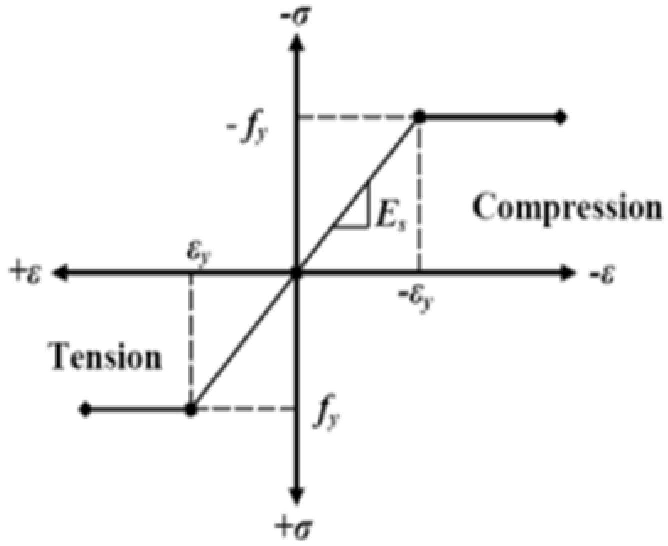

Figure (B.13) Stress-strain curve of Reinforcing steel bars.

It is also assumed that the reinforcing steel is capable of transmitting a axial force only. In the current study. Figure (B.14) shows the alternative curve of stress-strain for reinforcing steel used in the ANSYS program. The curved part consists of two parts. The first part is a slanted line with a slope equal to (Es) from the original until (fy), the second part is a line with a slope equal to (0.01Es) instead of horizontal. and this last case is limited to the strain 0.01 according to **(De-Xin, and Xiao-Xiong, 2007).**

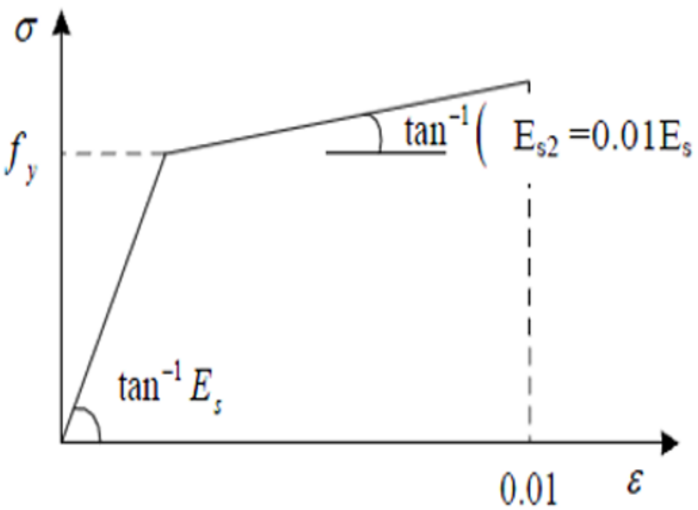

Figure (B.14) Modeling of reinforcing steel bars **(De-Xin, and Xiao-Xiong, 2007).**

B.3 Nonlinear Solution Techniques

Curved load - deflection shows the non-linear behavior of reinforced concrete elements due to the constant change in the hardness of these members arising from cracking, crushing concrete, yielding of reinforcing steel in tension, and plastic deformation of steel bars and concrete. The following techniques are used to solve nonlinear problems:

1- Iterative technique
2- Incremental technique
3- Incremental – iterative technique

As shown figure (B.15)

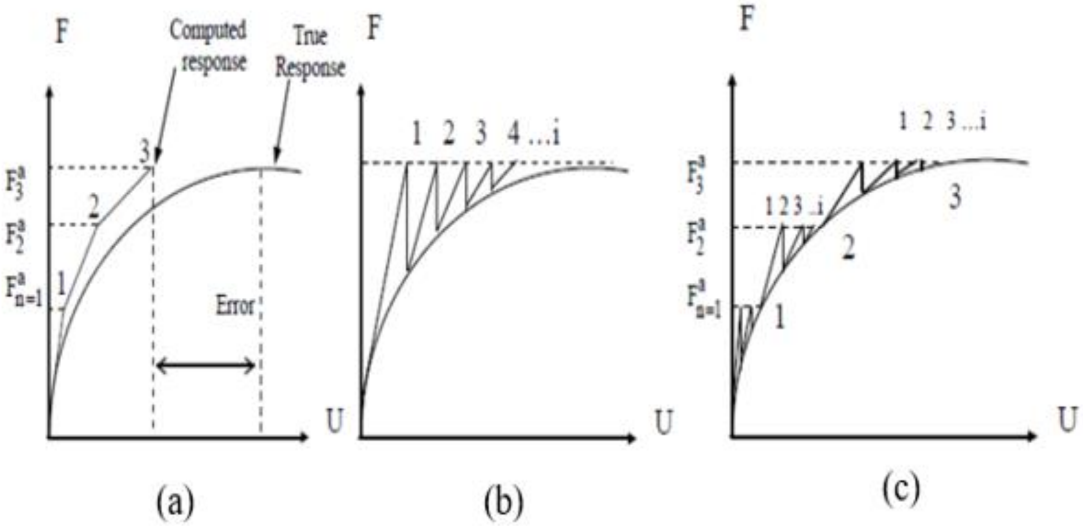

Figure (B.15) Basic techniques for solution of nonlinear equations

(B) Incremental (b) Iterative (c) Incremental-Iterative **(McGuire et. al, 2000)**

B.3.1 Incremental – Iterative Technique

This technology is characterized by its high accuracy and its ability to provide information throughout the loading period **(Ansys Help, 2004)** and widely used in the analysis of reinforced concrete structures. Nonlinear equations are solved this way by applying external loads as a series of small increments, within each increment of loading, iterations are performed until equilibrium is achieved according to the specified convergence criterion, as shown figure (B.15.c).

The incremental-iterative solution procedures comprise the following procedures **(Ansys Help, 2004).**

B.3.1.1 Initial-Stiffness Procedure

In this procedure, the stiffness matrix is formed and solved only once at the beginning of the analysis, and the program uses this initial stiffness matrix at every equilibrium iteration. For this procedure, the computation cost per iteration is significantly reduced, but in case of strong nonlinearities (such as large deformation analyses), the method often fails to converge, Figure (B.16).

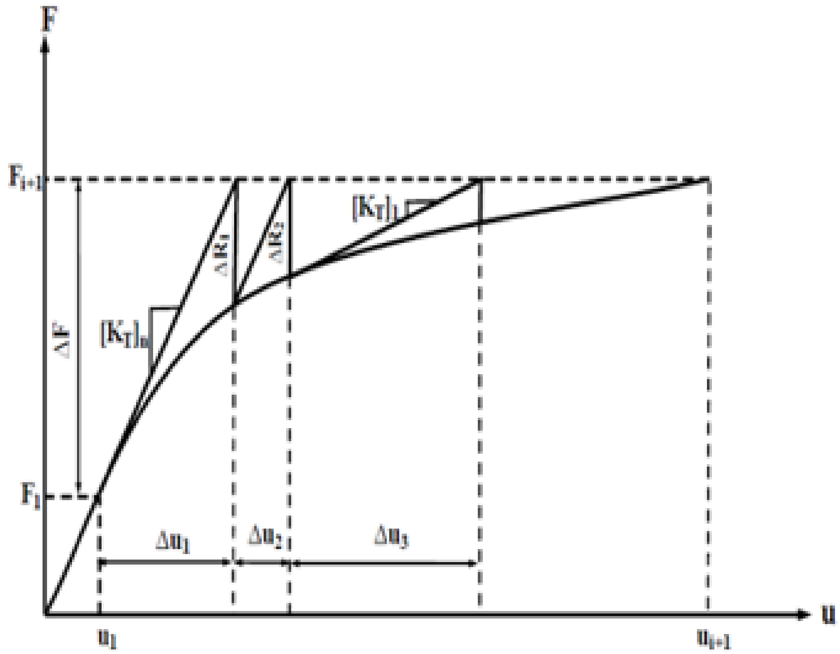

Figure (B.16) Initial stiffness method

B.3.1.2 Full Newton - Raphson Procedure

In this procedure, the stiffness matrix is updated at every equilibrium iteration, thus a large amount of computation may be required to form and solve the stiffness matrix, Figure (B.17).

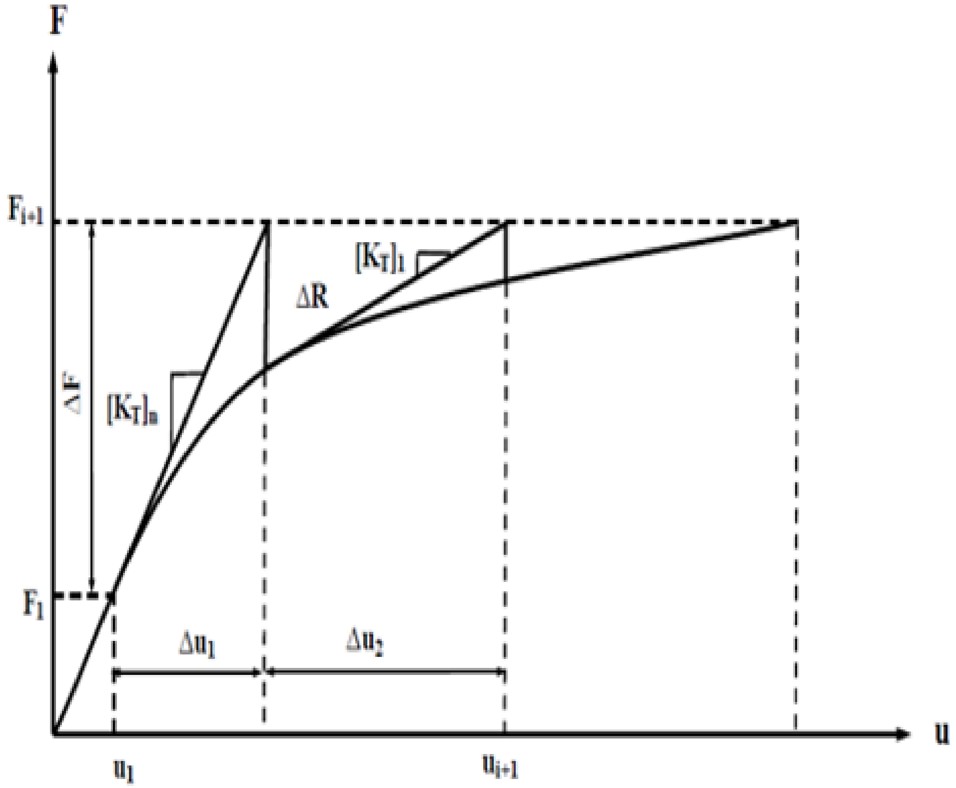

Figure (B.17) Full Newton‑Raphson method.

B.3.1.3 Modified Newton - Raphson Procedure

In this method, the stiffness matrix is updated only once for each increment of loading. As compared with the full Newton-Raphson method, the modified Newton-Raphson method is more economical and common because it involves fewer stiffness matrix reformulations, but the convergence is slower and a large number of iterations are required to achieve a converged solution, Figure (B.18).

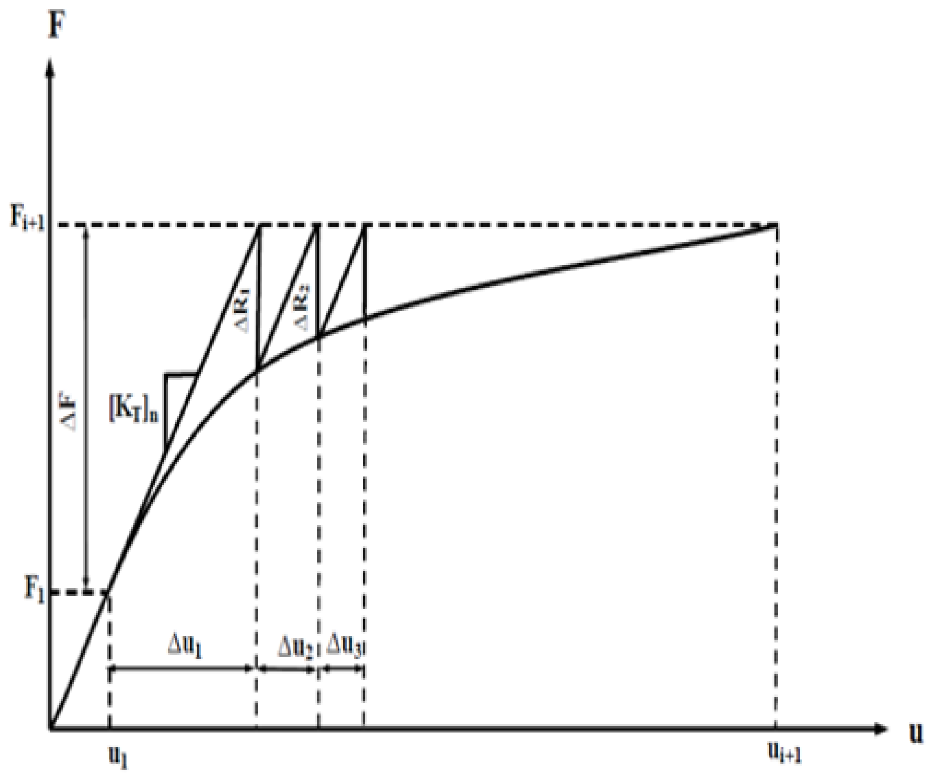

Figure (B.18) Modified Newton-Raphson method

B.4 Convergence Criterion

A convergence criterion is required in order to terminate the iterative process when the solution is considered to be sufficiently accurate. For nonlinear structural analysis, several convergence criteria can be used to monitor equilibrium. The convergence criterion for the nonlinear analysis of structural problems can be classified as:

1- Force criterion.

2- Displacement criterion.

3- Stress criterion

Only the force criterion is adopted in the present study. In the force convergence criterion, the norm of the residual forces at end of each iteration is checked against the norm of the current applied forces as:

$$\|\{R\}\| = \left(\sum R_i^2\right)^{0.5} \leq T_n\left(\sum F_i^{a\,2}\right)^{0.5} \tag{B-24}$$

and, $\{R\} = \{F^a\} - \{F^{in}\}$ (B-25)

where:

T_n = tolerance (taken equal to 0.1%)

$\{R\}$ = residual load vector

B.5 Analysis Termination Criterion

The nonlinear finite element analysis used in simulating the response of reinforced concrete structures must include as well a criterion to terminate the analysis when failure of the structure is reached. In a physical test under load control, collapse of a structure takes place when no further loading can be sustained; this is usually indicated in the numerical tests by successively increasing iterative displacements and a continuous growth in the dissipated energy. Hence, the convergence of the iterative process cannot be achieved and therefore it is necessary to specify a suitable criterion to terminate the analysis.

In the present study, a maximum number of iterations for each increment of load are specified to stop the nonlinear solution if the convergence tolerance has not been achieved. This maximum number of iterations depends on the type of the problem, extent of nonlinearities, and on the specified tolerance **(Fenner, 1996).** In this study the selected maximum number of iteration is 100.

الخلاصة

الهدف الرئيسي من البحث هو دراسة فائدة استخدام تقنية التهجين في العتبات الخرسانية العميقة من خلال دراسة سلوك القص في العتبات الخرسانية العميقة المسلحة ذات مقطع عرضي هجين يحتوي على نوعين مختلفين من الخرسانة, خرسانة المساحيق الفعالة (RPC) و خرسانة عادية المقاومة (NSC) تجريبيا" وعدديا".

تضمن البرنامج العملي فحص ثمان نماذج من العتبات الخرسانية المسلحة العميقة بابعاد (mm (800×300×150)) بسيطة الاسناد وتحت تأثير حملين مركزيين متناظرين . قسمت العتبات العميقة الى اربعة مجاميع : المجموعة (A) تضمنت العتبات العاديه, المجموعة (B) شملت العتبات الهجينه مع RPC (75 ملم في منطقة الشد) , المجموعة (C) تضمنت العتبات الهجينه مع RPC (75 ملم في منطقة الانضغاط) و المجموعة (D) شملت العتبات الهجينة مع RPC (125 ملم في منطقة الشد) لدراسة تأثير: نسبة مسافة القص/ العمق ($^{a}/_{h}$) وكانت (2/3 و 1.25/3) وسمك طبقة (RPC) وكانت (75 ملم و 125 ملم) و موقع طبقة RPC (في منطقة الضغط او منطقة الشد) على كلا من الحمل النهائي وحمل التشقق الاولي ومنحني الحمل – الهطول ونوع الفشل. بينت النتائج العملية ان استخدام تقنية التهجين حسن من سلوك العتبات العميقة الهجينة مع زيادة في حمل التشقق الاولي والحمل النهائي , أكبر زيادة في حمل التشقق الاولي والحمل النهائي حوالي (17.8 و 54) % على التوالي للعتبات الهجينة التي تمتلك طبقة RPC (125 مم) في منطقة الشد عند مقارنتها مع العتبات العادية. الحمل النهائي في العتبات الهجينة مع طبقة RPC في منطقة الشد أكبر من العتبات الهجينة مع RPC في منطقة الانضغاط حوالي (6.7 و 28.7) % عند (a / h = 2/3 و 1.25 / 3) على التوالي. أيضا ، زاد كلا من حمل التشقق الاولي والحمل النهائي مع زيادة سمك طبقة RPC حوالي (2.4 و 8.6) % على التوالي عند (a / h = 1.25 / 3). سلوك منحني (الحمل-الهطول وسط الفضاء) في العتبات العميقة كان أكثر مطاوعة مع زيادة (a / h) ، منحني (الحمل-الهطول وسط الفضاء) في العتبات العميقة الهجين أكثر صلابة من العتبات العميقة العادية ، منحني (الحمل-الهطول وسط الفضاء) في العتبات العميقة الهجينة أكثر صلابة مع زيادة سمك طبقة RPC. كان أفضل سلوك لمنحنى (الحمل-الهطول وسط الفضاء) في العتبة الهجينة مع RPC (125 ملم في منطقة الشد) وعند (a / h = 1.25 / 3). تحمل العتبات زاد مع انخفاض (a / h) حول (21.5 ، 27.4 ، 5.6 و 22.6)% في المجموعات (A، B، C و D) على التوالي ، ولكن تأثير a / h كان ضئيل على حمل التشقق الاولي.

تضمن الجزء العددي استخدام طريقة العناصر المحددة (FEM) لمحاكاة سلوك العينات وتحسين البحث بإضافة المزيد من المتغيرات. أظهر التحليل الذي تم إجراؤه مع (ANSYS-2016-R 17.2) اتفاقاً مقبولاً بين النتائج التجريبية والنتائج العددية. كانت الأحمال النهائية التجريبية للأحمال النهائية العددية بين (0.19 - 6.67) %.

جمهورية العراق
وزارة التعليم العالي والبحث العلمي
جامعة كربلاء- كلية الهندسة
قسم الهندسة المدنية

دراسة سلوك القص في العتبات العميقة الهجينة المتكونة من خرسانة المساحيق الفعالة وخرسانة الاعتيادية المقاومة

رسالة

مقدمة إلى كلية الهندسة في جامعة كربلاء

كجزء من متطلبات نيل درجة ماجستير في علوم الهندسة المدنية

(بنى تحتية)

من قبل

علي يونس سعد

(بكالوريوس في الهندسة المدنية 1994)

إشراف

الأستاذ المساعد الدكتور ليث شاكر رشيد

كانون الثاني **2018**

جمادي الاول **1439**